THESIS FOR THE DEGREE OF DOCTOR OF PHILOSOPHY (PHD)

Neuromodulatory actions on ion channels of neuronal populations of the reticular activating system

by **Dr. Tsogbadrakh Bayasgalan**

UNIVERSITY OF DEBRECEN

DOCTORAL SCHOOL OF MOLECULAR MEDICINE

DEBRECEN, 2021

THESIS FOR THE DEGREE OF DOCTOR OF PHILOSOPHY (PHD)

Neuromodulatory actions on ion channels of neuronal populations of the reticular activating system

by **Dr. Tsogbadrakh Bayasgalan**

Supervisor: Dr. Balázs Zoltán Pál

UNIVERSITY OF DEBRECEN

DOCTORAL SCHOOL OF MOLECULAR MEDICINE

DEBRECEN, 2021

1. TABLE OF CONTENTS

1. TABLE OF CONTENTS 3
2. LIST OF ABBREVIATIONS 5
3. INTRODUCTION AND LITERATURE BACKGROUND 8
3.1. The reticular activating system 8
3.2. Cholinergic structures of the midbrain and basal forebrain 10
3.2.1. Pedunculopontine nucleus (PPN) 12
3.2.2. Morphological properties and relationships of PPN 13
3.2.3. Cell types and markers of PPN 15
3.2.4. Raphe nuclei 27
3.3. The M-current 29
3.3.1. Ion channels responsible M-current and channelopathies related to them 30
3.3.2. Selective KCNQ channel openers and blockers and neurological diseases 31
3.3.3. Electrophysiological properties and regulation 32
3.3.4. M-current of different brainstem structures 34
3.4. Optogenetics 37
4. Aims of the study 40
5. MATERIALS AND METHODS 41
5.1. Solutions 41
5.2. Animals and preparation 41
5.3. Electrophysiology 42
5.4. Morphological identification of the investigated neurons 47
5.5. Immunohistochemistry 47
5.6. Activity wheel test 48
5.7. Statistics 48
6. RESULTS 49
6.1. Electrophysiological characterization of the M-current and localization in neurons from PPN 49
6.1.1 The M-current of different PPN neuronal populations 49
6.1.2 Modulation of M-current on PPN cholinergic neurons 50
6.2. The role of the M-current on neuronal synchronization of PPN cholinergic neurons 52
6.3. M-current properties mediated by KCNQ4 subunits 53
6.3.1 M-current properties in KCNQ4 KO mice 53
6.3.2 Presence of functional KCNQ4 subunits in PPN 56

6.4. Functional roles of KCNQ4 in the RAS 58
6.5. Localization of the M-current in neurons from dorsal and median raphe 61
6.6. PPN glutamatergic neurons are physiologically different from CnF neurons 66
6.6.1 Morphological features of glutamatergic neurons of the mesencephalic locomotor region 66
6.6.2 Ionic currents and firing properties of the PPN and CnF 68
6.6.3 Functional subgroups of MLR glutamatergic neurons 70
6.6.4. High threshold membrane potential oscillations of the MLR glutamatergic neurons 73
7. Discussion 76
7.1. The M-current is a hallmark of cholinergic neurons of the PPN 76
7.2. The M-current synchronizes neighboring PPN cholinergic neurons 78
7.3. The KCNQ4 subunit is present on a subset of PPN cholinergic neurons 78
7.4. Ion channels formed by KCNQ4 subunits critically affect adaptations to changes in light-darkness conditions 81
7.5. The M-current of raphe serotonergic neurons is topographically distributed 82
7.6. CnF and PPN glutamatergic neurons are functionally distinct 85
8. SUMMARY 86
10. KEYWORDS 87
11. Acknowledgements 88
12. References 89

2. LIST OF ABBREVIATIONS

5-HT	subtypes of the 5-hydroxytryptamine receptor receptor family
AAV	adeno-associated viral vectors
aCSF	artificial cerebrospinal fluid
AI	adaptation index
AM	acetoxymethyl ester
Arch	archaerhodopsin-3
ATP	adenosine 5'-triphosphate
BAS	nucleus basalis
BF	basal forebrain
BLA	basolateral amygdala
BR	bacteriorhopsin
CEA	central amygdala nucleus
ChAT	choline acetyltransferase
Ch1-6	cholinergic nuclei
ChR2	channelrhodopsin-2
CnF	cuneiform nucleus
CNS	central nervous system
DA	dopamine
D-AP5	D-2-amino-5-phosphopentanoate
DAG	diacylglycerol
DBS	deep brain stimulation
DCN	dorsal cochlear nucleus
DD	complete environmental darkness
DR	dorsal raphe nuclei
DFNA2	non-syndromic sensorineural deafness type 2
DRG	dorsal root ganglion
EC	entorhinal cortex
ECoG	electrocorticography
EEG	electroencephalography

EGTA	ethylene glycol tetraacetic acid
fAHP	fast afterhyperpolarization
GABA	gamma-amino-butyric acid
GAD	glutamic acid decarboxylase
GFAP	glial fibrillary acidic protein
GPi	globus pallidus internus
GPCR	rhodopsin-G protein-coupled receptor
GPR55, GPR119	G protein-coupled cannabinoid receptors (G protein-coupled receptor)
GtR3	guillardia theta rhodopsin-3
Hcrt	hypocretin
HDB	horizontal diagonal band nucleus
HEPES	4- (2-hydroxyethyl) -1-piperazinetanesulfonic acid, (4- (2-hydroxyethyl) -1-piperazineethanesulfonic acid)
HR	halorhodopsin
HTO	high threshold oscillations
Hyp	hypothalamus
ICU	imaging control unit
Icj	islands of Cajella
ILT	intralaminar thalamus
IP 3	inositol 1,4,5-triphosphate
IPN	interpeduncular nucleus
ISI	interspike interval
KCNQ	alternative name for Kv7 voltage-gated potassium channel
KO	knockout
LC	locus coeruleus
LD	alternating light-darkness condition
LDT	laterodorsal tegmental nucleus (laterodorsal tegmental nucleus)
LH	lateral hypothalamus
LHb	lateral habenula
LV	lentiviral vector

mAChR	muscarinic acetylcholine receptor
mAHP	medium afterhyperpolarization
mGluR	metabotropic glutamate receptor
MLR	mesencephalic locomotor region
MN	tuberomammillary nucleus
M1,3,5	muscarinic acetylcholine type 1 receptor
MR	median raphe nuclei
MS	medial septal nucleus
NBQX	2,3-dihydroxy-6-nitro-7-sulfamoylbenzo [f] quinoxaline-2,3-dione, (2,3-dihydroxy-6-nitro-7-sulfamoyl benzo [f] quinoxaline-2,3-dione)
NpHR	Natronomonas pharaonis
OptoXR	photoactivatable protein G coupled metabotropic receptor
Orx	orexin
PAG	periaqueductal gray
PALc	caudal pallidum
PB	phosphate buffer
PBS	phosphate-buffered saline
PFC	prefrontal cortex
PGi	paragigantocellular nucleus
PGO	ponto-geniculo-occipital
PIA	pontine inhibitory area
PIP 2	phosphatidylinositol 4,5-bisphosphate
PKA	protein kinase A
PKC	protein kinase C
PLC	phospholipase C
PPN	pedunculopontine nucleus (pedunculopontine nucleus)
RAS	reticular activating system
REM	rapid eye movement
RMP	resting membrane potential
RMTg	rostromedial tegmental nucleus

RN	raphe nuclei
PS	paradoxical sleep
sAHP	slow afterhyperpolarization
Sert	serotonin transporter
SFA	spike frequency adaptation
SI	substantia innominata
SN	substantia nigra
SNr	substantia nigra pars reticulata
SP5	spinal trigeminal nucleus
STD	short-term depression
STN	subthalamic nucleus
STR	striatum
SWS	slow wave sleep
TTX	tetrodotoxin
VCN	ventral cochlear nucleus
VDB	vertical diagonal band nucleus
VGLUT2	type 2 vesicular glutamate transporter
VP	ventrolateral preoptic nucleus
VTA	ventral tegmental area
XE991	10,10bis (4-Pyridinylmethyl) -9 (10H) -anthracenone dihydrochloride
W	wakefulness
WT	wild type

3. INTRODUCTION AND LITERATURE BACKGROUND

3.1. The reticular activating system

The reticular activating system (RAS) is a part of the pontine and mesencephalic reticular formation. The RAS is a network of neurons sending ascending fibers to the hypothalamus and the thalamus, as well as directly to the cortex to facilitate EEG desynchronization and awake state, as well as to modulate behavior (Moruzzi and Magoun,

1949; Jones and Leavitt, 1974; Steriade et al., 1991; Jones, 1993; Stevens and Hening, 2007; Garcia-Rill, 2009; Arguinchona et al., 2020).

The RAS is formed by three main cell groups, which consist of the cholinergic pedunculopontine nucleus (PPN) and the laterodorsal tegmental nucleus (LDT); the noradrenergic locus coeruleus (LC), and the serotonergic raphe nuclei (RN). The RAS receives inputs from all afferent sensory systems as collaterals of primary afferent sensory pathways (Steriade and Glenn, 1982; Link and Sloan, 2003; Garcia-Rill, 2009).

The RAS relays 'arousal' information through the intralaminar thalamus (ILT) to the cortex (Macchi and Bentivoglio, 1982, Gonzalez-Lima and Scheich, 1985, Kaufman and Rosenquist, 1985). This system operates in parallel with 'specific' sensory innervation to the cortex via the primary sensory thalamic nuclei (Link and Sloan, 2003; Garcia-Rill, 2009).

The RAS also sends descending projections to systems regulating posture and movement, in order to activate higher centers in parallel with acting on motor systems to respond appropriately to sudden stimuli. These descending projections regulate the pontine inhibitory area (PIA) that controls the atonia of rapid eye movement (REM) sleep, pontine neurons responsible for startle reflex (a flexor response to sudden, potentially harmful stimuli acting on the motor system), and the reticulospinal systems that control locomotion. The RAS, particularly its cholinergic part, projecting to the dorsal subcoeruleus region also generates the ponto-geniculo-occipital (PGO) waves during REM sleep (Nelson et al., 1983; Garcia-Rill, 2009; Bernardi et al., 2019). This region triggers high-frequency bursts of activity (such as those required for long-term potentiation) that have been proposed to participate in sleep-dependent plasticity. (Fig. 1.; Garcia-Rill, 2009; Renouard et al., 2018).

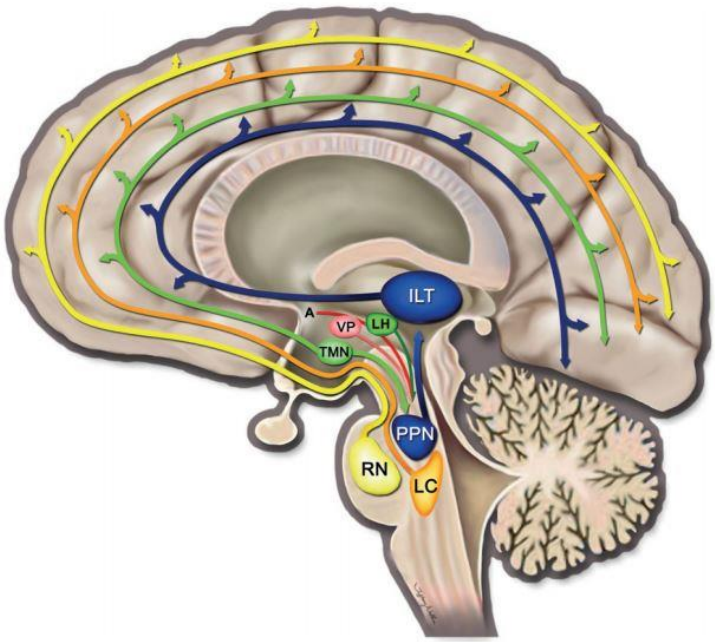

Fig. 1. Ascending projections of the RAS. A, adenosine; ILT, intralaminar thalamus; LC, locus coeruleus; LH, lateral hypothalamus; PPN, pedunculopontine nucleus; RN, raphe nucleus; MN, tuberomammillary nucleus; VP, ventrolateral preoptic nucleus (Garcia-Rill, 2009)

Furthermore, most of the neurons in the RAS located in the midbrain reticular formation are found dorsally and laterally to the red nuclei. Cooperation between several neurotransmitters modulates the action of the RAS with the key roles of both cholinergic and adrenergic neurotransmission. (Jones, 1991; Walter and Shaikh, 2014).

The ascending projections of the RAS boost the cortical activation and stimulate conscious perception of sensory stimuli. The brainstem reticular formation also modulates autonomic function especially muscle reflexes and tone (Walter and Shaikh, 2014).

3.2. Cholinergic structures of the midbrain and basal forebrain

Immunohistochemical labeling studies have demonstrated four major groups of ChAT-positive neurons located in the (1) the striatum; (2) the magnocellular basal nucleus; (3) the pontine tegmentum; and (4) the cranial nerve motor nuclei (Armstrong et al., 1983). The well-known brainstem and forebrain cholinergic structures are also grouped into six main central pathways (Ch1–Ch6) associated to the nuclei from where the cholinergic fibers originate (Fig.2; Mesulam et al., 1983; Lucas-Meunier et al., 2003).

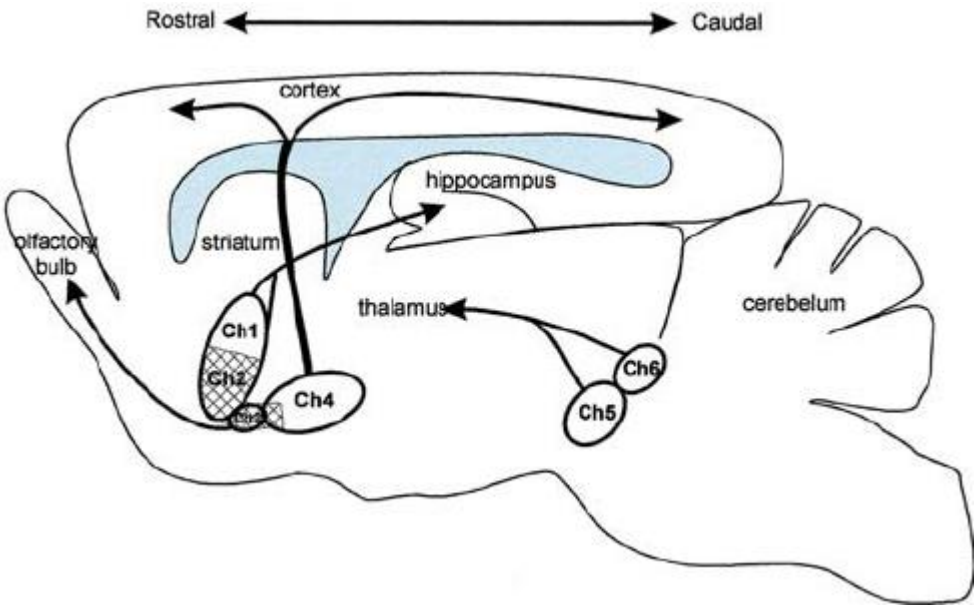

Fig. 2. Central cholinergic pathways and regions of the rat. Hatched area: diagonal band (Lucas-Meunier et al., 2003)

Cholinergic nuclei of the septum (Ch1) and the vertical limb of the diagonal band (Ch2) innervate only the hippocampus. The pedunculopontine nucleus (PPN; part of Ch5)

and the laterodorsal tegmental nucleus (LDT; Ch6) project to the thalamus. Cholinergic nuclei of the lateral part of the horizontal limb of the diagonal band (Ch3) send projections to the olfactory bulb. The pathway innervating the cortex mainly comes from the nucleus basalis magnocellularis (Ch4; Bigl et al. 1982; Lehmann, 1980; Wenk et al, 1980; Henderson, 1981; Johnston et al., 1981; Mesulam et al., 1983)

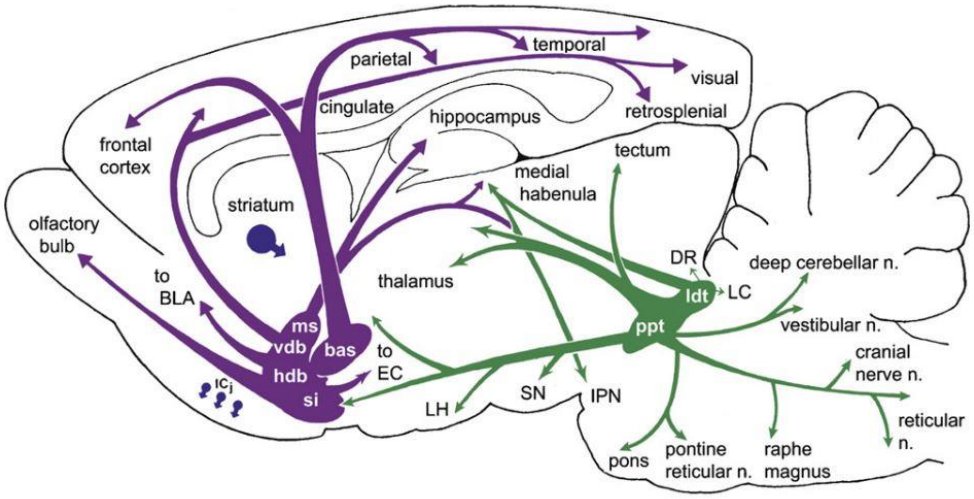

Fig. 3. Cholinergic nuclei and main projections in the brain. Abbreviations: bas, nucleus basalis; BLA, basolateral amygdala; DR, dorsal raphe; EC, entorhinal cortex; hdb, horizontal diagonal band nucleus; Icj, islands of Cajella; IPN, interpeduncular nucleus; LC; locus ceruleus; ldt, laterodorsal tegmental nucleus; LH, lateral hypothalamus; ms, medial septal nucleus; ppt, pedunculopontine nucleus; si, substantia innominata; SN, substantia nigra; vdb, vertical diagonal band nucleus (Woolf and Butcher, 2011)

The most abundant cholinergic neuronal populations are found in the basal forebrain (BF) and centered on the output of the nucleus basalis (Goard and Dan, 2009). The human nucleus basalis comprises approx. 200,000 neurons (Woolf and Butcher, 2011). The topography of BF cholinergic cells projecting to several cortical targets has been studied considerably. Cholinergic and non-cholinergic projections to the neocortex are well organized into separated (but sometimes also overlapping) neuronal groups that spread information from specific locations in the BF to different cortical areas (Fig. 3; Armstrong et al., 1983; Sofroniew et al., 1985; Zaborszky et al., 2015a).

The cholinergic neurons can be divided into three rostrocaudal regions in BF. Cholinergic neurons of the medial septal nucleus and vertical diagonal band nucleus project to the hippocampus (Woolf et al., 1984; Wainer et al., 1985). It is typically named as septohippocampal pathway. The intermediate region of the cholinergic basal forebrain comprises of the horizontal diagonal band nucleus and magnocellular preoptic nucleus. These

cholinergic nuclei send projections to olfactory bulb, amygdala, and the cingulate, retrosplenial, entorhinal, perirhinal, insular cortices, as well as to the frontal cortex (Saper, 1984; Woolf et al., 1984). Cholinergic neurons in the substantia innominata, magnocellular preoptic nucleus, and nucleus basalis give rise to projections for the neocortex, involving primary and secondary visual, auditory, somatosensory, and higher association cortex (Bigl et al., 1982; Rye et al., 1984). As a complex structure, the cholinergic basal forebrain plays an important role in attention, learning, memory, perception, and consciousness (Sarter et al., 2003; Woolf, 1998).

In the tegmentum, a continuous group of cholinergic neurons is located in the lateral reticular formation beginning rostrally at the caudal end of the substantia nigra and moving dorsocaudally towards the parabrachial region to pass into the rostral halves of both the ventral and dorsal parabrachial nuclei (LDT; Paxinos and Watson, 1982; Sofroniew et al., 1985).

The main sources of acetylcholine in the brainstem are the PPN and laterodorsal tegmental nucleus (LDT) collectively known as the mesopontine tegmental area or ponto-mesencephalo-tegmental complex. (Fig. 3; Woolf and Butcher, 1986; Woolf and Butcher, 1989). The major cholinergic inputs of the thalamus arising from Ch5 including PPN, which is located in the reticulum of the pontomesencephalic formation, and Ch6 comprising of the LDT found inside the periventricular area nucleus (Woolf and Butcher, 2011).

3.2.1. Pedunculopontine nucleus (PPN)

One of the main cholinergic areas of mesopontine region is the pedunculopontine nucleus (PPN) which does not only give rise to cholinergic innervation but also a target of it by inputs from the neighboring laterodorsal tegmental nucleus (LDT) and the contralateral PPN. Apart from cholinergic fibers from neighboring nuclei, local cholinergic collaterals were also shown in the PPN (Mena-Segovia et al, 2008; Honda and Semba, 1995).

The PPN is composed of cholinergic ,GABAergic and glutamatergic neurons, which present different activity patterns during different global brain states. The PPN shows different neuronal activity patterns in slow wave sleep (SWS), paradoxical sleep (PS) and wakefulness (W).

3.2.2. Morphological properties and relationships of PPN

Identification of the PPN can be easily based on labelling of the cholinergic neurons. This labelling is typically done by immunohistochemistry with monoclonal antibody against the choline acetyltransferase (ChAT) enzyme (Eckenstein and Sofroniew, 1986; Mesulam et al., 1984; Satoh and Fibiger, 1986; Vincent and Reiner, 1987). Cholinergic cells in this area are 40% greater than non-cholinergic ones (Rye et al., 1987; Honda and Semba, 1995). It was shown that there is a rostrocaudal gradient in the density of PPN cholinergic neurons, i.e. the number, proportion and density of cholinergic cells increase towards the caudal part of PPN (Mena-Segovia et al., 2009; Baksa et al., 2019).

Ascending projections of PPN have been also extensively studied with several methods. By injecting the tritriated amino acids into the PPN, an anterograde and retrograde labeling was seen in many rostral structures such as the substantia nigra, globus pallidus, lateral part of the hypothalamus, basal forebrain, frontal cortex (Lavoie and Parent, 1994b, 1994c; Saper and Loewy, 1982; Sugimoto and Hattori, 1984; Benarroch, 2013). In another study, wheatgerm-agglutinin conjugated horseradish peroxidase was directly administered into the PPN, which anterogradely marked further structures in addition to the former, such as intermediate lamina of the spinal cord in the cervical and thoracic levels (Fig. 4; Canteras et al**.,** 1990; Goldsmith and Van Der Kooy, 1988; Jackson and Crossman, 1981, 1983, Redgrave et al**.,** 1987).

One of the important connections of PPN is reciprocal relationship with the basal ganglia (Jackson and Crossman, 1983; Moon Edley and Graybiel, 1983; Sugimoto and Hattori, 1984). The PPN neurons with different functions innervate the basal ganglia, and basal ganglia sends fibers to the PPN where they contact with another neuronal population (Pahapill and Lozano, 2000; Mena-Segovia et al., 2004). This fact is also an example for the heterogeneity of PPN.

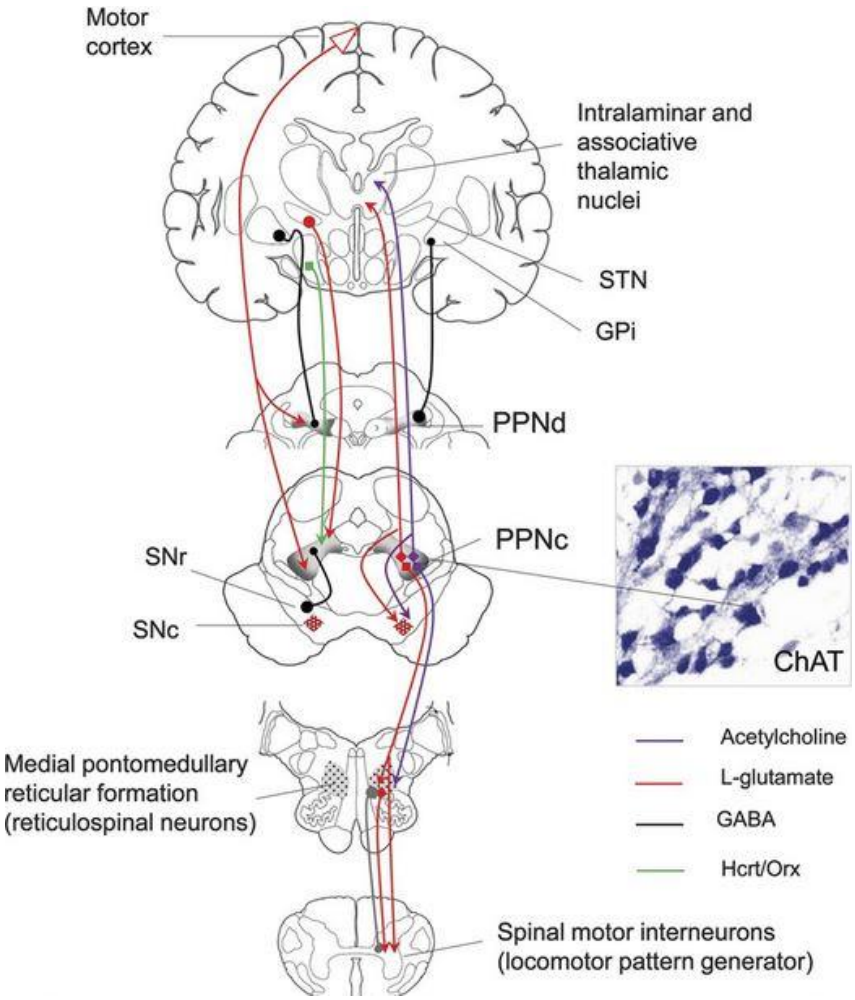

Fig.4. Main connections of the pedunculopontine nucleus. The pedunculopontine nucleus (PPN) is subdivided into a pars dissipata (PPNd), present throughout the rostrocaudal extent of the nucleus, and a pars compacta (PPNc), and contains neurons that synthesize acetylcholine, g-aminobutyric acid (GABA), or L-glutamate. The cholinergic neurons, identified by the expression of choline acetyltransferase (ChAT), predominate in the PPNc. The PPN receives direct glutamatergic inputs from the motor cortex and GABAergic inputs from the globus pallidus internus (GPi) and substantia nigra pars reticulata (SNr), as well as inputs from the subthalamic nucleus (STN) and deep cerebellar nuclei (not shown). Both cholinergic and non-cholinergic neurons of the PPN provide ascending and descending projections. Ascending projections mainly target the GPi, substantia nigra pars compacta (SNc), and the intralaminar and associative nuclei of the thalamus. Descending projections target the pontine and medullary reticular formation and the spinal cord involved in control of muscle tone and locomotion. The PPN also receives inputs from wake active hypocretin/orexin (Hcrt/Orx) neurons of the posterior lateral hypothalamus, as well as inputs from histaminergic neurons of the tuberomammillary nucleus, serotonergic neurons of the dorsal raphe, noradrenergic neurons of the locus coeruleus, and cholinergic input from the laterodorsal tegmental nucleus and contralateral PPN (not shown). (Benarroch, 2013)

The reciprocal relationship between the substantia nigra and the PPN was both anatomically and electrophysiologically revealed (Beninato and Spencer, 1987; Clarke et al., 1987). Electron microscopic studies found synaptic terminals from the substantia nigra on the dendrites of the PPN neurons (Nakamura et al., 1989). The two main mesopontine cholinergic nuclei, the PPN and LDT overlap in many parts in their projections, but the LDT projects more toward the midline and limbic structures, while PPN projects to lateral motor structures (such as the substantia nigra and dorsomedial striatum) and the colliculus superior (Woolf and Butcher, 1986). Descending projections of the PPN include the deep cerebellar

nuclei (Newman and Ginsberg, 1992), pontomedullary reticular nuclei (Mitani et al., 1988; Rye et al., 1988), the medioventral medulla (Garcia-Rill and Skinner, 1987a, 1987b; Rye et al., 1987; Spann and Grofova, 1989), and there are minor projections to the spinal cord (Goldsmith and Van Der Kooy, 1988, Spann and Grofova, 1989).

The areas of PPN, LC, and LDT are overlapped at the transition between PPN and LC and between LC and LDT. Furthermore, the anterior part of the PPN is attached to the posterior edge of the substantia nigra. (Beckstead et al., 1979; Moore and Bloom, 1979; Garcia-Rill, 1991). It has been shown that some of their projections also run in parallel. The cholinergic (from PPN and LDT) and catecholaminergic (from LC) innervations are in balance in the regulation of certain areas (DeFeudis, 1974), such as the striatum (Barbeau, 1962), the mesopontine region (Hobson et al., 1986) and the spinal cord (Jones et al., 1986). In these areas the innervation is reciprocal between cholinergic and cholinoceptive structures. Similar reciprocal communication is known even in serotonergic raphe nucleus (Jackson and Grossman, 1983; Moon-Edley and Graybiel, 1983; Sugimoto and Hattori, 1984; Jones and Yang, 1985; Nauta, 1958; Sakai et al., 1977; Leonard and Llinas, 1994; Reiner and Vincent, 1987).

The descending connections of the PPN include the reticulospinal tract. Its activation through repeated activation of PPN is able to affect motor activity. Descending cholinergic (and presumably glutamatergic) fibers innervate the nucleus pontis oralis and nucleus pontis caudalis, the gigantocellular nucleus and the spinal cord (Mena-Segovia et al., 2008, Martinez-Gonzalez et al., 2013, Spann and Grofova, 1989). PPN is also involved in startle reflex and it has a role in prepulse inhibition as well (Mori et al. 1989). The locomotor activity can be initiated in many neural pathways and cannot be completely eliminated by PPN lesions (Swerdlow and Koob, 1987). An interesting observation is that injecting a cholinergic agonist into the PPN also decreases the locomotor activity. This presupposes the existence of an inhibitory, possibly muscarinic cholinergic receptor in PPN (Brudzynski et al., 1988) and the presence of a cholinergic feedback inhibition system makes it likely.

3.2.3. Cell types and markers of PPN

3.2.3.1. Morphological markers

The PPN consists of three neuronal populations such as cholinergic, GABAergic, and glutamatergic neurons (Clements and Grant, 1990, Ford et al., 1995) and several further neuronal markers, e.g. neuropeptides and calcium binding proteins (Fortin and Parent, 1999;

Vincent, 2000; Martinez-Gonzalez et al, 2012). It is known that the the PPN glutamatergic neurons (identified with in situ hybridization for VGluT2) overwhelms the cholinergic ones with a very low level of overlap (Wang and Morales, 2009; Baksa et al, 2019).

According to their location, GABAergic and glutamatergic neurons show a strong rostrocaudal gradient (Mena-Segovia et al. 2009; Wang and Morales, 2009). In the rostral part of the PPN, GABAergic neurons are more abundant than cholinergic and glutamatergic neurons, and the proportion of GABAergic ones decreases towards the caudal part of the PPN (Mena-Segovia et al. 2009). In contrast, glutamatergic population is more numerous in the caudal part of the PPN (Wang and Morales, 2009). Out of these three main cell types, other neurochemical markers and different subpopulations can also be defined within these neuronal groups.

Large numbers of cells containing different calcium binding proteins have been reported in the PPN (Dun et al., 1995; Fortin and Parent, 1999). In the rat, the calcium binding proteins calbindin and calretinin were mostly detected in GABAergic and glutamatergic cells, whereas calretinin is rare and calbindin never occurs in cholinergic cells. In GABAergic cells, calcium binding proteins were found in greater numbers in the rostral part of the PPN. Glutamatergic cells also expressing calbindin and calretinin were predominantly in the caudal PPN (Martinez-Gonzalez et al., 2012).
The PPN neurons vary in shape (spindle-shaped, polygonal, triangular, rarely oval or round) with a soma size between 15 and 80 μm. The neurons have 2-5 dendrites which often leave the boundaries of the nucleus and enter adjacent structures (Kamondi et al., 1995). In the same study, significant difference was not found between cholinergic and non-cholinergic neurons in soma diameter and the size of dendrites (Kamondi et al., 1995).

A cholinergic subpopulation possesses dendritic spines, whereas all of the glutamatergic neurons possess morphologically diverse dendritic spines (Muller et al., 2011). There is also a difference in the morphology of their axons. Axons of cholinergic neurons have 5 collaterals in average, which are dorsally and ventrally give rise to projections with ascending trajectory to several nuclei of the thalamus as well as to the hypothalamus and basal forebrain. In addition, the cholinergic neurons have one or more descending axon collaterals. In contrast, the axons of non-cholinergic neurons are less complex and shorter than cholinergic and mainly innervate the substantia nigra, ventral tegmental area and

hypothalamus. Within the PPN, the axons of cholinergic neurons have a several varicosities on local collaterals (Mena-Segovia et al., 2008; Mena-Segovia and Bolam, 2017).

3.2.3.2. Membrane properties and firing pattern

Based on the electrophysiological properties of membrane, the PPN neurons are grouped into three types (type I, II and III). The three neuronal types above can be distinguished on the basis of the following membrane properties: type I has low-threshold calcium spikes, type II with A-current (transient outward current, which delays depolarization from the initial membrane potential after a hyperpolarizing pulse), and type III, whose membranes do not possess these features, and do not fit the previous two groups, or possesses both properties (Kang and Kitai, 1990; Saitoh et al., 2003; Leonard and Llinas, 1990).

The first group of neurons was characterized by slow spike potentials with a burst of fast action potentials elicited with a long lasting depolarizing current injection. These slow spike potentials were TTX resistant calcium conductances elicited by depolarization preceded by hyperpolarizing prepulse, and generated burst firing pattern. A similar neuron type with low-threshold calcium spikes has been also described in the laterodorsal tegmental nucleus (Leonard and Llinas, 1990; Kang and Kitai, 1990; Wilcox et al., 1987; Kamondi et al., 1992; Saitoh et al., 2003). The second group of neurons was characterized by the presence of A-current.

The third group of neurons has the A-current and low-threshold calcium spike (Kamondi et al., 1992, Saitoh et al., 2003) or none of them (Kang and Kitai, 1990).

The neuronal A-current is elicited by depolarization after a hyperpolarizing step. Neurons with only A-current have a tonal repetitive firing pattern, whereas ones with calcium spikes are characterized by the burst type firing pattern (Steriade and McCarley, 1990). In those cases, when both calcium spikes and A-current are present, observations also indicated that either low threshold calcium spike or A-current without rebound hump depolarization occurred depending on the intensity of hyperpolarizing current pulses.

According to Ye et al. (2010) there is one more group referred as type IV. This latter group is also marked as IIIK (Baksa et al., 2019), where ‘K’ is indicating the acronym of the authors who first described this type (Kang and Kitai, 1990).

Type II neurons are the most common type of the PPN (Takakusaki et al., 1996; Leonard and Llinás, 1994; Ye et al., 2010), as they exist in the greatest proportion (52.2 to 75%). By contrast, Kang and Kitai (1990) referred that only one-third of the neurons can be grouped to this group. The cholinergic or non-cholinergic nature of the neurons was also identified by literature data and presented that all type II neurons are cholinergic (Kang and Kitai, 1990). In one of the early studies, non-cholinergic neurons belonged to group I (41%) and group II (59%). None of the cholinergic neurons belonged to group I (Takakusaki et al., 1996). According to Leonard and Llinás, 3% of the population identified as type I, 75% was type II and 22% was type III (Leonard and Llinás, 1994).

The latest study demonstrated that only a small proportion (12%) of the cholinergic neurons was type I and most neurons grouped to the type II category (48%) on transgenic mice (Fig. 5.; Baksa et al., 2019). Additionally, type II neurons were found in greater proportion in the caudal PPN and only one-third of the neurons belonged to this group rostrally.

High threshold oscillations (HTOs) are another crucial characteristic of certain PPN neurons. The characteristics were originally demonstrated by Takakusaki et al. (1997). More recent papers confirmed the existence of HTOs on PPN cholinergic neurons (Kezunovic et al., 2011, Bordas et al., 2015). Most recently, cholinergic neurons were grouped according to the frequency and amplitude of HTOs. Namely, low amplitude–high frequency and high amplitude–low frequency activities were found on type II cholinergic neurons. Oscillatory activity correlated with action potential width and spontaneous firing rate. The HTO frequency is directly proportional to the firing rate of the neuron in question. Inhibition of HTOs significantly increased firing frequency (Baksa et al., 2019).

Furthermore, neurochemically separable populations can be found in different proportions in distinct PPN regions: the rostral pars dissipata has less cholinergic and more GABAergic neurons, whereas the caudal pars compacta consists of glutamatergic neurons with high density, with minimal overlap between glutamatergic and cholinergic neuronal groups (Mena-Segovia et al., 2009, Martinez-Gonzalez et al., 2011, Luquin et al., 2018, Wang and Morales, 2009).

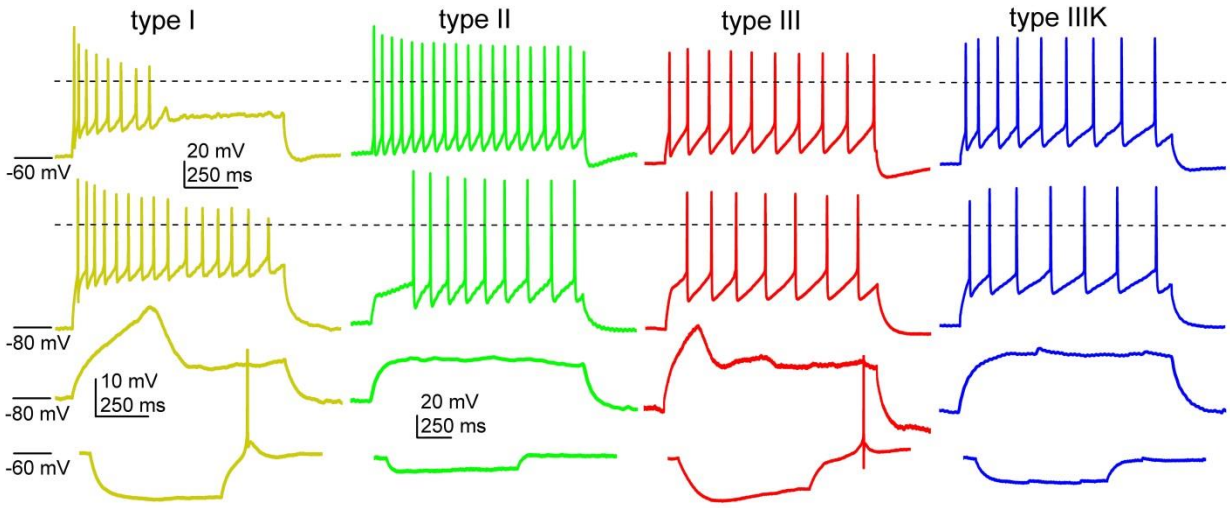

Figure 5. Functional neuronal groups in the PPN. Type I neurons (dark yellow). From top to bottom: Recordings with 100 pA depolarizing step, from -60 mV resting membrane potential in control solution; 100 pA depolarizing step, -80 mV resting membrane potential in control solution; 50 pA depolarizing step, -80 mV resting membrane potential in TTX; -30 pA hyperpolarizing step, -60 mV resting membrane potential, control solution. Note the lack of the delay in the first action potential, the calcium spike and the rebound hump. **Type II neurons (green**; with the same arrangement of panes as type I). Note the delay of the first action potential and the lack of calcium spike and rebound hump. **Type III neurons (red**; with the same arrangement of panes as type I). Note the delay in the first action potential, the calcium spike and the rebound hump. **Type IIIK neurons (blue**; with the same arrangement of panes as type I). Note the lack of the delay in the first action potantial, the calcium spike and the rebound hump. (modified from Baksa et al, 2019)

3.2.3.3. In vivo properties, relationships with cortical oscillations

Cholinergic and non-cholinergic neurons of PPN can also be sorted according to their *in vivo* firing properties. In anesthetized rats, which are in similar condition to physiological slow wave activity, synchronized cortical activity took place in parallel with two different firing patterns on PPN cholinergic cells. The larger population consisted of slow firing cholinergic neurons, which operate synchronously with the active, "up state" phase of the cortical slow oscillations. This population increased its firing rate during cortical desynchronization. There was also a smaller population with fast firing cholinergic neurons, which fired synchronously with cortical “down state". No neurochemical marker was found in the neurons to distinguish them (Fig. 6; Mena-Segovia et al., 2008).

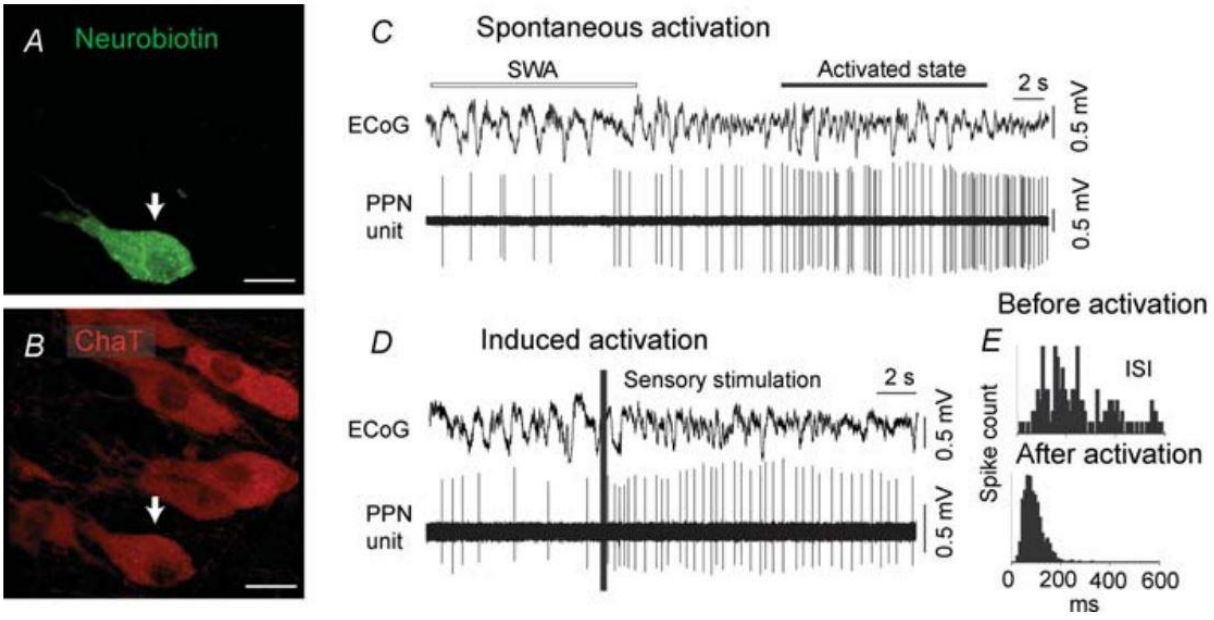

Fig.6. PPN cholinergic neurons fire with higher frequency during transitions from cortical slow wave activity to activated state. A-B. Identification of cholinergic neurons (green: neurobiotin; red: choline acetyltransferase immunoreactivity.). **C.** Spontaneous activation of a PPN cholinergic neuron during transition from cortical slow wave activity to an activated state. **D.** Induced activation of a cholinergic neuron by hindpaw pinch (vertical bar; sensory stimulation), cholinergic neurons fired more frequently and regularly. **E.** The interspike interval (ISI) before and after activation. Scale bars in A and B: 20 µm. (Mena-Segovia et al., 2008)

Non-cholinergic (glutamatergic and GABAergic) neurons in the PPN are highly heterogeneous and composed of at least three different groups: (1) "quiescent" neurons, which are much silent during slow-wave activity (SWA) but intensively respond to neocortical activation; (2) "tonic firing" neurons, with less changing firing rate that is independent of neocortical activity across different brain areas; and (3) "irregular firing" neurons, show a variable level of correlation with cortical activity (Ros et al., 2010).

The PPN does not only regulate cortical oscillation activity, but produces measurable extracellular oscillations (Brown, 2003). The optimal amplitude of alpha oscillations (7-12 Hz) has great physiological importance in PPN. The amplitude of these oscillations decreases in the development of Parkinson's disease (Thevathasan et al., 2012). Alpha oscillations were mainly present in the caudal part of the PPN. Beta oscillations (13–30 Hz) were also measured in the PPN cells, which appeared mainly in the rostral part of the PPN. The predominance of beta oscillations was observed in Parkinson's disease. This activity contributes to akinesia (Thevathasan et al., 2012; Li and Zhang, 2015).

Based on neuronal activity during REM sleep, two groups of PPN neurons were traditionally distinguished. The neurons increase firing frequency in parallel with the onset of REM are called "REM-on neurons." Conversely, another group of neurons termed "REM-off' totally decrease and stop firing with the approach and beginning of REM (Steriade et al., 1990a, b; see Garcia-Rill, 1991).

In summary, PPN neurons are synchronized during SWS but less synchronization is observed during REM and W (Fig. 7; Petzold et al, 2015; Mena-Segovia and Bolam, 2017). This synchronization mechanism has not been presented yet in detailed, considering the local neuronal networks of the PPN are not fully revealed.

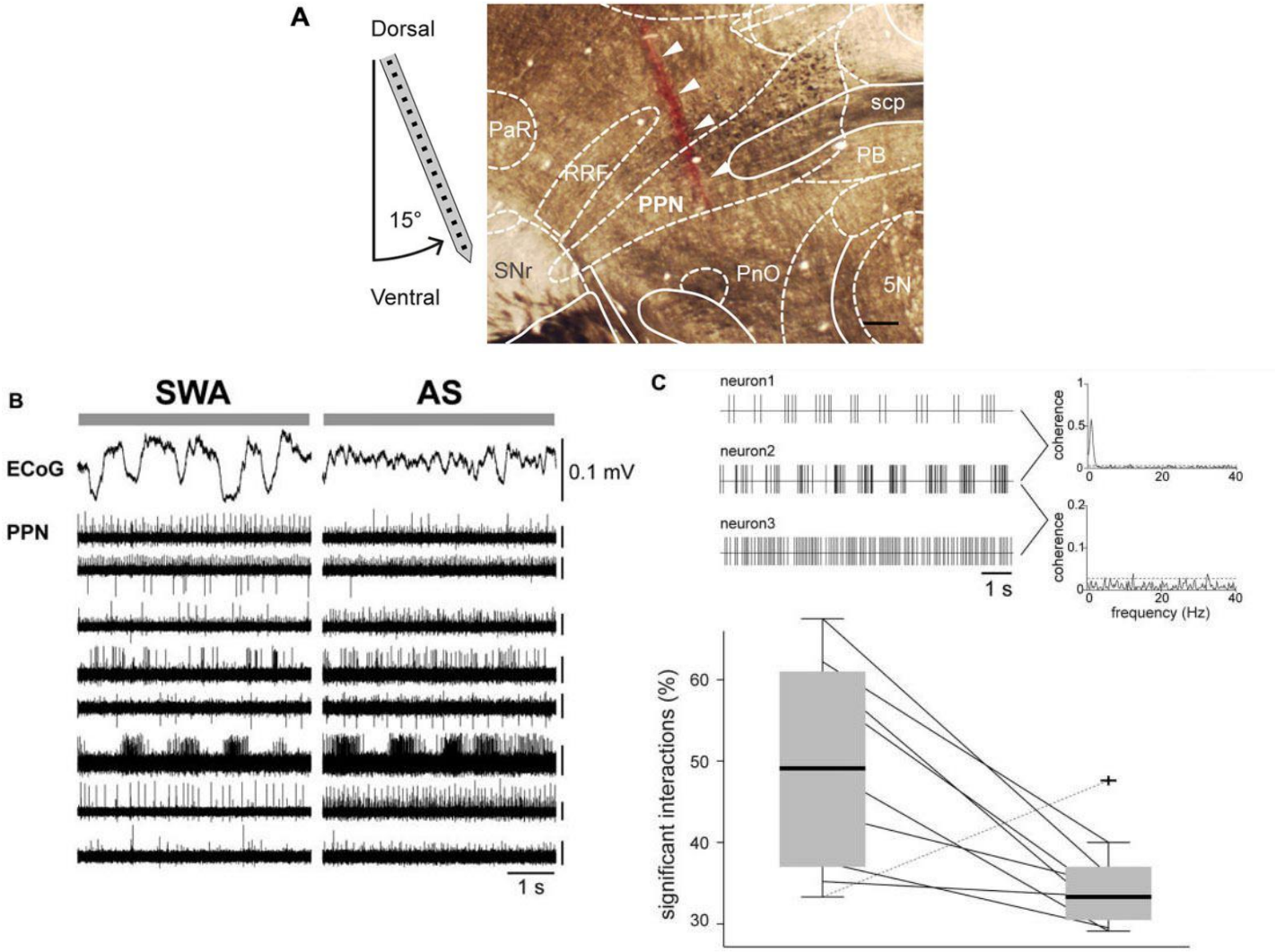

Fig. 7. PPN neuronal activity depends on global brain state. A. The recording site and the placement of a probe in the PPN (arrows indicate the probe track labeled with DiI). 5N, motor trigeminal nucleus; PaR, pararubral nucleus; PB, parabrachial nucleus; PnO, pontine reticular nucleus, oral part; RRF, retrorubral field; SNr, substantia nigra pars reticulata. Scale bar: 300 µm. **B.** Synchronized ECoG activity indicating SWA, and its replacement by desynchronized activity during "activated state" (AS). **C.** When SWA is detected, PPN neurons have synchronized activity (illustrated in the representative traces as examples of coherent [top] and non-coherent [bottom] neuronal activity; dotted lines represent significance levels), which significantly decreases during the AS (Petzold et al, 2015).

3.2.3.4. The role of PPN in the regulation of sleep-wakefulness cycle

The PPN, one of the cholinergic nuclei of RAS is involved in the regulation of sleep-wakefulness cycles (Moruzzi and Magoun, 1949, Steriade et al., 1991). According to the classical description, PPN neurons increase their firing frequency during REM sleep and

wakefulness, but reduce their firing frequency during slow-wave sleep (Sakai et al., 1990; Steriade et al., 1990a, b; 1991; Steriade and McCarley, 1990; Datta and Siwek, 2002).

It has been recently confirmed that PPN cholinergic neurons increase firing frequency during wakefulness and REM sleep (Boucetta et al., 2014; Cox et al., 2016). Importantly, this activation of the cholinergic neurons was proved to be temporary, as their firing frequency is increased at the beginning of cortical desynchronization, but quickly returned to original low activity level.

These results indicate that the activity of cholinergic neurons occur simultaneously with transitions of cortical activity (Boucetta et al., 2014; Petzold et al, 2015). Furthermore, optogenetic activation of PPN cholinergic neurons induced REM sleep in a sleeping animal (Van Dort et al., 2015). Similar optogenetic activation of the PPN reduced cortical slow wave activity during seizures and short-term development of cortical gamma oscillations was observed (Furman et al., 2015). Cholinergic neurons had high frequency action potential firing during REM sleep (Boucetta et al., 2014; Cox et al., 2016) and also it was revealed chemogenetic activation of glutamatergic neurons in PPN leads to prolong awake time (Kroeger et al., 2017).

3.2.3.5. The role of PPN and the cuneiform nucleus in the regulation of locomotion

The mesencephalic locomotor region (MLR) is a functionally-defined mesencephalic region consisted of the PPN and the cuneiform nucleus (CnF). These nuclei are known as output stations of forebrain systems innervating lower motor circuits (Fig. 8; Capelli et al., 2017; Kim et al., 2017; Garcia-Rill et al., 1983). The MLR was originally defined by showing that electrical stimulation of the area led to motor activation in decorticated cats (Shik et al., 1966; Garcia-Rill et al., 1987).

Optogenetic experiments also confirmed that the motor function of the MLR is related to the excitation via the glutamatergic neurons (Rosberry et al., 2015; Caggiano et al., 2018), which are the most important cell types in the MLR (Martinez et al., 2012; Wang et al., 2009). In the last two decades, the role of MLR was proposed in the functional circuits of posture (Lau et al., 2015; Josset et al., 2018; Pahapill et al., 2000). Furthermore, in Parkinson's disease, some of the motor abnormalities may be explained by degeneration of

neurons in the MLR (Hirsch et al., 1987; Zweig et al., 1987, 1989; Jellinger, 1988; Manaye et al., 1999; Hepp et al., 2013).

By deep brain stimulation into the PPN some improvements in abnormal gait has been revealed, which may have caused by the excitatory output from the MLR (Nandi, 2002; Jenkinson et al., 2004; Perera et al., 2018; Goetz et al., 2019). However, the contribution of excitatory MLR neurons to motor activity and association of motor functions to different neuronal types in the MLR has not been fully elucidated.

The PPN is a significant and heterogeneous component of the MLR. As mentioned in previous chapter, the nucleus is composed of cholinergic, GABAergic and glutamatergic neurons. PPN glutamatergic neurons are heterogenous in terms of their neurochemical properties (Martinez et al., 2012), connectivity and firing pattern (Roš et al. 2010; Petzold et al., 2015). There is less literature data about the cuneiform nucleus (CnF). Recent studies showed that activation of CnF glutamatergic neurons generated significant movements which differ from the activation of PPN neurons, suggesting that MLR neurons are functionally specialized (Fig. 8; Caggiano et al., 2018; Josset et al., 2018).

PPN and CnF are contiguous nuclei with undefined borders between them (Sherman et al., 2015), and this makes an issue for unambiguously separating these nuclei. Furthermore, these nuclei are interconnected which does not support the separation of their functions.

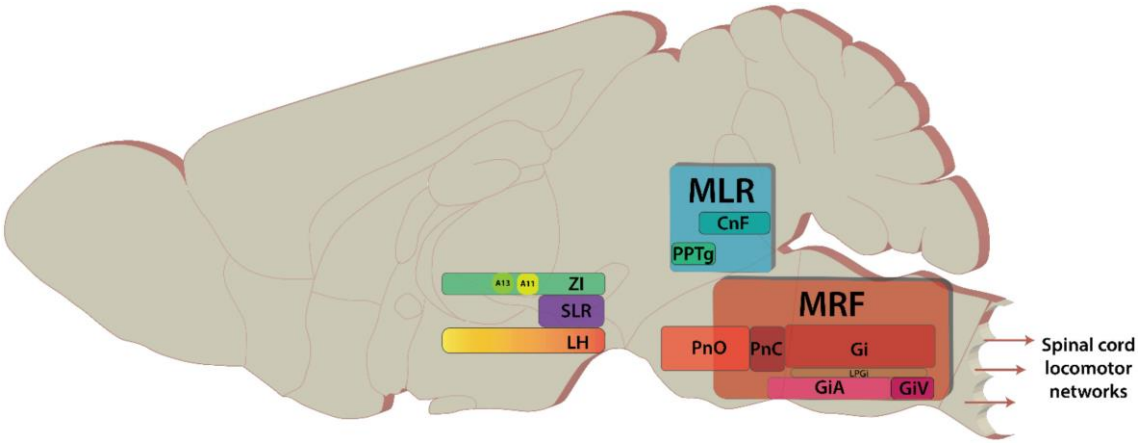

Fig. 8. Brain areas modulating motor activity. Sagittal view of the rodent brain. MLR-mesencephalic locomotor center, PPTg-pedunculopontine nucleus, CnF-cuneiform nucleus. MRF-medullary reticular formation, PnO –nucleus pontis oralis, PnC-nucleus pontis caudalis, Gi-gigantocellular area, GiA-gigantocellular reticular nucleus alpha, GiV- gigantocellular reticular nucleus ventral section. ZI-zona incerta, SLR-subthalamic locomotor region, LH-lateral hypothalamus (Kim et al, 2017).

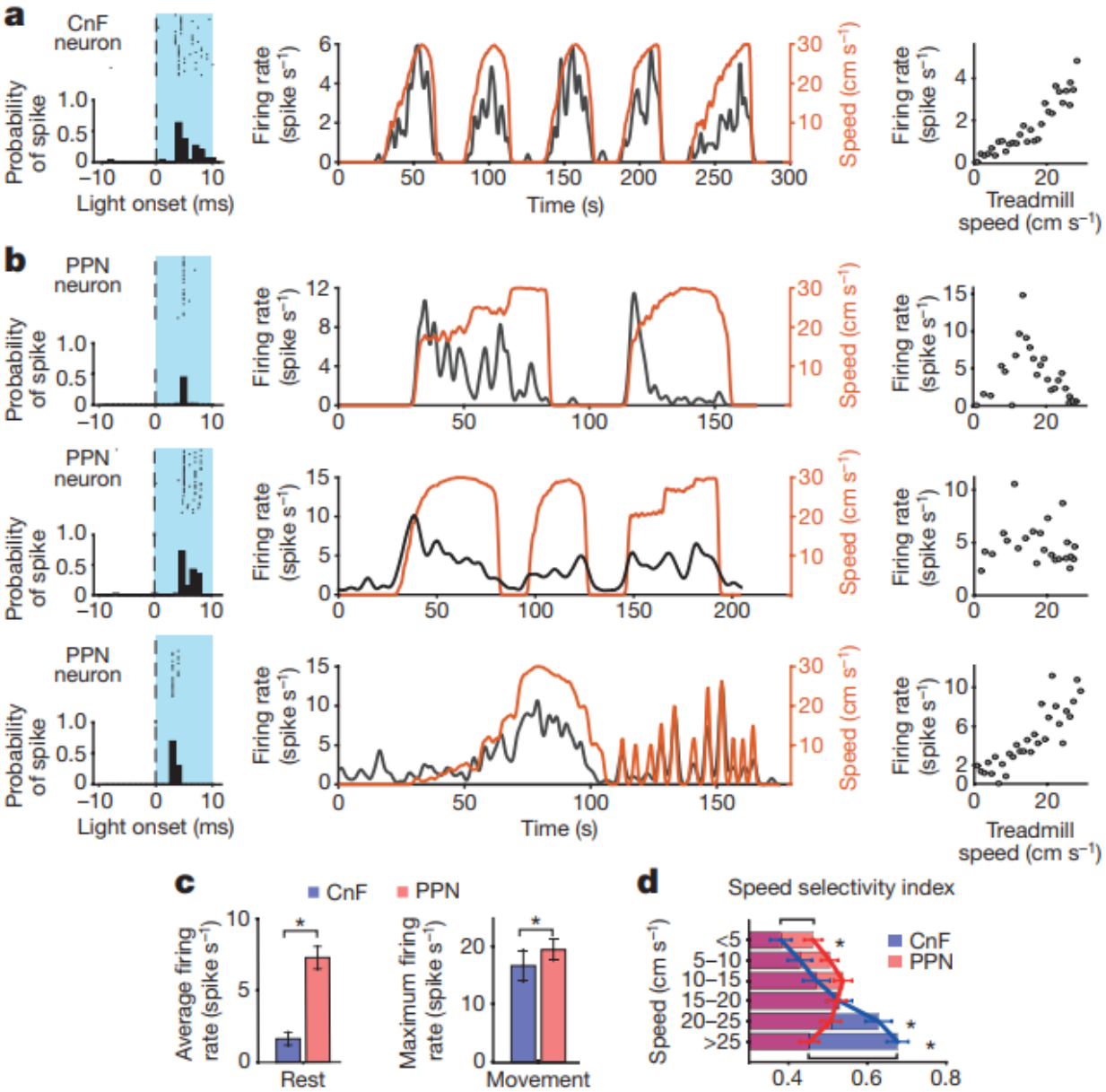

Fig.9. Determination of movement velocity in glutamatergic neurons in the CnF and the PPN. **A,B.** Discharge rate of representative neurons at different locomotion velocities, detected in the CnF (**A**) and the PPN (**B**). **C.** Average (left, at rest) and maximum (right, during movement) neuronal spiking frequencies in the CnF (n=79) and the PPN (n=105). $P < 0.001$. D. Speed selectivity index. Glutamatergic PPN neurons were involved at lower speeds, whereas glutamatergic CnF neurons were active at higher speeds. * $P < 0.05$ (Caggiano et al., 2018).

3.2.4. Raphe nuclei

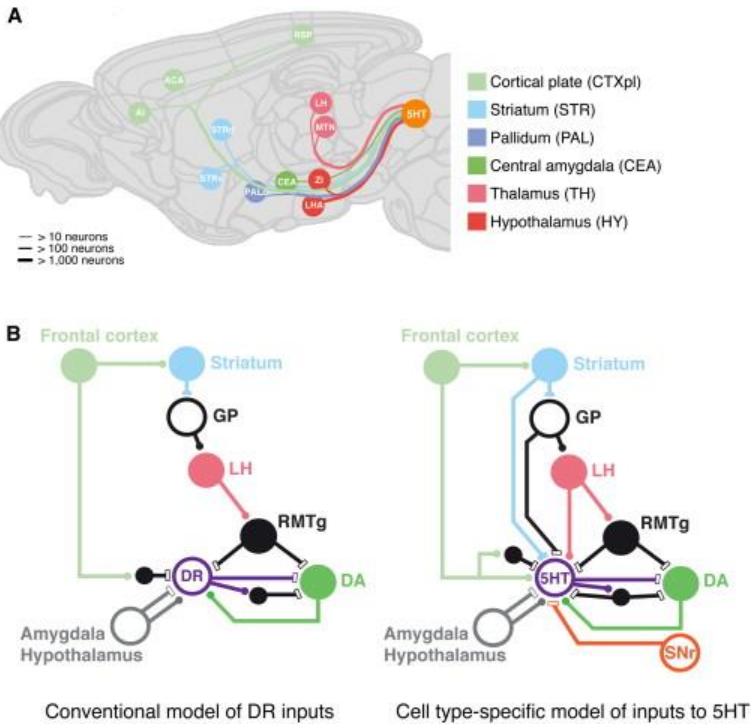

Fig.10. Direct synaptic connections of the serotonergic neurons. A. Inputs of serotonergic areas (5-HT) from isocortex (ACA, AI, RSP), striatum (STRd, STRv), caudal pallidum (PALc), thalamus (LH, MTN), central amygdala nucleus (CEA), and hypothalamus (LHA, ZI). Line thickness is proportional with input numbers. **B.** Conventional and updated models of inputs to serotonergic neurons (Dorocic et al., 2014)

Serotonin is an important modulator of neural circuits that mediate anxiety-related behavior. However, the mechanisms through these networks and the related physiological and behavioral responses are not fully clear (Iversen, 1984; Handley, 1995; Graeff et al., 1996; Maier and Watkins, 1998; Zhuang et al., 1999; Gray and McNaughton 2000; Graeff, 2002; Millan, 2003; Maier and Watkins, 2005; Ohmura et al., 2019).

Serotonergic systems are well organized within the brainstem raphe nuclei and the serotonergic neurons in topographically different regions of the brainstem raphe nuclei give rise to projection to distinct functional systems (Lowry, 2002; Hornung, 2003; Abrams et al., 2005).

Caudal serotonergic structures (as the nucleus raphe magnus, obscurus and pallidus) send projection to the spinal cord and the brainstem, whereas the rostral nuclei as median raphe (MR) and the dorsal raphe (DR) nuclei project to forebrain targets (Fig.10; Hornung, 2003; Dorocic et al., 2014). The MR innervates the hippocampus, nucleus accumbens, medial septum and hypothalamic nuclei. The DR sends projections to the frontoparietal cortex, amygdala, lateral septum, nucleus accumbens shell, ventral hippocampus and several

hypothalamic nuclei (Fig. 11; Lechin et al., 1979a, 1989, 2002b, 2006; Dorocic et al., 2014, Soiza-Reilly and Kathryn, 2014).

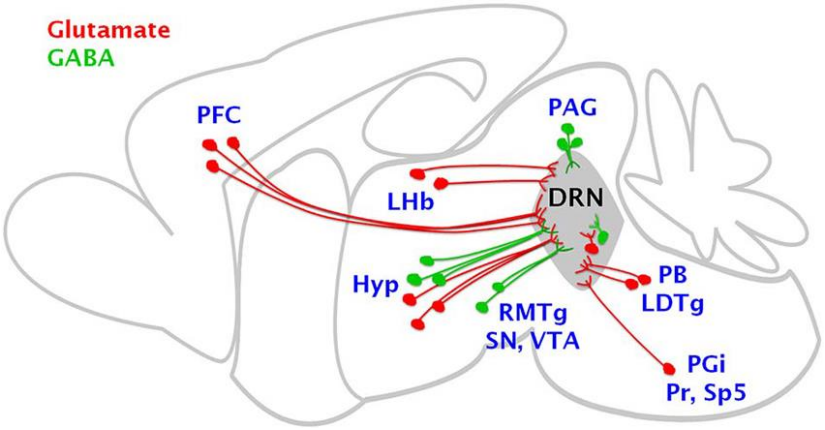

Fig.11. Brain regions sending glutamatergic and GABAergic axon projections to the DRN. Glutamatergic cells (in red) are located in the prefrontal cortex (PFC), lateral habenula (LHb), hypothalamus (Hyp), parabrachial nucleus (PB), laterodorsal tegmental nucleus (LDTg), paragigantocellular nucleus (PGi), prepositus hypoglossal nucleus (Pr) as well as the spinal trigeminal nucleus (Sp5), and in local sources including the DRN. GABAergic cells (in green) sending projections to the DRN are found in the hypothalamus, substantia nigra (SN), ventral tegmental area (VTA), rostromedial tegmental nucleus (RMTg) and locally within the periaqueductal gray (PAG) and DRN (Soiza-Reilly and Kathryn, 2014).

Moreover, DR and MR are parts of the RAS and involved in the regulation of sleep-wakefulness cycles, movement, and affective states. During wakefulness, the activity of DR is increased and it is more silent in REM sleep (Monti, 2011). Numerous subpopulations of DR and MR serotonergic neurons are determined by expressed markers, morphological characteristics, and in vitro and in vivo electrophysiological properties (Fig. 12; Hornung, 2003; Andrade and Haj-Dahmane, 2013).

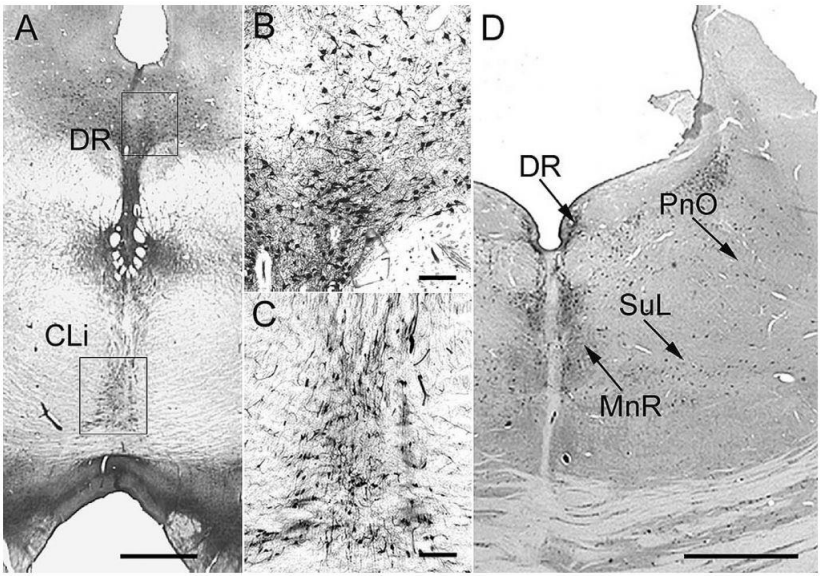

Fig.12. Location of serotonergic neurons on parasagittal brainstem slices. A. Overview of the mesencephalic raphe at the level of the trochlear nucleus (4) of a section immunoreacted for tryptophan hydroxylase. Serotonergic neurons of DR are found in the ventral periaqueductal gray and surrounding the medial longitudinal fasciculus (mlf). Ventrally, serotonergic cells in CLi are restricted to the midline. **B.** Higher magnification of the part of DR in box in (A). **C.** Higher magnification of the part of CLi in box in (A) illustrating the vertical orientation of the dendrite typical of this nucleus. **D.** Overview of the rostral pons of a section with tryptophan hydroxylase labelling (caudal division of the rostral group). DR is present as a thin stripe of neurons, while MnR has a well-developed median division and two lateral cell groups: SuL ventrally and PnO dorsally. Scale bars (A and D): 2 mm, band (C): 100 μm (Hornung, 2003)

3.3. The M-current

The M-current is a non-inactivating, voltage-gated potassium current, which is regulated by several receptors and neuromodulatory actions. Presumably the most characteristic neuromodulatory action on these channels is the inhibition by muscarinic acetylcholine receptors (Brown and Adams, 1980; Hernandez et al, 2008; Marrion, 1997). The neuronal M-current contributes to setting of resting membrane potential and regulates action potential firing by acting on the afterhyperpolarization and spike frequency adaptation (Brown and Passmore, 2009; Delmas and Brown, 2005). The M-current controls synaptic vesicle release in presynaptic locations (Huang and Trussell, 2011).

We previously reported that roughly all PPN cholinergic neurons have M-current, whereas GABAergic neurons lack it. The M-current of the cholinergic neurons contributes to

the afterhyperpolarization and spike frequency adaptation (SFA), and is responsible for modulating high threshold membrane potential oscillations (Bordás et al, 2015).

3.3.1. Ion channels responsible M-current and channelopathies related to them

Homo- or heterotetrameric ion channels formed by KCNQ (Kv7) subunits are responsible for M-current. KCNQ2-5 (Kv7.2-5) subunits are present in the central nervous system (CNS), from which KCNQ2, 3 and 5 are located more abundantly in various brain areas, but KCNQ4 is only found in the brainstem (Brown and Passmore, 2009; Delmas and Brown, 2005; Kharkovets 2000). These nuclei are the auditory brainstem nuclei as the cochlear nuclei, nuclei of the lateral lemniscus and the inferior colliculus; the principal and spinal trigeminal nuclei; and the reticular activating system (RAS) nuclei as raphe nuclei and the ventral tegmental area (Kharkovets et al, 2000; Hansen et al 2008; Koyama and Appel, 2006).

Mutations in the *KCNQ2* and *KCNQ3* genes encoding for Kv7.2 and Kv7.3 voltage-dependent K+ channel subunits, are cause of neonatal epilepsies known as benign familial neonatal epilepsy (BFNE) with broad phenotypic heterogeneity. Furthermore, KCNQ2 mutations are responsible for severe outcome, with drug-resistant seizures and psychomotor retardation, electroencephalogram (EEG) suppression-burst pattern (Ohtahara syndrome, Saitsu et al., 2012), and different neuroradiological characteristics, a condition that was named “KCNQ2 encephalopathy” (Weckhuysen et al., 2012, Soldovieri et al., 2014)

KCNQ4 gene mutations cause an autosomal progressive nonsyndromic hearing loss (DFNA2) caused by the degeneration of outer, and partially the inner hair cells of the cochlea (De Leenheer et al, 2002; Nie et al, 2008). This disease was reproduced in mouse models that also expressed a human KCNQ4-mutation or lacked KCNQ4 channel expression (Kharkovets et al., 2006; Carignano et al 2019). The mutation changes somatosensory functions as well because of the lack of expression on skin somatosensory receptors and dorsal root ganglia also in human and mouse (DRG, Heidenreich et al, 2011).

KCNQ4-positive brainstem areas overlap with cholinoceptive areas (Woolf and Butcher, 2011; Kharkovets, 2000).

The brainstem structures expressing KCNQ4 are involved in auditory startle reflex (ASR). The neural circuitry of ASR is under the neural control from the basal ganglia through

the pedunculopontine nucleus and superior colliculus, cerebellum and cerebral cortex (Koch et al., 1993; Yasin et al., 2018).

It has been revealed that the M-current formed by KCNQ4 subunits participate in neuromodulatory autoregulation (Su et al, 2019). Therefore, we sought evidence based on the hypothesis that M-current formed by KCNQ4 subunits presents on PPN cholinergic neurons.

3.3.2. Selective KCNQ channel openers and blockers and neurological diseases

3.3.2.1. XE991

Together with linopirdine, XE991 is a potent inhibitor of the native M-current. XE991 has both high affinity and selectivity for the native M-channel and KCNQ channels (Wang et al., 1998). Interestingly, XE991 was 5 to 10 times more effective than linopirdine (Zaczek et al., 1998).

3.3.2.2. Linopirdine

A selective M-current inhibitor linopirdine has been revealed to facilitate acetylcholine release and improved learning abilities in animal models of cognitive dysfunction. However, in Alzheimer's disease, phase 3 clinical trials of linopirdine did not reveal significant benefits, more effective derivatives of the drug might be potential candidates (Zaczek et al., 1998).

3.3.2.3. Retigabine

In the 1980's, retigabine, an M-current opener was discovered as part of the National Institute of Neurological Disorders and Stroke Anticonvulsant Screening Project. Retigabine was potent in preventing seizures induced by electrical shock or by chemical convulsants (e.g. pentylenetetrazol, N-methyl-D-aspartate, 4-aminopyridine, and picrotoxin). Retigabine prevented spontaneous and induced seizures in rodent models of epilepsy (Dailey et al., 1995). Numerous studies demonstrated that retigabine is an effective opener of channels composed of KCNQ2 and KCNQ3 subunits (Rundfeldt and Netzer, 2000). Retigabine opens the channels at more hyperpolarized membrane potentials, increases the rate of channel opening, and slows the rate of channel closing (Rundfeldt and Netzer, 2000; Cooper and Jan, 2003).

The indication was restricted in 2013, following reports of discoloration of the nails, lips, skin, and/or mucosa and pigmentation of ocular tissues, including the retina, in some

patients receiving retigabine and in 2017, retigabine was voluntarily withdrawn from the market (Shkolnik et al., 2014; Brickel et al., 2020).

3.3.2.4. ML213

The ML213 is a new Kv7 channel activator initially indicated as being selective for Kv7.2 and Kv7.4 channel subtypes displaying ~80-fold selectivity over other Kv7 channels (Yu et al., 2011), as well as greater potency than other Kv7 activators such as retigabine and BMS204352 (fluoro-oxindole potassium channel opener, Jepps et al., 2014). Subsequent in vitro electrophysiological and pharmacological studies in vascular smooth muscle cells have revealed ML213 as an effective activator of homomeric Kv7.4 and Kv7.5 channels and heteromeric Kv7.4/Kv7.5 channels (Brueggemann et al., 2014a). Currently the only known Kv7 channel activator with the unique pharmacological selectivity profile is ML213 (Provence et al., 2018).

3.3.2.5. ICA27243

ICA27243 is considered as a selective opener of Kv7.2 and 7.3 subunits and showed to be more selective than other Kv7 channel openers. The compound is much more effective at heteromeric Kv7.2/3 channels than at homomeric Kv7.4 channels and heteromeric Kv7.3/5 channels (Wickenden et al., 2008). The action of this drug on Kv7.2/3 is based to mechanism for producing a hyperpolarizing shift of the voltage dependence of activation and to increase the current amplitude at all activating potentials (Blom et al., 2010).

3.3.3. Electrophysiological properties and regulation

Neuronal functions and firing properties are significantly affected by ion channels. Certain ion channels setting firing rate and pattern are regulated by neuromodulatory actions, consequently providing an important way of action by neuromodulatory agents. One important participant of this regulation is the M-current. The M-current presents in wide range of areas of the brain including brainstem (Kharkovets et al., 2000; Koyama and Appel, 2006; Hansen et al., 2008). Previously, it was showed that the non-inactivating voltage-gated potassium channel is affected by various metabotropic receptors. M-current is blocked or inhibited by the activation of muscarinic acetylcholine receptor and other G-protein coupled

receptors as $5HT_{2C}$ receptor (Brown and Adams, 1980; Marrion, 1997; Hernandez et al., 2008; Linley et al., 2012).

Channels responsible for M-current are inhibited by several ligands acting on G protein-coupled receptors, mostly those coupled to Gq and/or G11. The first observation was done with muscarinic acetylcholine receptor (mAChR; M1, M3 or possibly M5) agonists (Brown and Adams, 1980). In addition, M-current can also be inhibited by several other receptors with similar signaling pathways, including mGluR1 and mGluR5 metabotropic glutamate receptors, histamine H1, 5-hydroxytryptamine 5HT2C and P2Y1, 2, 4 and 6 nucleotide receptors, and by numerous peptide receptors as well (e.g. GnRH, substance P, bradykinin, angiotensin; Marrion, 1997).

KCNQ channels require membrane PIP_2 to open and any receptor whose activation leads to the hydrolysis of PIP_2 and the generation of the messengers $(1,4,5)IP_3$ and diacylglycerol (DAG) blocks the M-current. On the respective subsequent events, Ca^{2+} release and protein kinase C (PKC) activation was suggested for inhibition (Brown and Higashida, 1988; Marrion, 1997). Another possible second messenger is arachidonic acid (AA). It can be generated by the metabolism of DAG by diglyceride lipase or can be produced by the action of phospholipase A2, which is activated by an increase in intracellular calcium that occurs upon production of (1,4,5)IP3 (Moore et al., 1988; Marrion, 1997).

Latest studies have been suggested that activation of phospholipase C (PLC) through G-protein-coupled receptors generates a large number of second messengers and involved in many regulations and processes. As above mentioned, M-channels require the PIP_2 for functioning. Activation of PLC can shut down their activity if it depletes the PIP_2. This mechanism leads to the muscarinic suppression of current in KCNQ channels (Hilgemann et al. 2001 Horowitz et al. 2005, Suh and Hille, 2006)

It is known that M-current plays important role in the medium, slow afterhyperpolarizations (AHPs) of the action potentials (mAHP, sAHP; e.g., Madison and Nicoll, 1984; Storm, 1989; Koyama and Appel, 2006; Tzingounis and Nicoll, 2008; Tzingounis et al., 2010; Mateos-Aparicio et al., 2014), spike frequency adaptation (e.g., Madison and Nicoll, 1984; Nigro et al., 2014) and sets spiking frequency. It is a potent regulator for setting the resting membrane potential (e.g., Madison and Nicoll, 1984; Koyama and Appel, 2006; Navarro-López et al., 2009; Guan et al., 2011; Nigro et al., 2014) and

controls presynaptic functions as releasing of neurotransmitters (e.g. Huang and Trussell, 2011). In addition, M-current is important to neuronal high threshold membrane potential oscillations at a characteristic frequency approximately 20 Hz (Bordas et al, 2015).

3.3.4. M-current of different brainstem structures

3.3.4.1. M-current on the PPN

In a study from our laboratory, it was revealed that almost all PPN cholinergic neurons have M-current, whereas GABAergic neurons completely lack it. There are characteristic functional differences between cholinergic and GABAergic neurons, as amplitude of medium afterhyperpolarization, spike frequency adaptation and firing frequency caused by presence or absence of M-current. Furthermore, the inhibition of the M-current fully terminated the oscillations of cholinergic neurons at 20 Hz and reduced it at other frequencies (Bordas et al., 2015; Bordas, 2017).

3.3.4.2. M-current on dorsal and median raphe nuclei

Previous electrophysiological studies showed that there are differences in membrane properties of DR and MR serotonergic neurons. It is known that the M-current is present in the DR but less is known about its functional significance and distribution in this nucleus and the neighboring MR. The MR serotonergic neurons had a shorter time constant and larger afterhyperpolarization (AHP) amplitude than DR serotonergic neurons. Interestingly, the main differences between the serotonergic and non–serotonergic neurons in the DR were the membrane time constant and the action potential width. The distinct time constant of the MR and DR neurons is likely because of the morphological differences of these neuronal populations. On the other hand, the rise time and amplitude of synaptic currents are reasonably greater in the MR, and the possibility that the synaptic inputs are temporally summating is less in MR than in the DR neurons. The MR neurons have crucially lower firing rate than the DR neurons (Hajos et al. 1995a; Beck et al. 2004; Marinelli et al. 2004). The lower firing frequency and the longer interspike interval are caused by greater AHP amplitude in median raphe. The greater AHP magnitude in the MR than the DR could be cause of the difference in firing frequency (Beck et al. 2004).

DR and MR serotonergic neurons are hypothesized to have several subgroups according to expression of markers, morphological characteristics, also in vitro and in vivo electrophysiological properties (Hornung, 2003; Andrade and Haj-Dahmane, 2013). It was recently shown that approximately 60% of DR serotonergic neurons express KCNQ4, the main ion channel subunit for M-current in this nucleus (Zhao et al., 2017; Hansen et al., 2008). The proportion of the neurons possessing M-current in the MR, the topographical distribution of the M-current possessing neurons in both DR and MR, as well as their significance in distinct electrophysiological parameters of the serotonergic neurons have not been reported yet.

Our research question was to differentiate the ratios of DR and MR serotonergic neurons possessing M-current and to identify the topographical organization of neurons possessing M-current. We also aimed to determine electrophysiological parameters of raphe serotonergic neurons influenced by the M-current.

3.3.4.3. M-current on VTA and other members of the RAS

The neurons in the VTA are grouped into two main subgroups in terms of their neurotransmitters: dopaminergic (DA) and GABAergic neurons (Grace and Onn 1989; Johnson and North 1992). It was reported that the KCNQ2 and KCNQ4 subunits are present on VTA neurons (Cooper et al. 2001; Kharkovets et al. 2000). Supporting findings with the presence of KCNQ subunits found with morphological methods, M-current was recorded from midbrain DA neurons electrophysiological recording in brain slices (Lacey et al. 1990). Considering these data, it raised the possibility that both homomeric KCNQ2 and homomeric KCNQ4 channels contribute to M-current in DA VTA (Koyama and Appel, 2006). Moreover, the maximal M-current amplitude in the DA VTA neurons was recorded at -45 mV with the deactivation protocol (Brown and Adams 1980; Passmore et al. 2003; Wang et al. 1998). Also the result indicates that M-current is active near the resting membrane potential to decrease excitability and during the slow AHP to decrease the interspike interval in DA VTA neurons. DA-induced inhibition of spontaneous firing of VTA DA neurons was also mediated by Kv7.4 (Su et al., 2019).

Furthermore, the M-current, which is present in dopaminergic cells in the substantia nigra pars compacta and ventral tegmental area, modulates the firing during bursting without affecting the background low-frequency pacemaker firing (Drion et al., 2010). It has not been

well-studied or there isn't enough evidence for presence of M-current in other members of RAS such as LDT and LC.

3.3.4.4. M-current on the auditory pathway

Cholinergic connections exist at all levels of the auditory pathway and participate in modulation of sound information processing (Schofield et al., 2010). A well-studied descending system is the olivocochlear innervation to the inner ear. The olivocochlear bundle sends projections into the cochlear nucleus (Guinan 2006; Baashar et al., 2015, 2019; Gillet et al., 2018; Horvath et al., 2000; Kishan et al., 2011). In addition, ventral cochlear nucleus (VCN) receives about one quarter of cholinergic connections from the pontomesencephalic tegmentum (Mellott et al., 2011). Immunohistochemical and in situ hybridization studies in mice revealed that KCNQ4 subunits are present in the central auditory pathways (Kharkovets et al. 2000), including the cochlear nuclei, superior olivary complex, lateral lemniscus, central nucleus of IC (ICc), and dorsal raphe (Liang et al. 2006; Caminos et al. 2007).

Immunohistochemical data also confirmed the presence of Gq/11 protein-coupled metabotropic receptors M1 and M3 expression in the VCN. According to an electrophysiological study it has been confirmed that the M-current was present in VCN neurons and it was inhibited by the perfusion of a muscarinic agonist. The activation of all muscarinic receptors by Oxotremorine-M as a muscarinic agonist on average hyperpolarized the resting membrane potential. The inhibition of M3 shifted the resting membrane potential to even more negative values (Gillet et al., 2020).

Our laboratory showed that the dorsal cochlear nucleus (DCN) is also a target of muscarinic neuromodulatory regulation with both presynaptic and somatic targets. For the latter one, M-current likely regulates excitability of DCN giant (and possibly fusiform) neurons (Pál et al, 2009).

KCNQ5 channels have been found in cochlear nucleus and inferior colliculus (IC) of rats with immunohistochemistry (Caminos et al. 2007), and KCNQ2–5 mRNA transcripts have also been reported in the cochlear nucleus of guinea pig and rat by RT-PCR (Liang et al. 2006; Caminos et al. 2007). Electrophysiological data showed that KCNQ channels are functionally involved in the regulation of IC neuron excitability and the specific Kv7 drugs modulate both membrane potential and excitability of IC neurons (Navarro-Lopez et al., 2009)

3.4. Optogenetics

Optogenetics can be explained as a combination of optics and genetics to activate or inhibit functions or well-defined events within specific cellular groups (Deisseroth et al., 2006; Scanziani and Häusser, 2009; Deisseroth, 2010, 2011). The microbial opsin genes are used for optical control of firing in specific targeted neurons. General process of the optogenetics requires (1) engineered control tools to target specific cells, (2) light stimulation of the given structures, and (3) appropriate system for the integration of optical control with compatible detection tools (fluorescent organic or genetically encoded activity indicators, electrical recording, fMRI signals, or quantitative behavioral analysis, Yizhar et al., 2011)

Optogenetics is not simply using photon absorption for excitation and inhibition of targeted cells; rather, optogenetics must be able to obtain gain or loss of function of precise events. In neuroscience, millisecond-scale regulation is needed for optogenetics, to keep rate and speed with the known functional membrane properties of the targeted cell events such as action potential firing properties (Zemelman et al., 2002; Banghart et al., 2004; Kramer et al., 2005; Lima and Miesenböck, 2005; Yizhar et al., 2011)

The temporally precise optical control of genetically distinct neuronal populations in intact circuits has been enabled by using the algal light-sensitive cation channels, the channelrhodopsins into neurons (Zhang et al., 2011). The channelrhodopsin genes derived from two algal species (Chlamydmonas reinhardtii and Volvox carteri) are widely used in both *in vivo* and *in vitro* studies. Most importantly, channelrhodopsin-2 from Chlamydmonas reinhardtii (ChR2) (Nagel et al., 2003; Boyden et al., 2005) and channelrhodopsin-1 from Volvox carteri (VChR1) (Zhang et al., 2008) are a powerful pair of ChRs for controlling entire neural networks by illumination. ChR2 is activated by blue light around 480 nm of wavelength and at 589 nm of wavelength ChR2 is no longer responsive, whereas VChR1 remains significantly light sensitive even at the wavelength. Both channels can be opened by light with time constants on the order of milliseconds. Therefore, they are able for deliver high frequencies of light flashes of millisecond scale duration with high frequencies into stably elicited action potentials (Mei and Zhang, 2012).

Light-activated anion pumps have been introduced for inhibition of neuronal activation. For instance, the chloride pump halorhodopsin of Natronomonas pharaonis (NpHR; Zhang et al.,

2007) has been revealed to hyperpolarize neurons through illumination with green or yellow light. Moreover, additional neural inhibitors to eNpHR3.0, such as archaerhodopsin-3 (Arch), a green light (~550 nm)–activated proton pump derived from the archaebacteria Halorubrum sodomense are discovered through ecological prospecting (Idnurm and Howlett, 2001, Chow et al., 2010). Arch is also effectively used in neurons in neurons and activation leads to robust outward currents. Further important inhibitory optogenetic actuators are bacteriorhopsin (BR) and Guillardia theta rhodopsin-3 (GtR3). BR is maximally activated at 560 nm (Park et al., 1989), GtR3 has a peak excitation at around 470 nm light (Gradinaru et al., 2010). The difference in their excitation wavelengths helps researchers to design experiments where different neuronal populations are selectively inhibited. The term 'OptoXR' covers engineered rhodopsin-G protein-coupled receptor (GPCR) chimeras which exert their actions on G-protein coupled signaling pathways. OptoXR is subsequent to engineering for replacing the intracellular domain of vertebrate rhodopsin with the intracellular loops from GPCRs (Fig. 13; Mei and Zhang, 2012; Zhang et al., 2008).

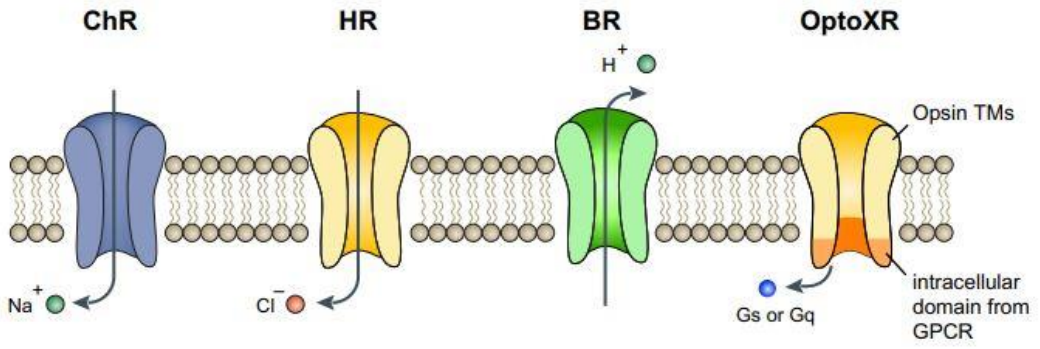

Fig.13. Microbial opsins as optogenetic tools. Channelrhodopsins (ChR) are light-activated non-selective cation channels capable to conduct Na+, K+, Ca+ ions and activate neurons by depolarizing the membrane potential. Halorhodopsins (HR) and bacteriorhodopsins (BR) are light-sensitive chloride and proton pumps are for inhibiting neurons by causing hyperpolarization. OptoXRs are used for controlling intracellular G-protein-coupled signaling pathways (Mei and Zhang, 2012)

In some cases, microbial opsin genes lead to appearance of light-induced photocurrents on the target cells, but further molecular modifications improved certain functions of the wild type actuators. After the first publications (Boyden et al., 2005; Li et al., 2005; Nagel et al., 2005; Bi et al., 2006; Ishizuka et al., 2006), a commonly used form of channelrhodopsin was generated in which algal codons were replaced by mammalian codons for a better expression level (humanized ChR2 or hChR2, Zhang et al., 2006; Adamantidis et

al., 2007; Aravanis et al., 2007; Zhang et al., 2007), and this procedure is typically used in case of several opsin genes.

The viral expression systems have various advantages for optogenetics, including flexibility and rapidity of experimental procedures, as well as specificity. Because of the obvious advantages, this is currently the most frequently used tool for delivering optogenetic actuators. Lentiviral vectors (LV, Dittgen et al., 2004) and adeno-associated viral vectors (AAV, Monahan and Samulski, 2000) have been widely used to express opsins in neural tissues of mouse (Adamantidis et al., 2007; Petreanu et al., 2009; Haubensak et al., 2010; Ciocchi et al., 2010; Lobo et al., 2010; Kravitz et al., 2010), rat (Aravanis et al., 2007; Gradinaru et al., 2009; Lee et al., 2010), and primate (Han et al., 2009; Busskamp et al., 2010; Diester et al., 2011). These vectors have high expression levels for long time with almost no unwanted side effects.

Transgenic animal lines are also generated to express the optogenetic actuators in a cell-type-specific model especially for promoters that exceed the packaging limit of viral vectors. Transgenic technology can be used into transgenic mice either using bacterial artificial chromosomes or with short transgene cassettes with recombinant cell-type-specific promoters (Gong et al., 2007). Various transgenic mouse lines expressing channelrhodopsin and halorhodopsin under the pan-neuronal Thy-1 promoter are frequently used (Arenkiel et al., 2007). Compared with viral expression system, one disadvantage is the amount of time needed to for maintenance of transgenic animal strains. Besides these, the unwanted consequences of genetic modifications should be also precisely checked and prevented.

For cell type–specific genetic manipulation, the Cre/loxP recombinase system is the most frequently used arrangement in mice (Fig.13.Gong et al., 2007; Madisen et al., 2010).

Through delivering an adeno-associated virus (AAV) that expresses an opsin in a Cre-dependent way, loxP-flanked ('floxed')-stop or floxed-inverse (FLEX) cassettes are used to deliver an opsin to a brain region with viral vectors, where only Cre-positive cells will express the actuator (Atasoy et al., 2008; Kuhlman and Huang 2008).

It has been difficult to generate transgenic mice with strong Cre-dependent expression of opsins, as indicated by recent characterization of a ChR2 Cre reporter (Katzel et al., 2011). Subsequently, efforts to overcome the limitations of early versions of inhibiting opsins, such as protein aggregation and low conductance (Zhao et al., 2008), have led to the development

of newer optical inhibiting molecules, including eNpHR (Gradinaru et al., 2008), eNpHR3.0 (Gradinaru et al., 2010) and various forms of Arch (Chow et al., 2010, Han et al., 2011), with considerable improvement in membrane expression and related increase in photoconductance, making reliable genetic inhibiting achievable now (Madisen et al., 2012).

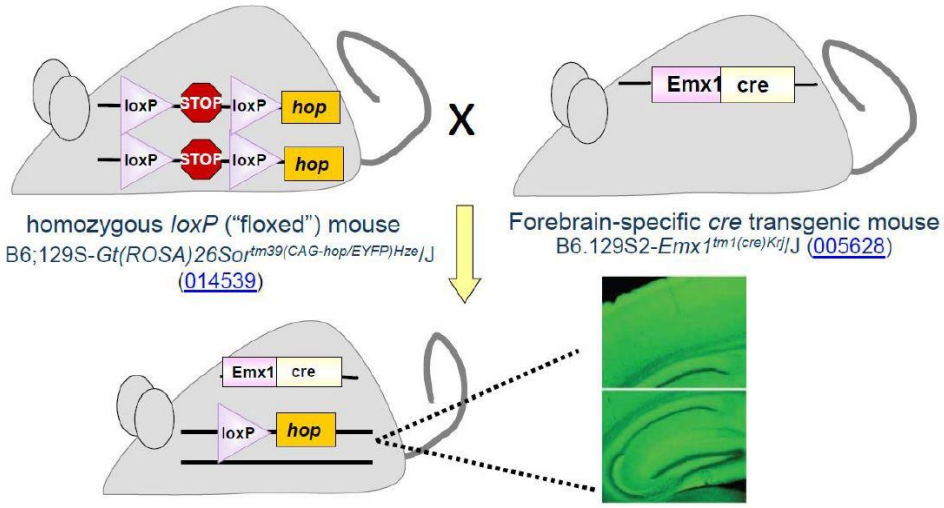

Fig.14. Breeding of transgenic mice using the cre-lox system (Madisen et al., 2012). The Cre-lox scheme is based on the Jackson Laboratory reference mouse breeding.

4. Aims of the study

In the frame of this PhD study, we were seeking to answer the following questions:

1. Is the M-current an electrophysiological hallmark of PPN cholinergic neurons?
2. How M-current contributes to synchronization of PPN cholinergic neuronal populations?
3. Do cholinergic neurons possess the KCNQ4 subunits?
4. Can M-current by channels with KCNQ4 subunit modulate circadian rhythm?
5. What proportion of serotonergic neurons in the DR and MR possess M-current and whether is there a topographical organization of neurons possessing M-current?
6. Are glutamatergic neurons in the PPN and CnF functionally distinct or do they form overlapping populations?

5. MATERIALS AND METHODS

5.1. Solutions

The composition of the artificial cerebrospinal fluid (aCSF) used in our experiments was as below (in mM): NaCl, 120; KCl, 2.5; $NaHCO_3$, 26; glucose, 10; myo-inositol, 3; NaH_2PO_4, 1.25; sodium-pyruvate, 2; CaCl2, 2; $MgCl_2$, 1; ascorbic acid, 0.5; pH 7.4. Low Na^+ aCSF was prepared for the procedure of slice preparation. In this solution, 95 mM NaCl was replaced by glycerol (60 mM) and sucrose (130 mM). The chemicals and drugs were purchased from Sigma-Aldrich (St. Louis, MO, USA), unless stated otherwise.

Internal solution was used for filling microelectrodes with the following composition: 120 mM potassium gluconate; 5 mM NaCl; 10 mM 4- (2-hydroxyethyl) -1-piperenethanesulfonic acid (HEPES); 2 mM EGTA; 0.1 mM $CaCl_2$; 5 mM Mg-ATP; 0.3 mM Na_3 -GTP; 10 mM Na_2 -phosphocreatinine; 8 mM biocytin and the osmolarity 280-290 mOsm/l, pH 7.3.

5.2. Animals and preparation

Animal experiments were performed according to the appropriate institutional, national and international laws (EU Directive 2010/63/EU for animal experiments), guidelines on the care of research animals. The protocols used for experiments below were registered by the University of Debrecen Committee of Animal Welfare (6/2011/DEMÁB; 5/2015/DEMÁB; 19/2019/DEMÁB) and approved by Government Office for Hajdú-Bihar County.

For slice electrophysiology, 10-22 days old mice were employed and 52-69 days old mice were used for behavioral tests. Mice expressing tdTomato fluorescent protein (554 nm excitation maximum and 581 nm emission maximum) or channelrhodopsin2 (ChR2) optogenetic actuator in a choline acetyltransferase- (ChAT) dependent way (n = 59 and 5, respectively), as well as mice expressing tdTomato in a type 2 vesicular glutamate transporter (Vglut2) dependent way (n = 13) and in a Serotonin transporter- (Sert) dependent way (n = 12) from both sexes were employed (Fig.15A).

The Cre-lox system was used for gene expression, where one parent of experimental animal was expressed the cre-recombinase protein catalyzes site-specific recombination events between two DNA recognition sites. Another was expressed the loxP sites which are specific binding sites for cre-recombinase. Each site is 13 bp long, and an 8 bp spacer region separates the two sites. In order to get mice for slice electrophysiology, homozygous floxed-

stop- tdTomato (B6;129S6-Gt(ROSA)26Sortm9(CAG-tdTomato)Hze/J; Jax mice accession number: 007905); ChAT-cre (B6;129S6-Chattm2(cre)Lowl/J; Jax number: 006410); Vglut2-cre (Slc17a6tm2(cre)Lowl (also called Vglut2-ires-Cre); Jax number: 028863); and Sert-cre (B6.129(Cg)-Slc6a4tm1(cre)Xz/J; Jax number: 014554); or homozygous floxed-stop-channelrhodopsin-2 (B6;129S-Gt(ROSA)26Sortm32.1(CAG-COP4*H134R/EYFP)Hze/J) and ChAT-cre (see above) strains purchased from Jackson Laboratories (Bar Harbor, ME, USA) were crossed in our animal facility.

The KCNQ4 knockout (KO) strain was a kind gift of Prof. Thomas Jentsch (FMP/MDC, Berlin, Germany; Kharkovets et al, 2006). Heterozygous mice were bred in the animal facility of the Department of Physiology, University of Debrecen. Young pups were genotyped, knockout animals and wild type littermates were used in the experiments and tests. In total, 10 KCNQ4 knockout and 12 wild type mice were used for slice electrophysiology; 13 knockout and 15 wild type mice were employed for behavioral tests.

Coronal midbrain slices with 200 μm thick were prepared in ice-cold (cca. 0 - -2 ºC) low Na^+ aCSF by a vibratome Microm HM 650V (Microm International GmbH, Walldorf, Germany) while continuously oxygenated with 95% O_2 and 5% CO_2 (carbogen). The slices were incubated for 1 hour before starting recording in a chamber while bubbling continuously with carbogen in normal aCSF on 37°C.

5.3. Electrophysiology

Our experimental setup included a Zeiss Axioskop microscope (Carl Zeiss AG, Oberkochen, Germany) which was used to visualize the slices. The microscope was connected to a fluorescent imaging system (Till Photonics GmbH, Grafeling, Germany), which was including a xenon-based Polychrome V light source (Till Photonics GmbH, Grafeling, Germany), a CCD camera (SensiCam, PCO AG, Kelheim, Germany), the imaging control unit (ICU) and the Till Vision software (4.0.1.3 version). This system allows the fluorescence intensity to change over observation time. Axopatch 200A amplifiers (Molecular Devices, Union City, CA, USA) for whole cell patch-clamp measurements with both voltage clamp and current clamp modes were used. Data processing and recording was performed with Clampex 10.0 software (Molecular Devices, Union City, CA, USA), while data analysis was done by Clampfit 10.0 (Molecular Devices).

Measurements were performed at room temperature (22-25ºC). The slices were kept in normal aCSF perfused at a rate of 1 ml/min with Gilson Minipuls 3 peristaltic pump

(Gilson Inc., Middleton, WI, USA) during the measurement. The solution was continuously oxygenated with carbogen (95% O_2 and 5% CO_2).

Patch pipettes were made of borosilicate glass capillaries using Narishige PC-10 pipette puller (Narishige Group, Tokyo, Japan) with 5-8 MΩ resistance and filled with the potassium gluconate-based internal solution described in "Solutions".

Whole-cell patch-clamp experiments were performed on neuronal somata using the Axopatch amplifiers. Only stable recordings were considered with minimal leak currents and with series resistance below 30 MΩ, with less than 10% change.

Measurements were performed in both voltage- and current clamp modes. In certain experiments, 1 μM tetrodotoxin (TTX; Alomone Laboratories, Jerusalem, Israel) was used for elimination of action potential generation. 20 μM XE991 (10,10-bis(4-Pyridinylmethyl)-9(10H)-anthracenone dihydrochloride; Tocris Cookson Ltd., Bristol, UK) was used to inhibit M-current. The non-specific M-channel opener retigabine, the KCNQ2- and KCNQ4-specific ML213 (N-(2,4,6-Trimethylphenyl)-bicyclo[2.2.1]heptane-2-carboxamide) and the KCNQ2- and KCNQ3-specific ICA27243 (N-(6-chloro-pyridin-3-yl)-3,4-difluoro-benzamide; 20 μM; Tocris Cookson Ltd., Bristol, UK) were applied in certain experiments (Gunthorpe et al, 2012; Linley et al, 2012; Brueggemann et al, 2014; Wickenden et al, 2008).

For assessing the presence of M-current or the functional consequences of the M-current on PPN cholinergic and glutamatergic, as well as DR, MR serotonergic neurons, detailed protocols below were used. The current clamp configuration was used to determine spike train properties.

The voltage clamp configuration was used for recording of the M-current. Neurons were held on -20 mV holding potential and 1-s-long repolarizing voltage steps were employed with 10 mV decrement from -30 to -60 mV. The difference of the instantaneous and steady state current components during the repolarizing steps used to define M-current (Fig.15B).

1-s-long square current pulses were used between -30 pA and +120 pA with 10 pA increment in current clamp configuration to detect spike train pattern. Depending on the type of experiment, the resting membrane potential was set to -60 or -80 mV. Furthermore, early, medium and late afterhyperpolarizations were recorded as the differences of the firing threshold and the afterhyperpolarization; at the maximal negative deflection, and 100 ms or 300 ms after the peak potential, respectively (Fig.15C). For defining the spike latency of recordings at membrane potentials of -60 and -80 mV, the time difference between the start

of the current step and the peak potential of the first action potential was used at the sweep recorded with 100 pA depolarizing current injection (Fig.15D). The input resistance was acquired from the difference between the average voltages of 10 ms long periods prior to and at the end of the trace corresponding to the -30 pA steps (Fig. 15E). The firing frequency of the entire trace of action potentials during the square pulse was considered at 100 pA depolarizing pulse. The highest firing frequency was determined from the shortest interspike interval recorded in the depolarizing steps (the majority of cases, between the first two action potentials of the +120 pA square pulse).

Adaptation index (AI) was calculated with the following formula: $AI = 1- (F_{last}/F_{initial})$, where F_{last} is the frequency of the last 2 action potentials and $F_{initial}$ is the average frequency of the first 3 action potentials (Nigro et al., 2014; Bordas et al., 2015; Fig. 15F). Only those recordings were considered for analysis where at least 8 action potentials were seen in control. AI was considered as 1 in those cases where this number lowered below 5 due to the robust action of M-current openers.

A-current was recorded on PPN and CnF glutamatergic neurons in voltage-clamp mode. Neurons were kept on -60 mV holding potential. A 1-s-long depolarizing step with +20 mV amplitude was employed to elicit the current. The depolarizing step was preceded by -120 mV and a -10 mV prepulses with a duration of 200 ms.

Simultaneous recordings were performed on PPN cholinergic neuronal somata and proximal dendrites (20-35 μm away from the soma) utilizing patch pipettes with 6-8 MΩ resistance in certain cases. In other cases, synaptically non-coupled, neighboring cholinergic neurons were patched and both neurons were simultaneously depolarized by using 1-s-long depolarizing square current injections with amplitude of 100 pA in current clamp configuration.

When analyzing synchronization of neuronal activity, the absolute values of time differences between action potentials were plotted with using 20 ms bins, when synchronization in action potential firing of neighboring neurons was assessed. Under control conditions and after application of XE991, the individual graphs were fit with single exponential function ($y = a + b*e(\tau*x)$), and the parameter 'τ' was used as a measure of synchronicity.

In current clamp mode, high-threshold membrane potential oscillations were recorded from -60 mV resting membrane potential with a 2-s-long depolarizing ramp protocol from 0 pA to 800 pA (Bordas et al., 2015; Baksa et al., 2019), in the presence of TTX for blocking

action potential firing. Power spectra were assessed during the depolarizing steps and power maximum and frequency were determined for of the whole traces (Fig.15G-H).

For the optogenetics experiments, 500 µm thick coronal midbrain slices including the laterodorsal tegmental nucleus (LDT) and the pedunculopontine nucleus (PPN) were prepared. An optical fiber was attached to the LDT and illuminations with 50 ms long, 470 nm wavelength and 1 Hz frequency were used. Before and during optogenetic illuminations, whole cell patch clamp recordings of the M-current (see above) were performed on PPN cholinergic neurons.

The tdTomato and EYFP fluorescent markers were visualized by using a widefield fluorescent imaging system (Till Photonics GmbH, Gräfeling, Germany) containing a xenon bulb-based Polychrome V light source, a CCD camera (SensiCam, PCO AG, Kelheim, Germany), an imaging control unit, and the Till Vision software (version 4.0.1.3).

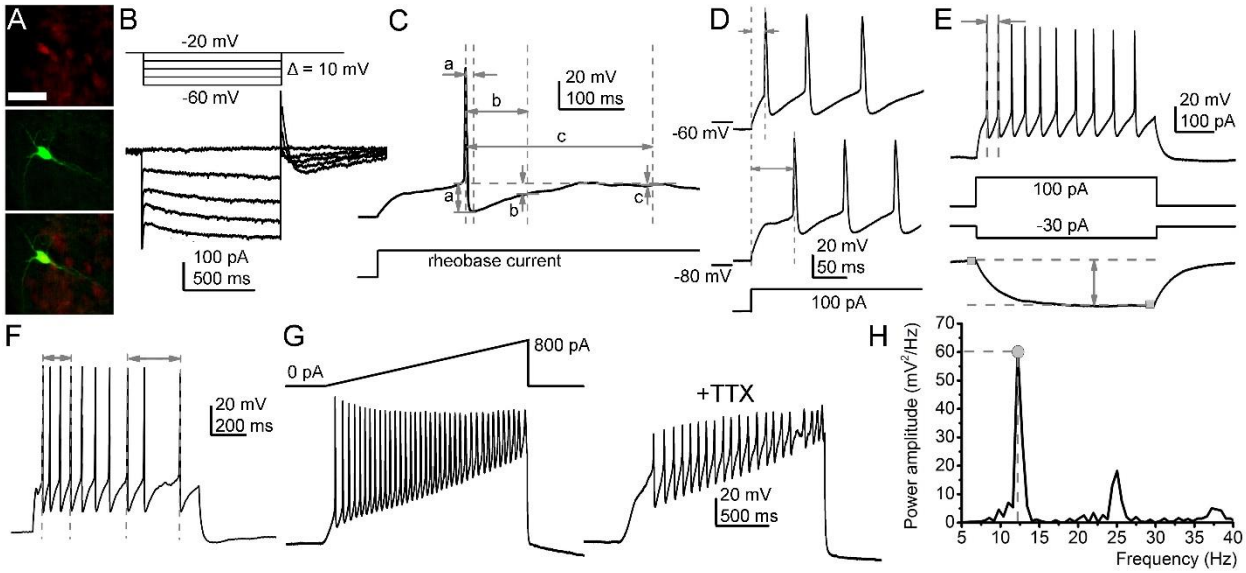

Fig. 15. Functional parameters for recordings. A. Identification of the neurons. Sert-dependent tdTomato expression (red, upper panel), biocytin labelling of the recorded cell (green, middle panel), merged image (bottom panel). Scale bar: 50 µm. **B.** A representative M-current trace (below) with the voltage protocol eliciting it (above). **C.** Measurement of afterhyperpolarization amplitudes on action potentials elicited with square rheobase current (20-50 pA; a. greatest deflection as the difference between the maximal negative peak and the firing threshold; b. amplitude at 100 ms from the action potential peak; c. amplitude at 300 ms from the action potential peak). **D.** Determination of the delay of the first action potential compared to the onset of the 100 pA depolarizing square current injection. The resting membrane potential was set to -60 (above) and -80 mV (below). **E.** Measurement of the maximal and average firing rate and the input resistance. (top) Voltage trace elicited by 100 pA depolarizing square current injection. For maximal firing rate, the time between the first two action potentials was used (arrows). (bottom) Voltage trace elicited with 30 pA hyperpolarizing square current injection. Gray squares indicate 20 ms-long segments where data points were averaged for calculation of the voltage difference prior to and at the end of the hyperpolarizing current injection. **F.** Trace used for calculation of the adaptation index. Arrows indicate the action potentials used for calculation of the frequency of the initial (F_i) and last action potentials (F_l). **G-H.** Methods for assessment of the oscillatory activity. **G.** Depolarizing ramp current injection from 0 to 800 pA with the duration of 2 s to elicit oscillatory activity (above left) and the voltage trace elicited by it (below left). The voltage trace with TTX (right). **H.** The power spectrum of the oscillatory activity with TTX. The gray circle and the dashed lines indicate the power maximum and the frequency belonging to power maximum.

5.4. Morphological identification of the investigated neurons

During patch clamp recording, neurons were labeled with biocytin and slices were fixed (4% paraformaldehyde in 0.1 M phosphate buffer; pH 7.4; 4 °C) for neuronal morphological analysis. For permeabilization, Tris buffered saline (in mM, Tris base, 8; Trisma HCl, 42; NaCl, 150; pH 7.4) supplemented with 10% bovine serum and 0.1% Triton X-100 (60 min) was applied. Then samples were incubated in streptavidin-conjugated Alexa488 (1:300; Molecular Probes Inc., Eugene, OR, USA) dissolved in phosphate buffer (90 min) for recovery.

The confocal microscope (Zeiss LSM 510; Carl Zeiss AG) was used to visualize the neurons and tile scan images were taken with 40x objective, 1 μm optical slices after the labeling procedure.

For the neuronal reconstruction, NeuroLucida software (MBF Bioscience, Williston, VT, USA) was used. On the basis of the Paxinos atlas (Paxinos, 2013), the topographical maps of functional properties, the three-dimensional location of the individual neurons (including the rostrocaudal location of the slice containing the labelled neuron) were set. A three-dimensional block reconstruction drawing included the contours of the brainstem and the cerebral aqueduct was made by parameters of the atlas, and positions of cell bodies were indicated with spheres.

5.5. Immunohistochemistry

For identification of cholinergic neurons in strains lacking genetically encoded fluorescent markers, choline acetyltransferase immunohistochemistry was performed in parallel with morphological identification; in collaboration with the Department of Anatomy, Histology and Embriology. Slices of KCNQ4 knockout and wild type mice used for electrophysiology were fixed in 4% paraformaldehyde for 24 hours. After 3x10 minutes incubation with PBS, the slices were permeabilized with 2% Nonidet and 1% BSA throughout 60 minutes.

Anti-choline acetyltransferase (anti-ChAT) primary antibody from goat (Millipore, Temecula, CA, USA) was incubated throughout 48 hours in 1:100, with anti-KCNQ4 1:400 from rabbit. Donkey anti-goat Alexa 555 and Donkey anti-rabbit Alexa 488 antibodies (Vector Laboratories Inc., Burlingame, CA, USA) were incubated for another 24 h. Confocal images were snapped in a similar way described in previous chapter after completion of the protocol above.

5.6. Activity wheel test

Activity cycle durations and distances moved per day were tested by activity wheel test (Campden Instruments Ltd., Loughborough, UK). KCNQ4 knockout young adult (52-69 days old) mice (n = 16) and wild type littermates (n = 16) were employed. Mice were settled individually in cages with activity wheel. There is a known progress in deafness of KCNQ4 KO mice and the activity wheel performance also changes with age. Therefore, we aimed to use as young animals as possible and to minimize the progress during the experiment by setting the experimental animals to shorter circadian periods (Kharkovets et al, 2006, Fodor et al, 2020).

Animals were in a room for 7 days to accommodate to alternating 6 h illumination and 6 h darkness periods and had voluntary and unlimited access to the activity wheel. The protocol with 6 hours of darkness and 6 hours of light was set to exclude vision impairment (as it is known about the original C3H strain; Gorman and Elliot, 2003; Harrison et al, 2016).

After accommodation, recording was started with the same conditions of illumination (LDLD conditions) and lasted for 5 days. After that, recording process was continued during 5 days of complete darkness (DD conditions). The recording data of last 3 days were taken into account. Period time was calculated by Lomb-Scargle periodogram (www.circadian.org). Due to technical problems, 3 of the knockout and 1 of the wild type animals were excluded, thus 13 knockout and 15 wild type mice were included to the study.

5.7. Statistics

All data tested by D'Agostino-Pearson normality test to compute the skewness and kurtosis to quantify how far the distribution is from Gaussian in terms of asymmetry and shape. Student’s t-test, one way ANOVA and post hoc Tukey Multiple Comparison tests were used for assessing statistical significance for pairwise comparison in case if the datasets had normal distribution, whereas Bonferroni's multiple comparison test was employed for multiple comparisons. Statistical analysis was performed using Microsoft Excel or IBM SPSS Statistics 25, SigmaPlot 12.0 and GraphPad Prism 5.01 (GraphPad software, San Diego, USA). In analysis, an alpha of 0.05 was used as the cutoff for significance.

6. RESULTS

6.1. Electrophysiological characterization of the M-current and localization in neurons from PPN

6.1.1 The M-current of different PPN neuronal populations

Our laboratory previously demonstrated that the M-current is almost exclusively present on PPN cholinergic neurons, by using genetically labelled cholinergic (ChAT+) and GABAergic (GAD65+), but not glutamatergic neurons (Bordás et al, 2015). First, we aimed to confirm it by recording M-current on genetically labelled Vglut2+ glutamatergic PPN neurons (Fig.15A). In accordance with our previous claim, almost all ChAT+ neurons possessed M-current but it was absent from GAD65+ (Fig. 16B-D). We recorded M-current from 6.8% of glutamatergic neurons (n = 32). A single neuron was ChAT-positive as well, belonging to the group of glutamatergic-cholinergic neurons (Wang and Morales, 2009; Baksa et al, 2019). In conclusion, almost all non-cholinergic neurons lack the M-current, but one cannot exclude existence of very few exceptions in the glutamatergic neuron population (Fig. 16E).

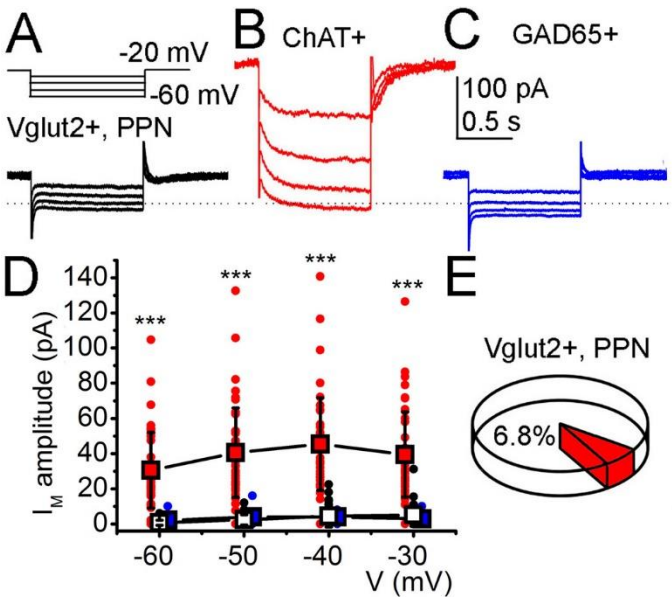

Fig. 16. Cholinergic neurons possess, glutamatergic and GABAergic PPN neurons lack M-current. A-C. Current traces recorded from a glutamatergic (Vglut2+) (A, the voltage protocol is above the current trace), cholinergic (ChAT+) (B) and a GABAergic (GAD65+) neuron (C). **D.** Statistical comparison of currents recorded with M-current relaxation protocol from a cholinergic (red square), glutamatergic (hollow square) and a GABAergic neuron (blue square) in the function of the repolarizing voltage steps (*** indicates significant difference from Vglut2+ at $p < 0.001$; dotted line: 0 pA). Red dots are the individual cholinergic, blue dots are the individual GABAergic and black dots are the individual glutamatergic data points. **E.** Percentage of glutamatergic neurons having M-current.

6.1.2 Modulation of M-current on PPN cholinergic neurons

Next, we tested whether an activation of a cholinergic input to the PPN resembling physiological situations (the LDT cholinergic neurons) is capable of inhibiting the M-current. In order to preserve as many cholinergic fibers arising from the LDT as possible, the M-current of PPN cholinergic neurons was measured from 500-µm-thick coronal midbrain block slices, which was cut from ChAT-ChR2 mice and it was optogenetically stimulated by 470 nm light flashes with 1 Hz frequency (Fig.17A-C). Optogenetic activation of the LDT lowered the holding current to 60.45 ± 6.49% of control (p= 0.008; Fig.17C-D). The relaxation current decreased at all voltage steps of the protocol we used. The magnitude of the current amplitude during optogenetic stimulation was 51-73% of the control (56.11 ± 12.75% at -60 mV, 51.1 ± 15.27% at -50 mV, 62.57 ± 12.53% at -40 mV, 72.7 ± 24.17% at -30 mV; Fig.17E). After 5 minutes' recovery following the optogenetic stimulation, the M-current was partially returned to control (88.6 ± 21.6 pA holding current, p = 0.093; 7.46 ± 5.15 pA M-current amplitude at -60 mV, p = 0.089; 24.63 ± 5.27 pA at -50 pA, p = 0.05; 35.07 ± 10.78 pA at -40 pA, p = 0.07; 33.57 ± 4.39 pA at -30 pA, p = 0.04). We concluded that the optogenetic stimulation for a single cholinergic input of the PPN can powerfully inhibit the M-current and it might serve physiological neuromodulatory processes.

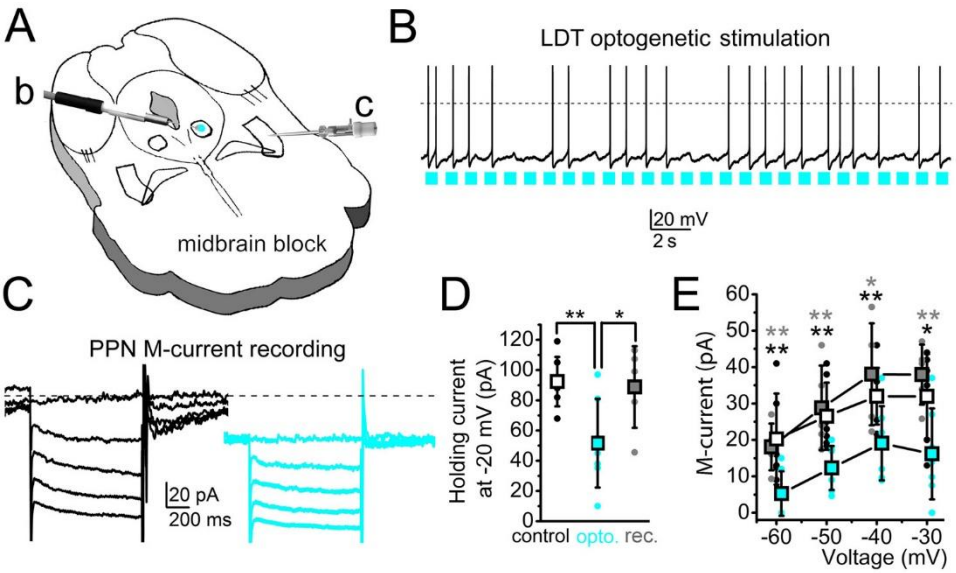

Fig. 17. Stimulation of a cholinergic input of the PPN can powerfully reduce the PPN M-current amplitude. A. Schematic drawing the block preparation. The LDT of the midbrain block originating from a ChAT-ChR2 mouse was optogenetically stimulated (blue spot; b; see panel B) in parallel with patch clamp recording from the PPN (c; see panel C). **B.** Optogenetic activation of an LDT cholinergic neuron with 1 Hz pulsatile blue light (blue squares) and spikes of the neuron elicited with the optogenetic stimulation. **C.** The M-current recorded from a PPN cholinergic neuron before (black) and during (blue) optogenetic stimulation of the LDT. **D.** Statistical comparison of the holding currents at -20 mV voltage recorded before (hollow squares, black dots), during optogenetic stimulation (blue squares, blue dots) and after recovery (gray squares, gray dots; **: $p < 0.010$). **E.** Statistical comparison of the repolarizing current steps recorded before (hollow), during optogenetic stimulation (blue) and after recovery (gray). Squares represent mean ± SD, dots represent individual data (*: $p < 0.050$; **: $p < 0.010$; black asterisks: significance between control and illuminated; gray asterisks: significance between illuminated and recovered datasets.)

6.2. The role of the M-current on neuronal synchronization of PPN cholinergic neurons

To show the contribution of the M-current to the synchronization of neighboring PPN neurons (e.g. during slow wave sleep), the KCNQ channel inhibitor XE991 was applied and we recorded firing of two synaptically non-coupled neurons, depolarized simultaneously with 100 pA square current pulses (Fig. 18A-C). The M-current inhibitor XE991 reduced the adaptation index of these neurons from 0.353 ± 0.026 to 0.277 ± 0.028 ($p = 0.0375$), to a similar magnitude as in KCNQ4 KO PPN cholinergic neurons (see below), representing the existence of the pharmacological actions of the drug we applied. We measured the time differences between the closest action potentials of the action potential trains from two synaptically non-coupled neurons (Fig. 18D-E). For the neuronal pairs in normal aCSF, a greater number of short delay values were recorded during control, delay values were showed longer and more variable values with XE991 (Fig. 18F, G, H). In control, higher than 50% of all cases, the delay values were less than 40 ms. The delay values became more uniformly distributed for the first 100 ms in the presence of XE991 (Fig. 18H). Moreover, decay tau of the distribution histograms was significantly decreased from -0.022 ± 0.010 to -0.007 ± 0.008 ($p = 0.0302$; Fig. 18I). We concluded that in the presence of the M-current inhibitor XE991, action potential firing of neighboring neurons was less synchronized.

Summarizing the findings above, we confirmed our previous results that the M-current exists on cholinergic and is absent on PPN non-cholinergic neurons. We also showed that the M-current is presumably effectively blocked by the physiological cholinergic inputs of the nucleus. Inhibition of M-current caused loss of synchronization between neighboring neurons.

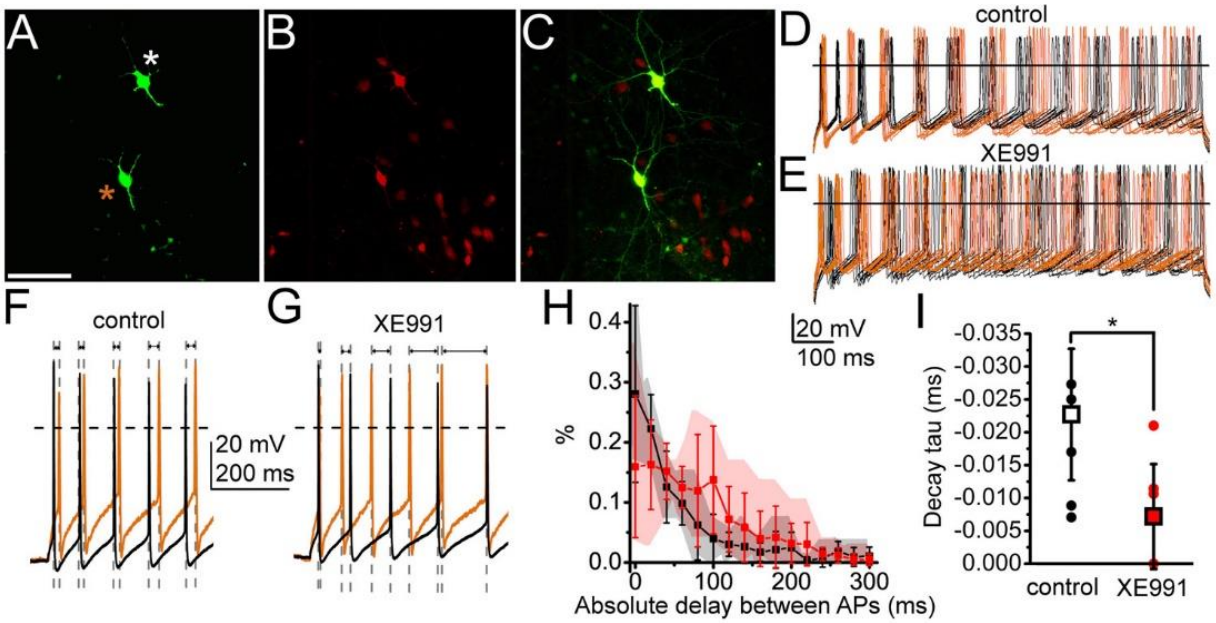

Fig. 18. The M-current of PPN cholinergic neurons can synchronize the neighboring neurons. A-C. Two cholinergic neurons labelled in the PPN (asterisks). **A.** Biocytin labelling (scale bar: 100 µm). **B.** ChAT-dependent tdTomato expression. **C.** Merged image. **D-E.** Trains of action potentials elicited by 100 pA depolarizing stimuli from the two neighboring neurons in normal aCSF (D, control, brown traces: recordings from the neuron labelled with brown asterisk; black traces: recorded from the neuron labelled with white asterisk) and in the presence of the M-current inhibitor XE991 (E). **F-G.** Representative trace pairs recorded from D-E at high temporal resolution under control conditions (F) and with XE991 (G) representing changes of delay intervals between spikes (indicated with gray dashed lines and arrows). **H.** Mean histograms of absolute delay between action potentials recorded from the neighboring neurons with 20 ms bins (mean ± SD; black: control, red: with XE991; gray and pink clouds: ranges of individual data). **I.** Decay tau values calculated by fitting the individual histograms of absolute delays in normal aCSF (hollow square, black dots) and with XE991 (red square, red dots). Squares represent average ± standard deviation and dots represent individual data.

6.3. M-current properties mediated by KCNQ4 subunits

6.3.1 M-current properties in KCNQ4 KO mice

The KCNQ4 subunit expression is restricted to the brainstem but the presence of it has not been revealed in the PPN, an important member of the RAS. Thus, in our next experiments, we studied PPN neuronal electrical properties from KCNQ4 KO animals using electrophysiological techniques. We performed experiments to investigate the presence of the

M-current in these neurons. For neuronal identity, we labeled all recorded neurons with biocytin and judged their cholinergic nature with post hoc ChAT immunohistochemistry (Fig. 19A, C). The holding current at -20 mV was much lower in KO than WT animals. For the WT animals, mean values were 175.97 ± 27.67 pA and 66.95 ± 19.8 pA for the KO ($p = 0.0060$; Fig. 18B). Also, we identified that the M-current was absent (< 10 pA at -40 mV) in 62.5% of the KO cases while WT animals only showed its absence in 7.7% of the cases ($n = 13$ for WT, and $n = 8$ for KO; Fig.19B, F). Furthermore, the average relaxation current at -40 mV was 42.57 ± 7.95 pA in the WT and 14.85 ± 6.12 pA in the KO animals ($p = 0.013$; Fig. 19F). On ChAT-negative neurons, M-current was not recorded neither in WT ($n = 5$) nor in KO ($n = 5$) (Fig. 19D).

As the M-current significantly contributes to SFA, setting synchronization of the neighboring neurons, we tested and analyzed whether the lack of KCNQ4-dependent M-current can alter SFA. By depolarizing square current injections, we obtained trains of action potentials and then we calculated the adaptation index (AI) of the trains. In cholinergic neurons from KCNQ4 KO animals, the AI were significantly lower than WT (0.34 ± 0.02 in WT and 0.23 ± 0.04 in KO, respectively; $p = 0.04$; $n = 6$ for KO and $n = 9$ for WT; Fig. 19G, I). 66.7% of the KO neurons presented lower AI, in agreement with the experiments shown above. In this experiment, the SFA for non-cholinergic neurons from KCNQ4 KO mice was also studied. The AI of the cholinergic neurons was significantly lower than non-cholinergic, as expected in accordance with our previous studies. Interestingly, a marked decrease of AI was observed in KO compared to WT (0.28 ± 0.06 in WT and 0.11 ± 0.11 in KO, $p = 0.0094$, $n = 5$ for both; Fig. 19H-I).

In conclusion, these experiments revealed that KCNQ4 is important for KCNQ channel assembly in a subset of PPN neurons and for forming the M-current. This alteration affected cholinergic and non-cholinergic neuronal firing pattern by changing SFA.

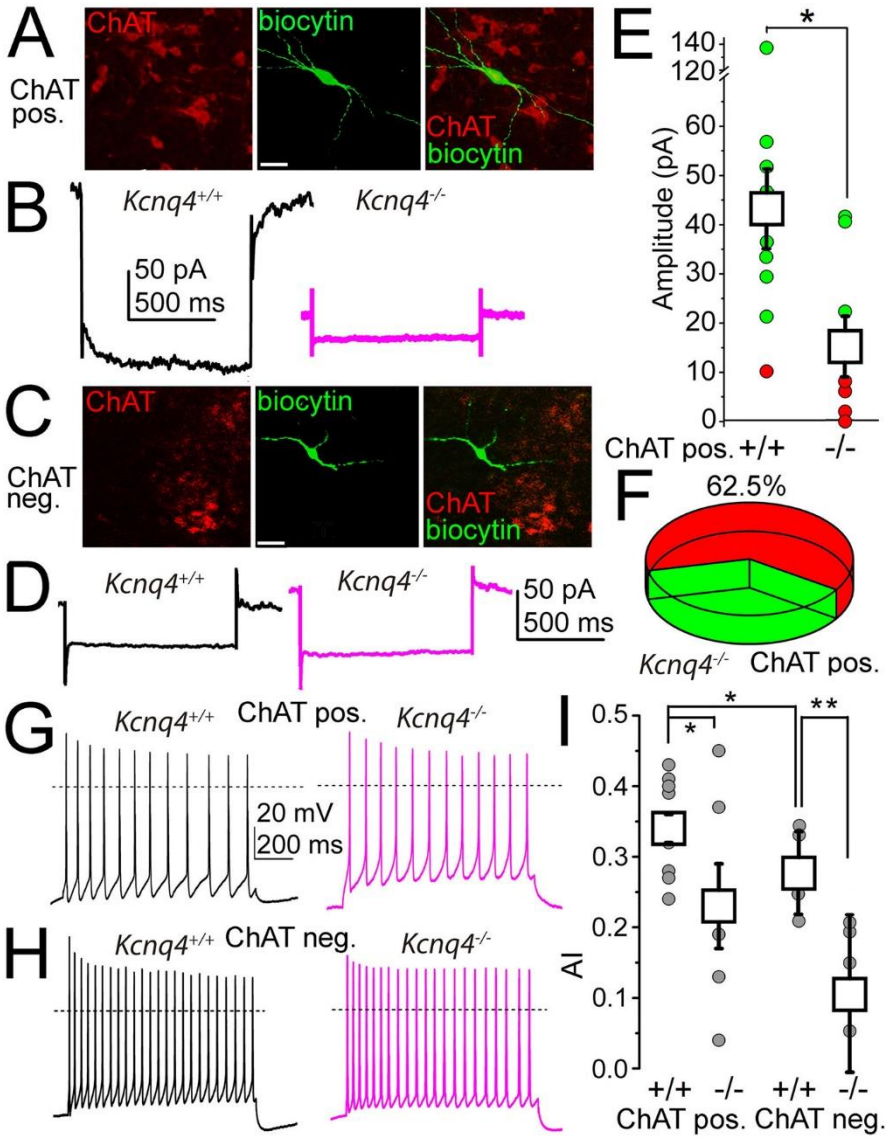

Fig. 19. A great population of cholinergic neurons lack M-current in KCNQ4 KO preparations. **A.** Labelling of a cholinergic neuron by choline acetyltransferase (ChAT) (left, red: ChAT immunohistochemistry; middle, green: biocytin labelling, right: merged image; scale bar: 50 µm). **B.** Representative current traces from of cholinergic neurons of a WT (*Kcnq4*$^{+/+}$, black) and a KO (*Kcnq4*$^{-/-}$, purple) sample. **C.** Non-cholinergic neuronal labelling by ChAT (left, red: ChAT immunohistochemistry; middle, green: biocytin labelling, right: merged image; scale bar: 50 µm). **D.** Individual current traces from non-cholinergic neurons of WT (*Kcnq4*$^{+/+}$, black) and KO samples (*Kcnq4*$^{-/-}$, purple). **E.** Statistical comparison of relaxation current of cholinergic neurons at -40 mV from WT (+/+) and KO (-/-) samples (green: M-current exists, red: no M-current detected; white squares: mean ± SD). M-current was absent on all non-cholinergic neurons. **F.** Percentage of cholinergic neurons from KO samples lacking (red) and having M-current (green). **G-H.** Representative voltage traces acquired from WT (*Kcnq4*$^{+/+}$, black) and KO (*Kcnq4*$^{-/-}$, purple) samples from cholinergic (G) and non-cholinergic (H) neurons. 0 mV indicated by dotted lines. **I.** Statistical comparison for adaptation index (AI) of cholinergic (ChAT pos.) and non-cholinergic (ChAT neg.) neurons from WT (+/+) and KO (-/-) samples (gray circles: individual data, white squares: mean ± SD; *: $p < 0.050$; **: $p < 0.010$.)

6.3.2 Presence of functional KCNQ4 subunits in PPN

In order to differentiate the function of KCNQ4 in PPN cholinergic neurons in WT animals, we dissected its contribution by employing various subunit-specific KCNQ channel openers. First, we conducted holding current analysis using 20 μM retigabine, a non-specific KCNQ channel opener. An outward shift of the holding current at -20 mV on 100% of the neurons was elicited by retigabine (n = 11; Fig.20A, D). The holding current at -20 mV was increased from 95.25 ± 11.96 pA to 140.23 ± 12.24 pA (p= 0.009; 43.3 ± 8.4% increase; Fig. 20A, E).

Next, we administered ML213 (20 μM), a KCNQ2- and KCNQ4-specific M-current opener. This generated an outward shift in the holding current in 69.2% of the cholinergic neurons tested and the rest were non-sensitive to it (Fig. 20B, D). The average rise of the outward current at -20 mV holding potential was 25.61 ± 5.94 pA (from 143.99 ± 28 pA to 169.61 ± 29.66 pA; 41.815 ± 10.7% increase; n =13; Fig. 20E).

Then, we tested a KCNQ2- and KCNQ3-specific opener ICA27243 (20 μM). In the majority of the cases, the opener did not cause changes in the holding current (Fig.20C-D). KCNQ channels activation signs were observed on 42.9% of the neurons (n = 7; Fig.20E). It elicited an averaged additional rise in the outward current of 19 ± 8.61 pA at -20 mV holding potential (from 165.04 ± 23.23 pA to 174.96 ± 25.78 pA; Fig.20E).

We identified the effects of the openers on the SFA in the next series of experiments. For retigabine, it was observed a rise of AI in the vast majority (88.9%) of the cases, from 0.33 ± 0.035 to 0.755 ± 0.10 (p = 0.0005; n = 9; Fig.21A, E, D), demonstrating that the participation of M-current in the SFA of cholinergic neurons, although other channels also contribute. It caused a weaker action as it increased the AI only in 44.4% of the cases by ML213 (from 0.36 ± 0.06 to 0.61 ± 0.13; n.s.; n = 10; Fig.21B, E, D). For ICA27243, its effect on AI was even weaker: it increased only in 20% of all cases (from 0.39 ± 0.02 to 0.43 ± 0.07; n.s.; n = 10; Fig.21C-D).

Based on these results, we concluded that not all PPN cholinergic neurons have KCNQ4-mediated M-current. According to the data for percentages of activated neurons elicited with all openers and their selectivity, we can assume that functional KCNQ4 subunits have only on subpopulation of PPN cholinergic neurons. This population is possibly one-fourth of the whole PPN cholinergic neuronal population.

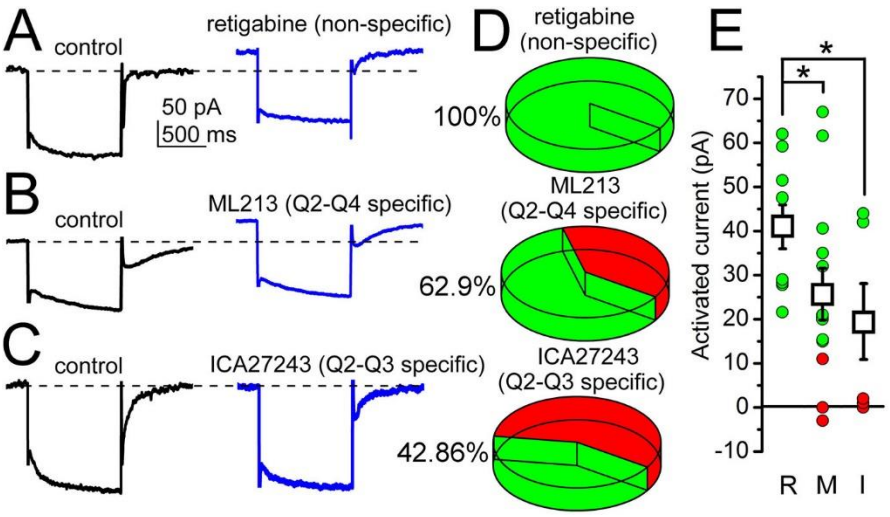

Fig. 20. The KCNQ4 subunit can be found on PPN cholinergic neuronal subpopulation. A. The non-specific KCNQ opener retigabine actions on the M-current (black: control trace, blue: trace with retigabine). **B.** Individual M-current traces in control conditions (black) and with ML213, KCNQ2- and KCNQ4-specific opener (blue). **C.** Representative M-current traces in control conditions (black) and with ICA27243, KCNQ2- and KCNQ3-specific opener (blue). The holding currents in control indicated by dashed lines. **D.** M-current activation percentage of neurons by the openers shown above (hollow: M-current activation, gray: no-M-current activation). **E.** Statistical comparisons for currents activated by retigabine (R), ML213 (M) and ICA27243 (I) at -20 mV holding potential (green: outward currents greater than 10 pA, red: currents less than 10 pA, black squares: mean ± SD).

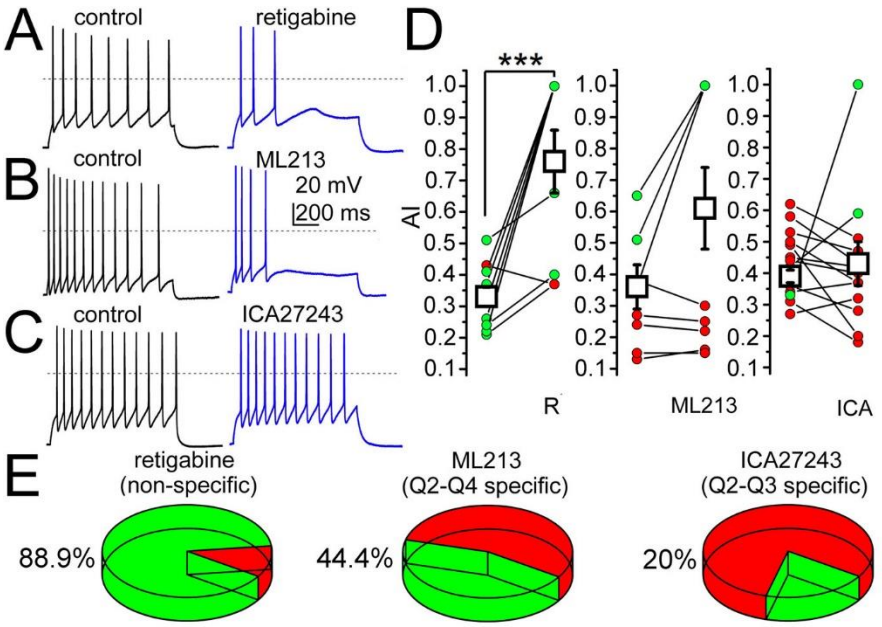

Fig. 21. Changes in AI by KCNQ-selective openers in PPN cholinergic neurons. A-C. Individual voltage traces acquired with 100 pA depolarizing current injections under control conditions (black) and with non-selective (A, retigabine), KCNQ2- and KCNQ4-selective (B, ML213) and KCNQ2- and KCNQ3-selective (C, ICA27243) openers. 0 mV indicated by dotted lines. E. Percentage of PPN cholinergic neurons increasing adaptation index (AI) to different M-current openers (hollow) and lacking response (gray). **D.** Statistical comparison for changes in AI by openers with various selectivity (green: increase, red: no change or decrease in individual data; black squares: mean ± SD; *** show significant difference at $p < 0.001$).

6.4. Functional roles of KCNQ4 in the RAS

The PPN is a nucleus of the RAS which participates in modulation of the circadian rhythm. We identified the presence of KCNQ4 in this structure and its functional role in neuronal properties. At that point, we investigated how this subunit is involved in the regulation of the circadian rhythm by the PPN by voluntary wheel running test in young adult KCNQ4 KO and WT mice (n = 13 and 15, respectively). For discarding any potential impairment in the visual pathway, we made mice circadian bifurcation by altering the LD cycle to a 6-h LDLD periods. In this condition, the actogram showed two activity bouts during both scotophases for each genotype (Fig. 22A, B), demonstrating a proper function of the visual pathway. It had been showing no difference of the period time between genotypes under LDLD condition (14.55 ± 2.64 h for WT and 14.92 ± 2.77 h for KO; Fig. 22C). Next, we measured the distance ran by both mouse genotypes under LDLD conditions. There was no significant difference in distance traveled between WT and KO in LDLD conditions (Fig. 22E).

For identifying the intrinsic circadian rhythm in both genotypes, we made analysis of mice in the free-running or constant darkness conditions (DD). In DD condition, the period time was significantly reduced in WT compared to LDLD (to 10.2 ± 7.72 h; p = 0.0242) but exhibited only an increasing tendency in KO (17.88 ± 12.9 h; Fig. 22C). For distance of travels in DD condition, we observed an increasing tendency in WT animals, though it was not statistically significant compared to LDLD (from 2203 ± 1804 m/day to 3091 ± 2083 m/day). Nevertheless, a ~2-fold increase was revealed in the distance traveled of KO mice in DD compared to LDLD condition (from 1445 ± 1088 h/day in LDLD and 3919 ± 2075 h/day, p = 0.0049; Fig.22E). All parameters exhibited a higher variability of individual measurements in DD conditions. The period time was significantly longer in KO mice than in WT under DD condition (p = 0.0331; Fig.22C) and for the distance traveled, it was not statistically significant (Fig.22E). Also the period time in DD condition was normalized to LDLD condition in each cases, this parameter was 0.71 ± 0.56 in WT and 1.15 ± 0.76 in KO (p = 0.0461; Fig.22D). However, when distances in DD conditions were normalized to LDLD conditions, the parameters confirmed to be significantly higher in KO with a much greater standard deviation (1.58 ± 0.55 in WT and 3.6 ± 3.39 in KO; p = 0.0482; Fig. 22F).

In conclusion, lack of KCNQ4 exhibits to have mild but detectable effect on adaptation to changes in LD cycle, also on movement regulation related to activity cycles.

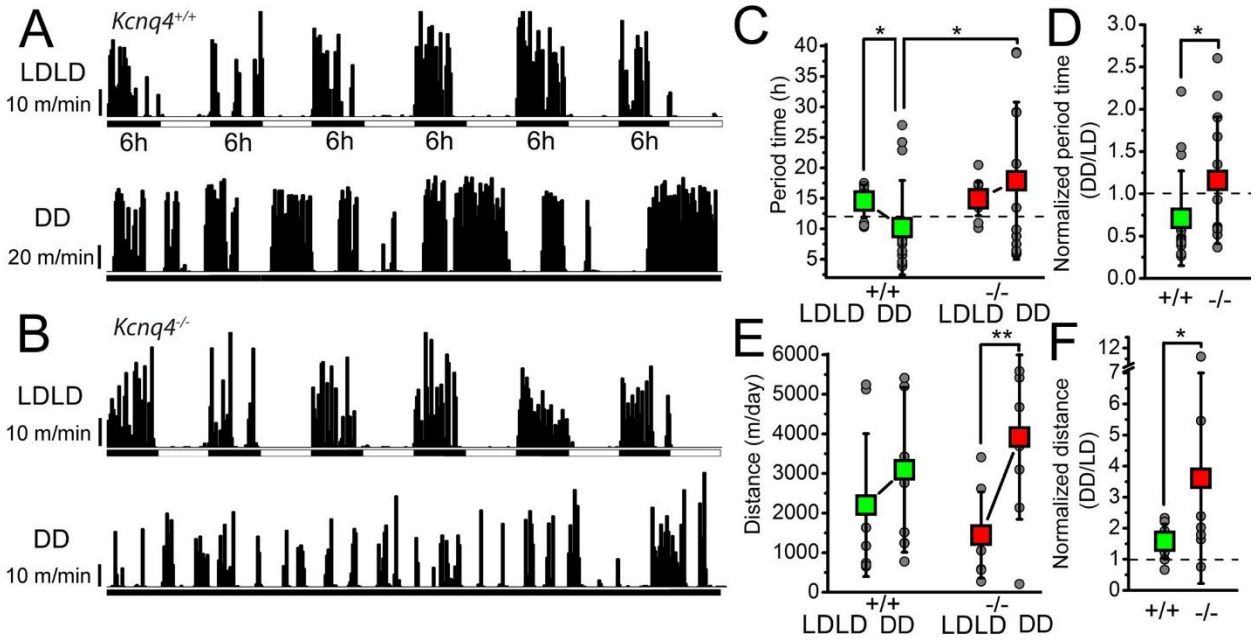

Fig. 22. KCNQ4 KO mice display altered activity cycle adaptation to changes in light-darkness conditions in the activity wheel test. **A.** Activity cycles of a WT mouse (*Kcnq4*$^{+/+}$) with 6 h alterations of light-darkness cycles (LDLD) and in full darkness (DD). Black vertical bars indicate distances ran in 10-minute bins. **B.** Activity cycles with the same arrangement as A for KCNQ4 KO mouse (*Kcnq4*$^{-/-}$). **C.** Statistical comparison of changes in period length under DD conditions with WT (+/+) and KO (-/-) mice (green squares: WT; red squares: KO; gray circles: individual data). Dashed line indicates 12 h. **D.** Period times under DD condition normalized to LDLD conditions of individual cases with the same arrangement as on panel C (dashed line: 1). **E.** Comparison of distances ran in 3 days by WT (+/+) and KO (-/-) under LD and DD conditions (the arrangement is the same as on panel C; *, and ** show significant difference at $p < 0.050$, and $p < 0.010$, respectively). **F.** Distances ran under DD condition normalized to LDLD conditions of each animal with the same arrangement as on panel C (dashed line = 1).

6.5. Localization of the M-current in neurons from dorsal and median raphe

Next, we investigated whether the M-current possessing raphe serotonergic neurons are topographically organized. We also investigated whether this current influences other membrane properties of these neurons. For addressing these questions, 56 genetically identified serotonergic neurons were patched (n =31 from the DR and n =25 from the MR; Fig. 15A).

Neurons possessing relaxation current amplitude higher than 20 pA (at -40 mV repolarizing step) were considered as ones having M-current. In these cases, (n =24), the holding current was recorded at -20 mV was 153.94 ± 23.28 pA. 25.9 ± 3.7 pA relaxation current was recorded at -60 mV repolarizing step; 39.16 ± 4.8 pA at -50 mV; 49.04 ± 6.64 pA at -40 mV and 44.26 ± 9.24 pA at -30 mV. After the administration of the M-current inhibitor XE991 (20 µM), the holding current was decreased to 120.78 ± 46.1 pA ($p = 0.2$), the relaxation current at -60 mV was 4.14 ± 2.64 pA ($p = 0.0002$), 11.72 ± 5.6 pA at -50 mV ($p = 0.0033$), 17.06 ± 9.27 pA at -40 mV ($p = 0.013$) and 19.14 ± 9 pA at -30 mV ($p = 0.07$; Fig. 15B; Fig. 23A,C).

In neurons without M-current (n =25), the holding current was recorded as 62.4 ± 9.12 pA at -20 mV; also the relaxation current was 0.75 ± 0.32 pA at -60 mV, 4.1 ± 0.1 pA at -50 mV, 6.8 ± 1.18 pA at -40 mV and 7.6 ± 1.8 pA at -30 mV. Administration of XE991 did not show any significant changes on recorded currents; as the holding current was 39.05 ± 9.38 pA at -20 mV ($p =0.12$), 0.17 ± 1.42 pA at -60 mV ($p =0.45$), 0.66 ± 1.12 pA at -50 mV ($p =0.24$), 1.46 ± 0.74 pA at -40 mV ($p = 0.22$) and 2.17 ± 2.77 pA at -30 mV ($p = 0.28$; Fig.23B, C) in the presence of XE991.

Regarding the amplitudes of the M-current on DR and MR serotonergic neurons, there was no significant difference between them (DR: 53.51 ±9.31 pA, n =16; MR: 38.8 ±3.11 pA, n =7; at -40 mV; $p =0.15$). 38.1% (8 from 21) of the MR serotonergic neurons possessed M-current, whereas this proportion was somewhat greater in the DR (48.6%; 17 from 35; Fig. 23D). In the lateral wings of the dorsal raphe, it was revealed that even more neurons had M-current (60%, 6 from 10).

We also evaluated the topographical organization of the neuronal somata having or lacking M-current (Fig.23E-G). We found that neurons with M-current are more likely located rostrally in the DR (-4.74 ± 0.05 mm from the bregma for the ones having and -4.9 ±

0.05 mm for the ones lacking M-current, p = 0.02) and found in dorsal locations of the MR (3.99 ± 0.07 mm from dorsal for the ones with and 4.36 ± 0.09 mm for the ones without M-current; p = 0.007; Fig.23H-K).

In the next step, statistical correlations were analysed between the M-current and other membrane properties. We found that the M-current can effectively determine average firing frequency and spike frequency adaptation (SFA). The average firing frequency at 100 pA depolarizing step was 5.3 ± 0.9 Hz for neurons having M current (n = 13) and 7.56 ± 0.84 Hz for the ones without M-current (n = 16; p= 0.04). Similarly, the SFA, calculated and numerically expressed by the adaptation index (AI), was also significantly different in the two groups. The AI was 0.77 ± 0.08 (n = 6) in neurons with M-current, whereas this parameter was 0.44 ± 0.04 in ones lacking M-current (n = 11; p = 0.0006; Fig. 15E-F; Fig. 24A-D).

The relationship of the M-current and the AHP was also measured and maximal, medium and slow AHPs were recorded and analyzed. The maximal amplitude of AHP was 20.27 ± 1.6 mV on neurons having M-current (n = 13) and 15.37 ± 1.44 mV (n = 16) on ones lacking M-current (p = 0.015). The medium AHP amplitude recorded 100 ms after the AP peak potential was 17.01 ± 2.95 mV with the neurons having M-current and 11.65 ± 1.54 mV lacking M-current (p = 0.046). The slow AHP recorded 300 ms after the AP peak was 10.87 ± 4.39 mV with the neurons possessing M-current and 3.77 ± 1.25 mV lacking M-current (p = 0.024; Fig. 15C; Fig. 25A-D).

There were electrophysiological parameters independent from the M-current. The input resistance of neurons with M-current was 966.54 ± 118.14 MΩ and 841.5 ± 64.74 MΩ for the ones without M-current (p = 0.16; Fig. 15E).

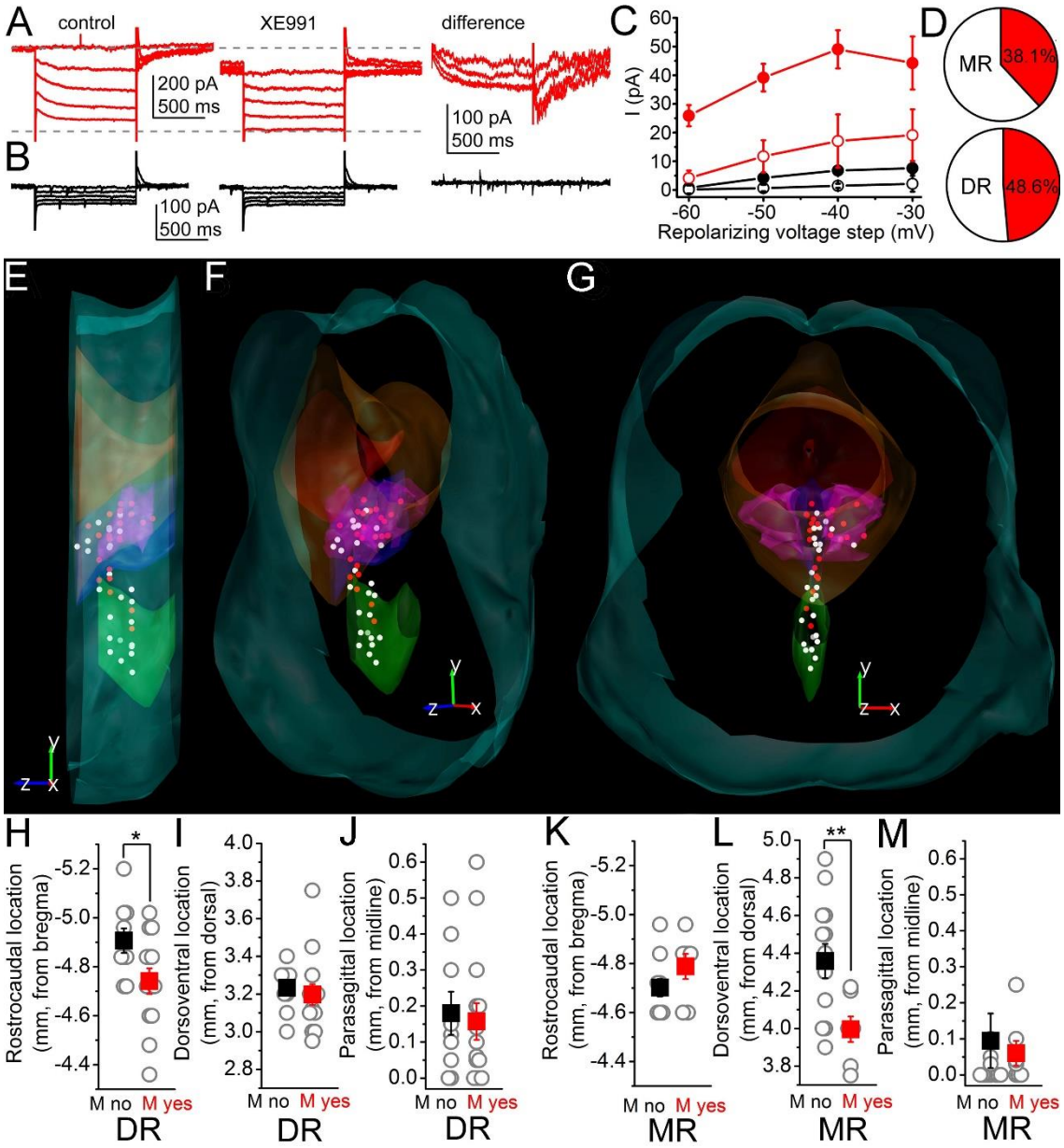

Fig. 23. Topographical organization of the M-current in median and dorsal raphe nuclei. A. An example of current traces when M-current was found (left: control current trace, middle: with the M-current blocker XE991, right: XE991-sensitive component). **B.** Individual current trace with the lack of M-current. For panel arrangement, see (A). **C.** Average relaxation currents in the function of the repolarizing voltage steps (red filled circles: M-current exists, control; red hollow circles: M-current exists, TTX; black filled circles: M-current is absent, control; black hollow circles: M-current is absent, TTX). **D.** Proportion of neurons possessing M-current (red area) in the median and dorsal raphe. **E-G.** The topographical organization of the somata with M-current in the raphe nuclei. **E.** Lateral view. **F.** 45º rotation towards the front view. **G.** Front view from caudal. White dots: somata lacking M-current. Red dots: somata with M-current. Light blue contours brainstem surface; red: aqueduct; orange: periaqueductal gray; blue: DR; purple: DR, lateral wing; green: MR. **H-J.**

Comparison of the rostrocaudal (H), dorsoventral (I) and parasagittal (J) locations of somata in the DR on which M-current was found (red squares) with those where no M-current was measured (black squares). **K-M.** Comparison of the rostrocaudal (K), dorsoventral (L) and parasagittal (M) locations of somata in the MR with the same arrangement as in H-J.

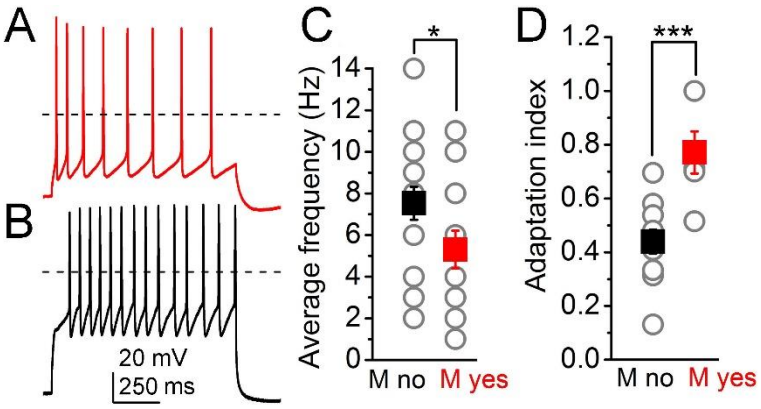

Fig. 24. The M-current influences firing frequency and adaptation index of raphe nuclei. A-B. Voltage traces elicited by 100 pA depolarizing current injections from a neuron having (A, red) and from another one lacking M-current (B, black). **C-D.** Statistical comparison of the average firing rate (C) and the adaptation index (D) of cells possessing (red squares) and lacking (black squares) M-current (gray circles: individual data; * $p<0.05$; *** $p<0.001$).

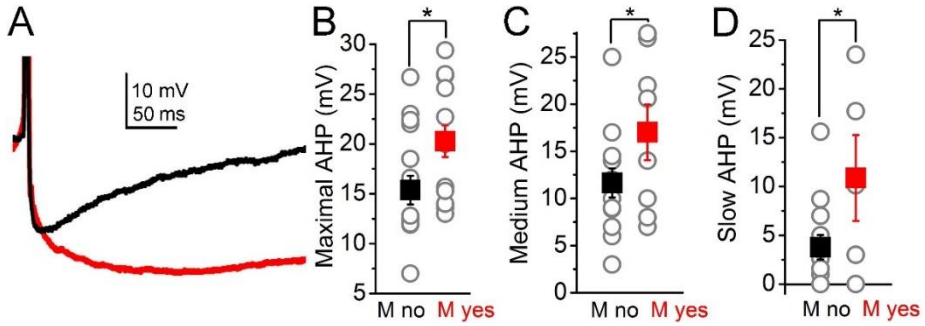

Fig 25. Differences in afterhyperpolarization by M-current in raphe serotonergic neurons. A. Two superimposed individual traces of afterhyperpolarization (AHP) from neurons with (red) and without M-current (black). **B-D.** Statistical comparison of the maximal (B), medium (C) and slow (D) afterhyperpolarization amplitudes.

Raphe serotonergic neurons display TTX-insensitive high threshold membrane potential oscillations with various amplitude and frequency. The presence or absence of M-current was not proved to be related to the intrinsic oscillatory activity. The oscillatory frequency at the power maximum was 21.67 ± 2.86 Hz for neurons possessing and 19.69 ± 2.21 Hz for lacking M-current (p = 0.29), whereas the power maximum was 1.95 ± 1.31 mV2/Hz for neurons possessing and 3.82 ± 3.39 mV2/Hz for ones lacking M-current (p = 0.33; Fig.14 G-H; Fig. 26).

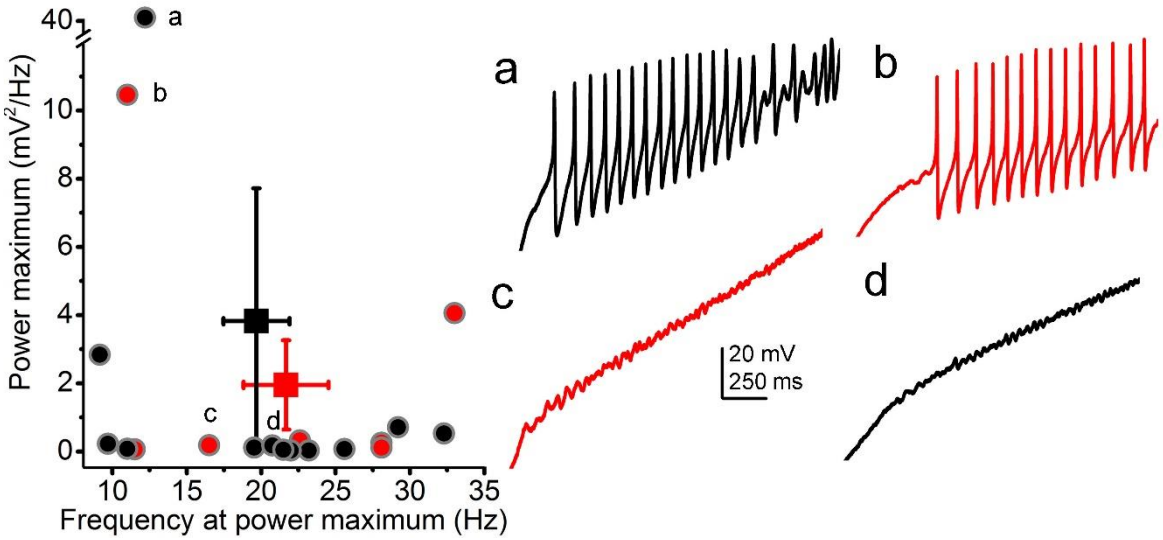

Fig. 26. Power maxima of raphe neuronal HTOs plotted against frequency values belonging to them (black: no M-current, red: M-current is present; gray circles filled with black or red color: individual data). Letters a-d indicate individual data and representative voltage traces belonging to them (black: no M-current, red: M-current is present).

Out of the correlations presented above, further correlations were identified between membrane properties that are not related to the M-current. The frequency of high threshold membrane potential oscillations was inversely proportional to the input resistance at power maxima (R^2 = 0.57), but the power amplitude was directly proportional to the input resistance (R^2 = 0.21; Fig. 27A-F). Moreover, the delay of the first action potential from the beginning of the depolarizing impulse from -80 mV was inversely proportional to the maximal firing rate (R^2 = 0.24; Fig. 27G-I).

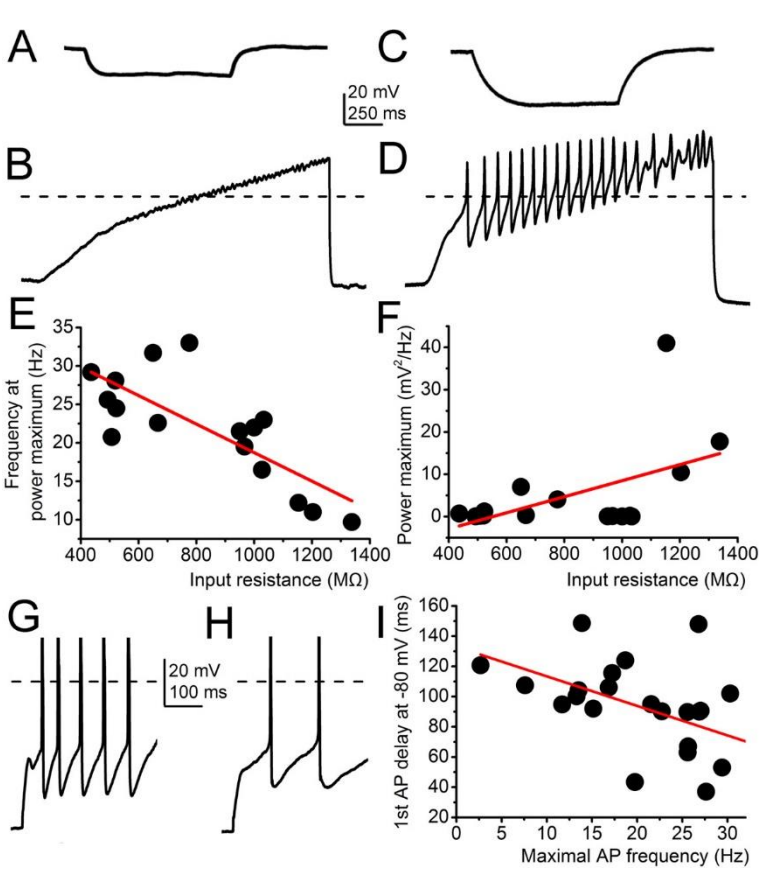

Fig. 27. Correlations of electrophysiological parameters not related to the M-current. A-F. Correlation between the input resistance and the parameters of high threshold membrane potential oscillations. **A.** Representative voltage trace elicited by hyperpolarizing current injection with -30 mV. **B.** High threshold membrane potential oscillations from the same neuron in the panel A. **C.** Representative voltage trace by hyperpolarizing current injection with -30 mV from another cell. **D.** High threshold membrane potential oscillations from the same neuron as on panel C. **E-F.** Correlations between the input resistance and oscillatory frequency (E) and oscillatory power maximum (F). **G-H.** Two representative voltage traces indicate the short delay and high maximal firing rate (G) and also another one with long delay and low maximal firing (H). **I.** Correlations for the two parameters described above (for arrangement see panels E and F).

6.6. PPN glutamatergic neurons are physiologically different from CnF neurons

6.6.1 Morphological features of glutamatergic neurons of the mesencephalic locomotor region

Slice electrophysiological experiments were achieved on PPN (n = 77) and CnF (n = 41) glutamatergic neurons of Vglut2-tdTomato mice (Figure 28-30). From the recorded tdTomato-positive neurons, randomly selected ones (PPN: n=15, CnF: n=11; Fig. 28A-B) were visualized with biocytin labelling, showing morphological differences between the two neuronal populations. CnF glutamatergic neurons had significantly higher number of dendrites than the PPN (5.11 ± 0.42 vs. 3.66 ± 0.33; p = 0.007). Similarly, there was also significantly larger number of endings in the CnF than in the PPN (20 ± 4.56 vs. 11.58 ±

1.73; p = 0.03). Furthermore, the number of nodes was also larger in the CnF, although with borderline significance (15 ± 4.38 vs. 8.08 ± 1.51; p = 0.05; Fig. 28C-D).

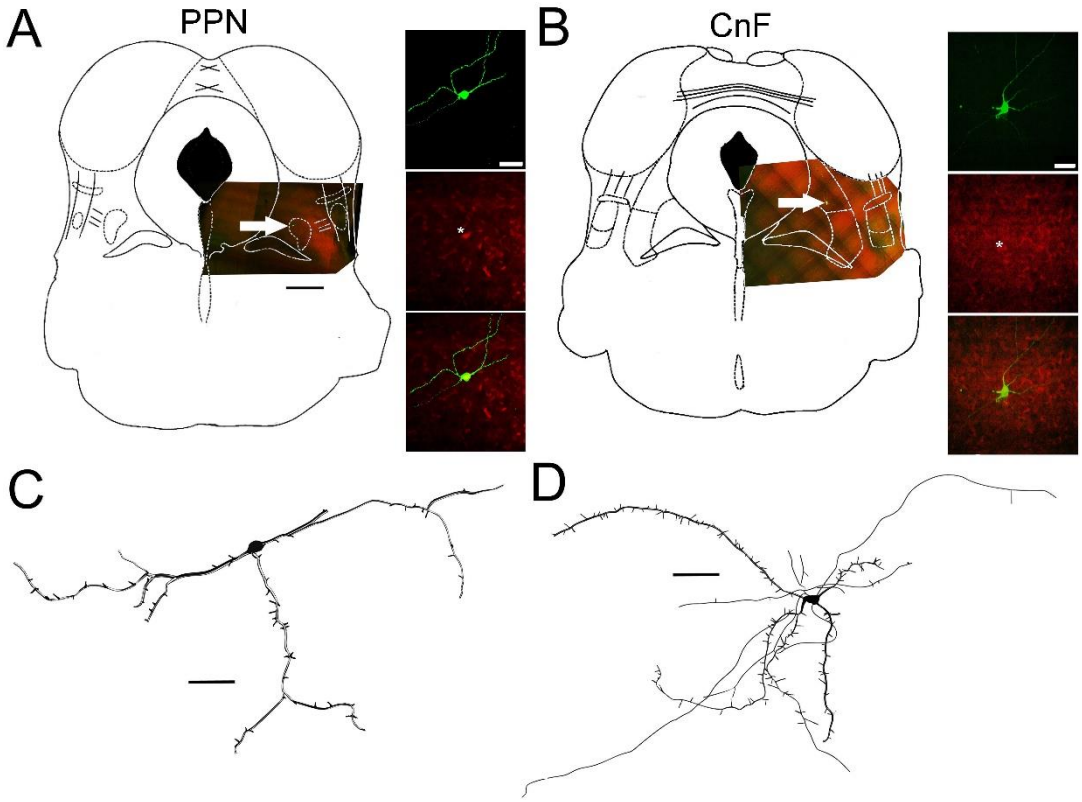

Fig. 28. Morphological differences of PPN and CnF glutamatergic neurons. A-B. Fluorescent images for PPN and CnF glutamatergic neurons acquired from VGLUT2-tdTomato mice after biocytin labelling. **C-D.** Representative glutamatergic neurons. Reconstruction from the PPN (C) and the CnF (D), from which the number of proximal dendrites, endings and nodes were analyzed.

6.6.2 Ionic currents and firing properties of the PPN and CnF

Several parameters were assessed from the functionally characterized neurons (Table 1). In 64 cases when depolarization-activated outward currents were assessed in the presence of TTX, we found that 91.4% of PPN and 79.3% of the CnF glutamatergic neurons possessed this current. The transient outward current can be recorded in the beginning of the depolarizing voltage step, which showed amplitude increase with hyperpolarizing prepulse (-120 mV), and fully disappeared after a depolarizing prepulse (+10 mV). The amplitude of the transient outward current was 395.13 ± 44.6 pA in the PPN and 352.49 ± 52.15 pA in the CnF, ranging between 158 and 1052 pA. Similarly, when depolarizing current injections were applied in current clamp mode from different resting membrane potentials, a marked increase in the delay of the first action potential appeared in several cases at hyperpolarized membrane potentials. When the resting membrane potential was kept on cca. -60 mV, the delay between the beginning of the 100 pA depolarizing square current injection and the first action potential was 31.27 ± 4.07 ms (ranging from 9.7 to 108 ms) in the PPN and 27.23 ± 7.95 in the CnF (ranging from 7.6 to 118.4 ms). When the resting membrane potential was set to -80 mV, the delay with the same current injection was 61.39 ± 8.9 ms in the PPN (ranging from 17.1 to 231 ms; n = 35, p = 0.0009 between values obtained from -60 and -80 mV resting membrane potentials) and 44.67 ± 10.64 ms in the CnF (ranging from 20.8 to 96.3 ms; n = 25, p = 0.09 between values obtained from -60 and -80 mV resting membrane potentials). No significant differences were found between datasets obtained from PPN and CnF neuronal populations (Table 1).

28.6 % of 58 recorded PPN neurons possessed low threshold transient depolarization. The maximal amplitude of this phenomenon was 17.65 ± 3.09 mV (from 6.1 to 32.3 mV), and it was recorded after 38.7 ± 5.5 pA current injection (from 20 to 60 pA), from resting membrane potential at -80 mV. On the same neurons, rebound transient depolarization were also detected (15.17 ± 2.99 mV, after -30 pA hyperpolarizing square current injection, from a resting membrane potential ranging between -50 - -60 mV (n = 58; from 7.2 to 24.6 mV; Table 1). Similar to the PPN, 31.03% of the CnF neurons had transient depolarization. The low threshold depolarization and rebound depolarization had an amplitude of 12.07 ± 2.17 mV (ranging from 4.6 to 18.3 mV) and 13.09 ± 1.79 mV (ranging from 8.9 to 23.6 mV), respectively (Table 1). Amplitudes of low threshold transient depolarization were reduced to 47 ± 22% of control by 100 nM agatoxin, whereas adding 1 µM conotoxin further reduced it to 58 ± 18% of the control.

Morphological parameters			
Parameter	**PPN**	**CnF**	**p**
Dendrite number	3.66 ± 0.33	5.11 ± 0.42	**0.007**
Node number	8.08 ± 1.51	15 ± 4.38	**0.05**
Ending number	11.58 ± 1.73	20 ± 4.56	**0.03**
Spine number	28.83 ± 8.7	32.11 ± 15.08	**0.42**
ChAT positivity (%)	3.4 ± 1.8 %	0 %	
Functional parameters			
Parameter	**PPN**	**CnF**	**p**
A-current amplitude (pA)	395.13 ± 0.33	352.49 ± 52.15	0.32
M-current amplitude (pA; at -40 mV)	6.38 ± 1.76	11.5 ± 2.41	0.04
Persistent Na-current amplitude (pA)	26.61 ± 5.41	5.31 ± 3.11	0.005
Action potential delay at -60 mV resting membrane potential (ms)	31.27 ± 4.07	27.23 ± 7.95	0.311
Action potential delay at -80 mV resting membrane potential (ms)	61.39 ± 8.9 (p=0.0009 between delays at -60 and -80 mV)	44.67 ± 10.64 (p=0.09 between delays at -60 and -80 mV)	0.169
Low threshold depolarization amplitude (mV)	17.65 ± 3.09	12.07 ± 2.17	
Rebound depolarization amplitude (mV)	15.17 ± 2.99	13.09 ± 1.79	
Input resistance (MΩ)	818.93 ± 41.94	792.54 ± 77.9	0.21

Table 1. Morphological and functional parameters of PPN and CnF glutamatergic neurons (n = 77 and 41, respectively)

Input resistance of glutamatergic neurons was recorded under control conditions, with employing -30 pA current injections from -60 mV resting membrane potential. When compared with input resistance data recorded from genetically identified cholinergic and GABAergic neurons (ChAT- and GAD2-tdTomato positive neurons, respectively) from the PPN, we found that the input resistance was 818.93 ± 41.94 MΩ for the glutamatergic neurons (n = 58), 567.3 ± 30.8 MΩ for the cholinergic neurons (n = 46), and 515.7 ± 41 MΩ for the GABAergic neurons (n = 26). Significant difference was revealed between the glutamatergic and GABAergic and the glutamatergic and cholinergic populations ($p < 0.0001$). CnF glutamatergic neurons had the input resistance of 792.54 ± 77.9 MΩ, which

was not significantly different from the PPN glutamatergic population ($p = 0.21$; $n = 37$), but showed significant differences with the PPN cholinergic ($p = 0.007$) and PPN GABAergic populations ($p = 0.006$).

6.6.3 Functional subgroups of MLR glutamatergic neurons

According to the classical electrophysiological subgroups by Kang and Kitai (1990) and Leonard and Llinas (1990, 1994), PPN neurons are grouped by the presence or absence of the A-current and calcium currents (or parameters caused by these currents in current-clamp configuration as the delay of the first action potential or appearance of low threshold depolarizing humps). Group I neurons possess low threshold depolarizing humps but lack A-current; group II neurons have A-current; whereas group III neurons possess both. Kang and Kitai (1990) described a distinct population where none of the functional features described above appear. In order to prevent confusion by different classifications, we will refer to this subgroup as IIIK group. In the PPN, glutamatergic neurons mostly belonged to group II, as 65.7% of all cells fell into this category. The second most abundant group was the III, to which 28.6% of the neurons belonged. The rest of the neurons (2.85-2.85%) were classified as group I or IIIK. Similar to the PPN, among CN glutamatergic neurons, the greatest group of neurons (55.6%) was the group II; but, unlike the PPN, the second greatest group was the IIIK with 22.2%. The group III neurons were 18.5% of the whole population, whereas the rest (3.7%) belonged to group I. Taken together, the only difference between the distributions of the classical functional subgroups between PPN and CN glutamatergic neurons is the appearance of the neuronal population lacking both A-current and low threshold depolarizing humps.

Out of the classical electrophysiological neuronal subtypes of the PPN (Kang and Kitai, 1990; Leonard and Llinas, 1990, 1994), functional subgroups based on changes of spike frequency adaptation with increasing depolarization can also be defined. We observed that certain neurons have a more-or-less constant adaptation index (Nigro et al, 2014), other ones have a gradual increase of this parameter with increasing depolarizing steps, and further neurons cease firing at the end of the greater depolarizing step, but have a high frequency burst at the beginning of the trace. Although changes of the adaptation index might form a dynamical scale, we grouped the neurons according to the following criteria: the neurons with constant adaptation index (called „non-adapting") had less than 50% increase in the adaptation index of the action potential trains obtained with 50 and 120 pA current injections;

the ones with increasing adaptation index („slowly adapting") had more than 50% change of the adaptation index between the same traces, but fired during the entire 1-s-long depolarizing step, whereas the rest of the neurons stopped firing after application of higher depolarizing steps („rapidly adapting"). The amplitude of the last action potential compared to the first action potential of the train elicited with 120 pA depolarizing current injection on neurons of the "non-adapting" group was 79 ±5% (Fig. 29), whereas the action potential width was 117 ± 5% of the first action potential. The amplitude of the last spike in the slowly and rapidly adapting groups were 61 ± 3% and 39 ± 11% and the width was 162 ± 6% and 205 ± 30% of the first spike (n = 8 and 10), respectively (Fig. 30A-C). 30.2% of all neurons (13/43 neurons) in the PPN were non-adapting and were found mostly in the lateral areas, whereas 21% (9/43 neurons) were slowly adapting and 48.8% (21/43 neurons) were rapidly adapting. Contrarily, in the CnF most neurons (85.7%, 24/28 neurons) were rapidly adapting, and non-adapting and slowly adapting composed equally smaller proportions (7.15%, 2/28 neurons for each group; Fig. 30D). Therefore, the responses of MLR glutamatergic neurons to spike adaptation show important functional group differences in the composition of the PPN and the CnF ranging from firing frequency to adaptation index. Our results thus support differences in the connections of PPN and CnF glutamatergic neurons with different motor circuits (Fig 30E).

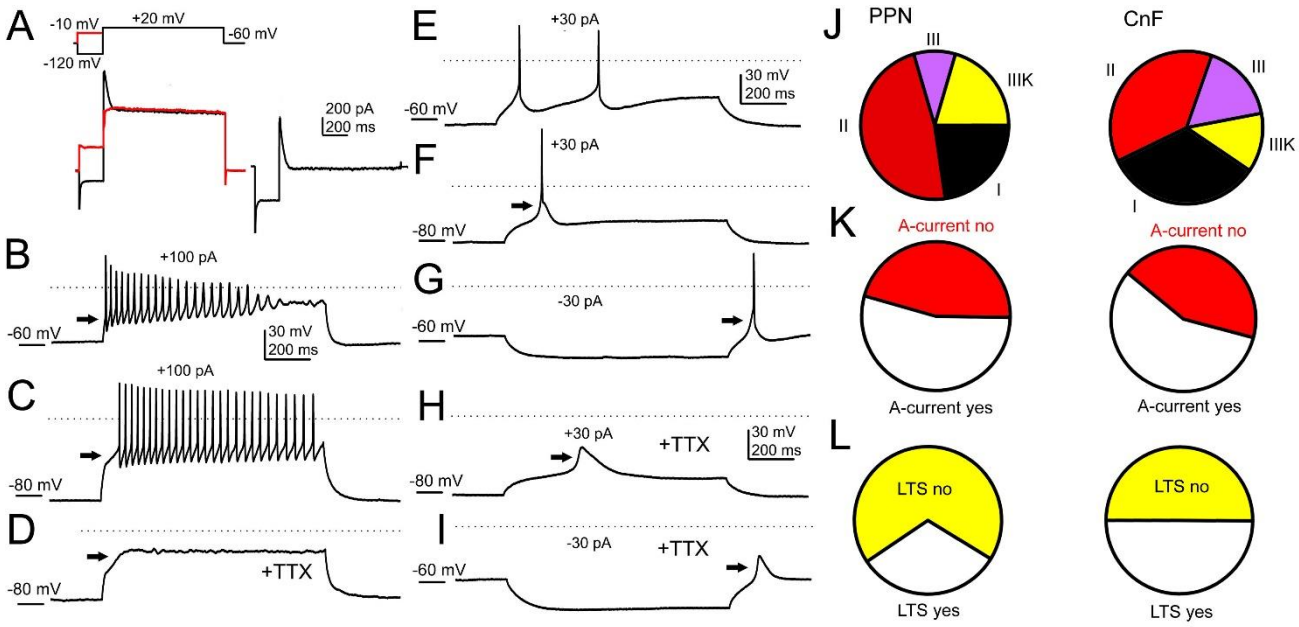

Fig. 29. Biophysical characteristics of the PPN and CnF glutamatergic neurons. A. Recording of A-current from PPN and CnF glutamatergic neurons. Current traces obtained by +20 mV voltage step, preceded by -120 mV (black) and -10 mV (red) voltage steps (example shows PPN). The difference of the current traces (black and red) is on the left side. B-D. Representative firing properties of PPN glutamatergic neurons. Trains of action potentials obtained by 100 pA depolarizing current injection from -59 mV (B), -87 mV (C) and -73 mV resting membrane potential (D, in the presence of TTX; the arrow shows the lack of delay). E-I. Depolarization and action potential firing obtained by 30 pA depolarizing square current injection from -66 mV (E) and -83 mV (F) resting membrane potentials. Note the low threshold depolarizing spike (black arrow). (G) 30 pA hyperpolarizing current injection from -53 mV resting membrane potential showed rebound spike and firing (black arrow). H-I. Low threshold spike and rebound depolarizing spike (respectively; arrow) in the administration of TTX. J. Proportion of functional neuronal types in the PPN and CnF. K. Proportion of A-current displaying neurons in PPN and CnF. L. Proportion of low threshold spikes (LTS) displaying neurons in PPN and CnF. All data are represented as average ± SEM.

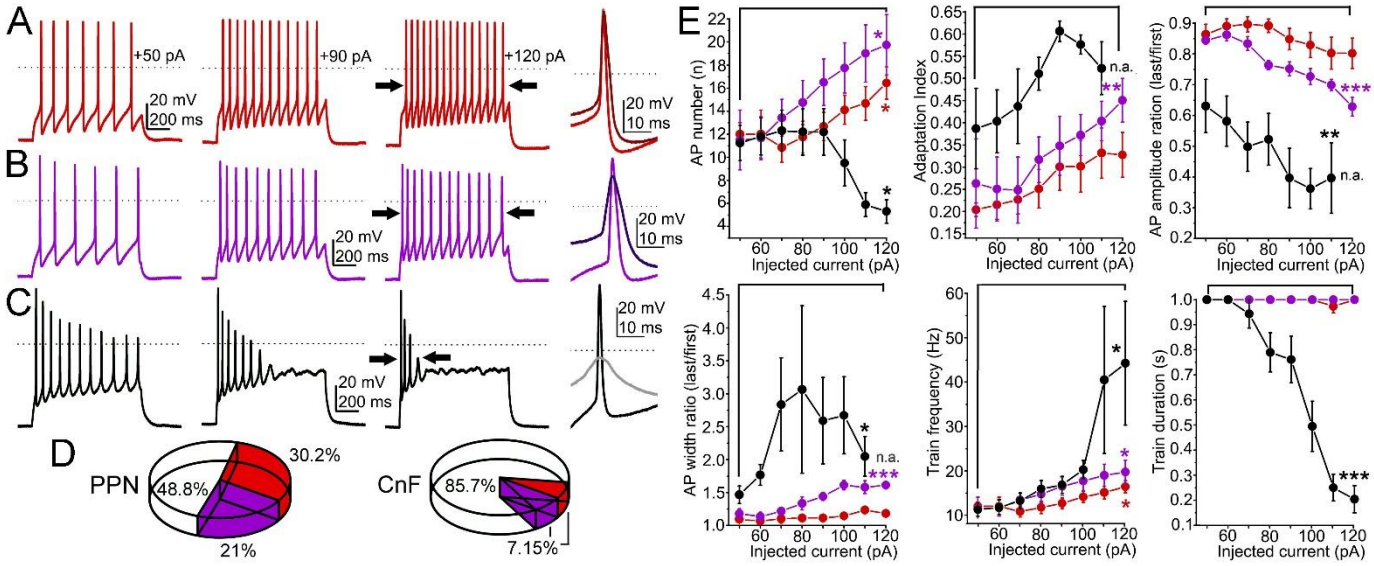

Fig. 30. Physiological properties of MLR glutamatergic neurons. A-C. Spike frequency adaptation changes by increasing depolarizing steps showed functional subtypes of glutamatergic neurons defined as (A) 'non-adapting': less than 50% increase in the adaptation index of the action potential trains acquired with 50 and 120 pA current injections; (B) 'slowly-adapting': greater than 50% change of the adaptation index but fired during the whole 1-s-long depolarizing step; and (C) 'rapidly-adapting': stopped firing after the higher depolarizing steps. **D.** Neuronal proportions with distinct spike frequency adaptation properties in the PPN and the CnF. **E.** Statistical summary for the number of action potentials obtained by 1-s depolarizing step, the adaptation index, the ratio of the amplitude and width of the last and first action potentials of the train; the frequency and the duration of the train in different functional subgroups (non-adapting, red; slowly adapting, purple; rapidly adapting, black). The significance was checked between the first and last datapoints within each trace. * $p<0.05$, ** $p<0.01$, *** $p<0.001$. All data are represented as mean ± SEM.

6.6.4. High threshold membrane potential oscillations of the MLR glutamatergic neurons

It was shown by several authors that certain PPN neurons possess calcium- and potassium-channel dependent high threshold membrane potential oscillations (Simon et al, 2010; Kezunovic et al, 2012). We previously confirmed that cholinergic neurons possess these oscillations even in the presence of TTX, but GABAergic and non-cholinergic populations lack it (Bordas et al, 2015). Using the same depolarizing ramp current injection, we showed that 28 from 29 glutamatergic neurons lacked oscillatory activity in the presence of TTX. However, in a single case, oscillatory activity similar to the ones observed on

cholinergic neurons was seen. This neuron belonged to the overlapping glutamatergic-cholinergic population. In the CnF, no TTX-resistant oscillation was observed.

In accordance with the literature (Simon et al, 2010), we observed TTX-sensitive oscillatory activity on the PPN glutamatergic neurons. On almost all PPN glutamatergic neurons, TTX-sensitive oscillatory activity was identified in the range of 7-40 Hz. Comparing power spectra before and after TTX application, significant difference was seen at the frequency range between 7 and 17 Hz. In the CnF, this oscillatory activity was weaker and restricted to certain neurons. Power spectra revealed similar average frequency ranges of oscillatory activity in both the PPN and CnF, but with a higher standard deviation in the latter population. When TTX was applied, power reduction was seen at all frequencies, but -due to the high standard deviation- no significant difference was found between the control and TTX action. One can conclude that TTX-sensitive oscillations can be found on PPN glutamatergic neurons, but only a subset of CnF neurons possess this oscillatory activity.

A potential reason of differences between TTX-sensitive oscillatory activity of PPN and CnF is the presence or absence of persistent sodium current. This current was revealed as the TTX-sensitive current recorded with using a depolarizing voltage ramp protocol. When recoded from PPN glutamatergic neurons, 9 from 11 possessed persistent sodium current with an average of 32.5 ± 4.5 pA (ranging from 26 to 58.7 pA). When all 11 cases were considered, the average current amplitude was 26.6 ± 5.4 pA. In the CnF, only 3 from 7 neurons had persistent sodium current, with an average of 12.4 ± 4.9 pA (ranging from 7 to 22.2 pA). When all cases were considered, the average current amplitude was 5.3 ± 3.1 pA. The difference between the two populations was statistically significant ($p = 0.0002$).

Furthermore, we characterized the oscillatory activity of glutamatergic neurons of the PPN and CnF. Oscillatory activity in the 10-20 Hz range was seen on PPN glutamatergic neurons ($n = 24$ neurons) was sensitive to TTX (Fig. 31A). Contrarily, oscillatory activity in the 20-40 Hz was rather characteristic for the CnF ($n = 19$ neurons) but it had smaller amplitude and it was predominantly insensitive to TTX (Fig. 31B). Power spectra showed similar average frequency ranges of oscillatory activity in the PPN and CnF, but with a higher standard deviation in CnF neurons. TTX-resistant oscillations were not found in these structures. Moreover, persistent sodium currents were characteristic for the PPN (9/11 neurons, range from 26 to 58.7 pA, average 32.5 ± 4.5 pA; Fig. 31D), and to a much minor extent in the CnF (3/7 neurons, range from 7 to 22.2 pA, average 12.4 ± 4.9 pA; Fig. 31I),

suggesting the role of such currents in the oscillatory activity observed in PPN neurons. In conclusion, PPN glutamatergic neurons form a heterogeneous group and display robust, wide-range oscillatory activity and the presence of persistent sodium currents. Contrarily, CnF glutamatergic neurons are rather fast-adapting with no persistent sodium currents.

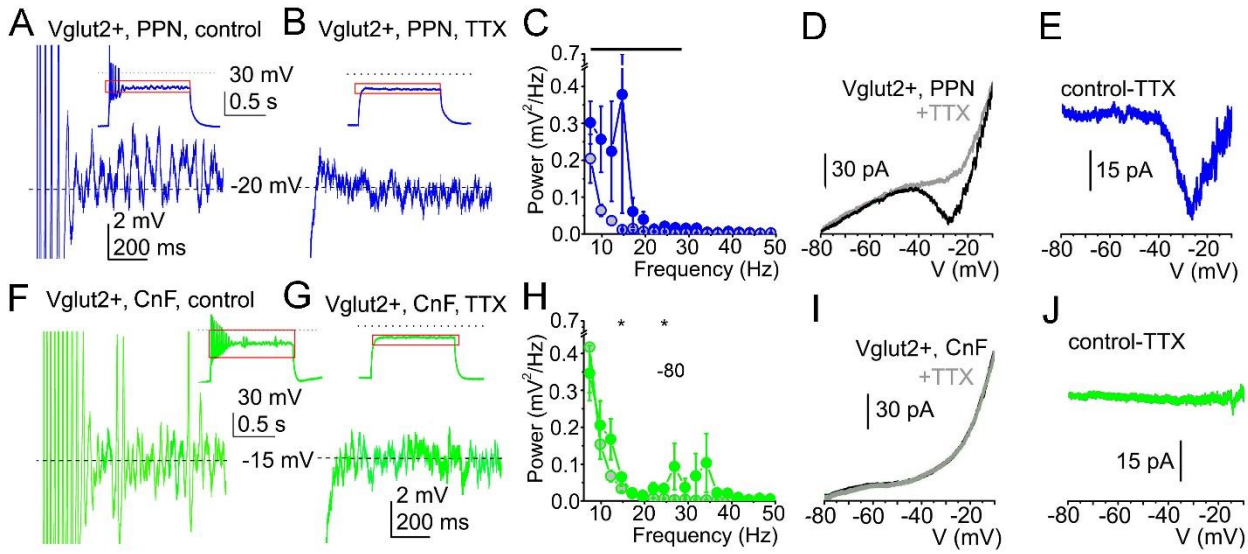

Fig. 31. Functional differences in oscillatory activity of PPN and CnF glutamatergic neurons. Voltage traces from PPN (**A-E**) and the CnF (**F-J**) glutamatergic neurons in the representing high threshold oscillations during 120 pA depolarizing square current injections in control conditions (**A,F**) and in presence of TTX (**B,G**). Power spectra **C,H** (average ± SEM; PPN control, blue circles; PPN+TTX, gray circles with blue contours; CnF control, green circles; CnF+TTX, gray circles with green contours). **D-E; I-J.** Representative current traces from the PPN (**D-E**) and the CnF (**I-J**) neurons obtained by voltage ramp injections in control conditions (black) and presence of TTX (gray; left). TTX-sensitive currents shown on the right panels (PPN, blue; CnF, green). Scale bars: A-B: 0.5mm, C-D: 50µm. * $P < 0.05$. All experiments have been repeated at least 3 times. Group value and statistics are provided in Table 1. All data are represented as mean ± SEM.

7. Discussion

In the frame of my PhD study, the following findings were presented.

1. The M-current can be considered an electrophysiological hallmark of PPN cholinergic neurons, as cholinergic neurons rarely lack it and glutamatergic or GABAergic neurons rarely possess it.
2. Inhibition of the M-current decreases synchronization of neighboring PPN cholinergic neurons.
3. A subpopulation of PPN cholinergic neurons possess the KCNQ4 subunits which are responsible for M-current.
4. Deletion of KCNQ4 subunit causes mild alterations in adaptation to changes of environmental changes of light and darkness.
5. The M-current possessing serotonergic raphe neurons are topographically organized, as they are found rostrally in the DR and dorsally in the MR.
6. Glutamatergic neurons of the PPN and CnF form overlapping but distinguishable populations but they can be distinguished on the basis of differences in somatodendritic morphology and certain electrophysiological parameters (as adaptation index, persistent sodium current and membrane potential oscillations).

7.1. The M-current is a hallmark of cholinergic neurons of the PPN

Several previous studies have shown that the M-current is present on different structures of the RAS (in the raphe nuclei and the VTA; Drion et al., 2010; Zhao et al., 2017; Su et al., 2019). It has been demonstrated in a previous publication and PhD defense from our laboratory that the M-current seems to be an electrophysiological hallmark of PPN cholinergic neurons; as cholinergic neurons had it but GABAergic ones lacked it. This current is capable of regulating excitability-related parameters and firing properties as SFA (Bordas et al., 2015). In this work, we involved glutamatergic neurons in our study and showed that the majority of this neuronal group lacks M-current. With this finding, we provided support for the previous findings. Immunohistochemical labelling of the KCNQ subunits also confirmed this statement. Our collaborating partners showed that different KCNQ subunits are present in the PPN on mRNA-and protein levels (Fig.32). Almost all

KCNQ subunits were found on identified cholinergic neuronal somata with the exception of KCNQ2. The KCNQ channels can be formed by heterotetramers of KCNQ3 and -4, KCNQ3 and -5 or KCNQ4 and -5 in the PPN. Our recent findings –based on novel electrophysiological results and immunohistochemistry- supports the previous claim that the M-current is a functional hallmark of PPN cholinergic neurons but absent from GABAergic and glutamatergic populations. Only one exception was found as there are neurons with both glutamate and acetylcholine as co-transmitters. This population is rather similar to cholinergic than glutamatergic neurons, as they possess M-current (Baksa et al, 2019).

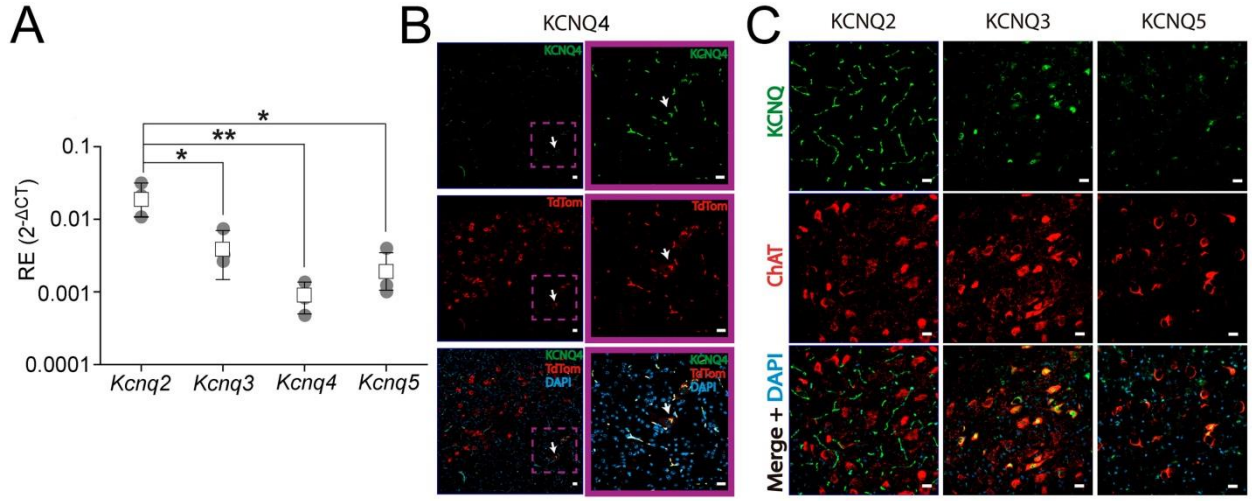

Fig.32. The presence of KCNQ subunits on mRNA- and protein levels. A. KCNQ2-5 subunit mRNA expression (hollow square: average ± SEM; gray circles: individual data; RE: relative expression level calculated with $2^{-\Delta CT}$). **B.** KCNQ4 immunohistochemical labelling (green, upper panel) on PPN of ChAT-tdTomato mice (tdTomato expression: red). Purple squares indicate the magnified area on panels with purple frames. Arrows indicate a KCNQ4-positive cholinergic neuron. **C.** KCNQ2, -3 and -5 immunohistochemical labelling on PPN neurons (green) and its co-localization with ChAT immunohistochemistry (red). Scale bar: 20 µm on all panels. This experiment was performed by the Spitzmaul Lab (Bahia Blanca, Argentina).

7.2. The M-current synchronizes neighboring PPN cholinergic neurons

Our laboratory previously demonstrated that the M-current can effectively set SFA (Bordas et al., 2015). In accordance with data based on modelling of cortical regions (Roach et al., 2015, 2016; Leão et al., 2009), we showed that SFA increases synchronization level of the neighboring cholinergic neurons. The M-current blockade decreased SFA. In parallel with this, the synchronization between two neighboring neurons was also reduced. Moreover, we demonstrated that this effect might have physiological significance as the M-current reduction can take place via stimulation of the cholinergic inputs to the nucleus.

These findings indicate that cholinergic inputs of the PPN are capable of desynchronization of its cholinergic neuronal populations. Under physiological conditions, this action can be even more robust, as there is an abundance of cholinergic inputs to the PPN. PPN cholinergic neurons give rise to local cholinergic collaterals, send cholinergic fibers to the contralateral PPN and targeted by cholinergic inputs from the LDT (Honda and Semba, 1995; Mena-Segovia et al., 2008). These inputs together might effectively desynchronize the cholinergic populations of the PPN. Desynchronization of PPN neuronal populations is observed in parallel with cortical desynchronization (Mena-Segovia et al., 2008; Boucetta et al., 2014; Petzold et al., 2015). One can conclude that blockade of the M-current by cholinergic inputs contributes to autoregulatory desynchronization of cholinergic areas, which, in turn, regulates global brain states.

7.3. The KCNQ4 subunit is present on a subset of PPN cholinergic neurons

Neuronal ion channels responsible for M-current are often composed of homomeric KCNQ2 or KCNQ5, as well as heteromers of KCNQ2 and 3 subunits in most cases (Shah et al., 2002; Brown and Passmore, 2009; Soldovieri et al., 2011; Huang and Trussell, 2011). In the Heteromers formed by KCNQ2/KCNQ3 subunits can be found on axon initial segments and nodes of Ranvier, which regulate action potential firing (Schwarz et al., 2006; Klinger et al., 2011). Neuronal networks of the hippocampus are synchronized by channels formed by postsynaptic KCNQ5 subunits (Fidzinski et al., 2015). KCNQ5 subunits were also shown on the axon terminal where channels formed by them regulate neurotransmitter release (Huang and Trussell, 2011). Heteromers of KCNQ3 and KCNQ5 subunits can also be found in the

brain (Jentsch, 2000; Delmas and Brown, 2005). Besides the best described locations of KCNQ4 in the peripheral sensory systems (cochlear outer hair cells, DRG, Merkel- and Pacinian corpuscules), this subunit is found in certain brainstem nuclei. It is only found in auditory nuclei and members of the RAS, as well as trigeminal nuclei (Kubisch et al., 1999; Kharkovets et al., 2000; Beisel et al., 2005; Heidenreich et al., 2011). Within RAS, the location and function of the KCNQ4 subunit was formerly demonstrated in the raphe nuclei and the VTA with morphological methods, but the functional descriptions of it has only been recently published (Zhao et al., 2017; McGuier et al., 2018; Su et al., 2019).

In this work, we employed morphological and pharmacological methods and transgenic animals to show the presence of the KCNQ4 in the PPN. Different research methods demonstrated the functional and morphological presence of KCNQ4 on a fraction of PPN cholinergic neurons in a range between 9 to 62.5%. Similar to our findings, it was previously found that only a subpopulation of the neurons has this subunit in the DRG and the DR (Heidenreich et al, 2011; Zhao et al, 2017). The significance of these subpopulations has not been determined yet and further investigation is needed to show it. However, it seems to be likely that this population might be somehow involved in regulation of the startle response (Kharkovets et al, 2000).

The KCNQ4 subunit is not the only identified KCNQ subunit of the PPN cholinergic neurons, as KCNQ3 and KCNQ5 were also found both in WT and KO animals. However, the expression of KCNQ3 was significantly altered in KO animals together with a great reduction in M-current. These findings might indicate that KCNQ4 has a role in KCNQ channel assembly and forms functioning heteromers with other KCNQ subunits (Kharkovets et al., 2000, Heidenreich et al., 2011).

A great difference was seen between the proportion of neurons possessing KCNQ4 subunits (9.0%) and the proportion of neurons having functional KCNQ4 subunits presented by subunit-specific openers (14.0-27.0%). These differences found by using WT animals could be due to the limitations of the techniques employed. One cannot exclude that the theoretically KCNQ2- and -4 subunit specific opener ML213 also slightly activate KCNQ5 subunits (Brueggemann et al., 2014). An even greater difference is seen between pharmacological experiments on WT animals revealing functional KCNQ4 channels and in the proportion of neurons lacking M-current in KCNQ4 KO mice (62.5%). The greater differences between data obtained from WT and KO mice are probably due to the changes in

expression of other KCNQ subunits or other potassium channels in KCNQ4 KO mice. The fact that differences in AI between WT and KO were seen on non-cholinergic cells also suggests that probably other potassium channels can be affected by the alteration in KCNQ4 expression.

Several changes of KCNQ subunit mRNA- and protein are seen in KCNQ4 knockout. As expected, the KCNQ4 subunit disappears and KCNQ2- and -5 does not change significantly. However, KCNQ3 subunit is upregulated and mostly appears in non-cholinergic neurons. It is very likely that these subunits do not form functional channels or homomers as we have not found M-current on KCNQ4 KO non-cholinergic neurons (Brown and Passmore, 2009).

However, we demonstrated alterations of other membrane properties of these neurons. The AI of the non-cholinergic was significantly smaller than on the cholinergic ones in WT mice. Unexpectedly, this parameter of the non-cholinergic cells was found to be significantly reduced in KO compared to WT. As several other potassium- and chloride channels influence AI, this finding is probably due to the altered expression of other potassium (or probably chloride) channels (Ha and Cheong, 2017).

In parallel with several pathological conditions (as retinal degeneration, hypertension or vascular tumors), alterations of KCNQ subunit expression and consequential changes of cellular membrane properties were described (Caminos et al., 2015; Jepps et al., 2011; Serrano-Novillo et al., 2020). In our project, we had similar findings, as the lack of KCNQ4 expression was capable of influencing expression and function of other ion channel subunits. One can conclude that the KCNQ4 is probably not only important as one of the ion channel subunits responsible for neuronal potassium currents, but also a potent regulator of the expression of other ion channel subunits.

7.4. Ion channels formed by KCNQ4 subunits critically affect adaptations to changes in light-darkness conditions

Based on our experiments, we concluded that the lack of KCNQ4 subunit (and further disturbances of other ion channel subunits) disturbed adaptation of the circadian rhythm to the changes of environmental light conditions. KO mice adapted to environmental darkness with longer distances ran. Compared to WT, the standard deviation of the datasets was also increased. These disturbances are likely due to the altered functions of the RAS, as the hearing loss is mild in this range of age (cca. 2-month-old mice; Carignano et al., 2019). One can also probably conclude that changes in environmental light conditions have no impact on tactile sensation, which strengthens the conclusion that the functions of the RAS are affected. With our experiments –as constitutional and not conditional knockout animals were employed- one cannot exclude that changes of neuronal excitability and firing pattern of the VTA and raphe nuclei also contribute to the observed actions (Zhao et al., 2017; McGuier et al., 2018; Su et al., 2019). These structures, together with the PPN, regulate movement and activity cycles (Monti, 2010; Mena-Segovia and Bolam, 2017; Zhao et al., 2017; McGuier et al., 2018; MacLaren et al., 2018; Su et al., 2019; Jing et al., 2019). One can draw the conclusion based on these findings and the literature that the KCNQ4 of the RAS can regulate sleep-wakefulness cycles, as well as movement (Kroeger et al., 2017).

The DFNA2 non-syndromic hearing loss is the best known pathological condition caused by KCNQ4 mutation. The term 'non-syndromic' was first challenged by the observation of enhancement of tactile sensation (Heidenreich et al, 2011). We provided further support of the previous finding that DFNA2 is probably not 'non-syndromic', as the adaptation to environmental light conditions and changes in movement are probably also affected by KCNQ4 loss. However, further research is needed to demonstrate whether humans with DFNA2 also have alterations in the same parameters.

As a conclusion, one can assume that M-current via channels from KCNQ4 subunits regulate adaptation of the circadian rhythm to environmental illumination.

As expression of KCNQ4 subunit is restricted to certain RAS nuclei in the PPN, KCNQ4-specific openers might serve as drugs for treating diseases related to anxiety or sleep disturbances (Sotty et al., 2009; Zhao et al., 2017; McGuier et al., 2018; Su et al., 2019). Furthermore, as KCNQ4-dependent M-current reduces the excitability of neurons possessing

it, these openers might have a role in slowing progression of neurodegenerative diseases with loss of PPN cholinergic neurons (as e.g. progressive supranuclear palsy; MacLaren et al., 2018). These openers might be also used for helping adaptation to artificial changes of the circadian rhythm by jet lag or space travel (Brainard et al., 2016).

7.5. The M-current of raphe serotonergic neurons is topographically distributed

Based on our data and consistent with the literature, we concluded that several but not all serotonergic neurons of the MR and DR possess M-current. DR serotonergic neurons have this current is a somewhat greater proportion than in the MR. As it has been already known from other structures, the M-current regulates AHP kinetics, SFA and firing frequency. In contrast with the previous findings of the laboratory on PPN cholinergic neurons, the M-current does not seem to regulate HTOs (Bordas et al, 2015).

We also showed that DR and MR serotonergic neurons possessing M-current is found in certain locations within these nuclei. Besides findings related to the M-current, it was also shown that parameters of HTOs correlate with the input resistance and the delay of the first action potential is inversely proportional to the maximal firing frequency.

As it is well known from the literature of other brain areas, the M-current determines SFA, AHP morphology and neuronal excitability (Koyama and Appel, 2006; Tzingounis et al, 2010; Nigro et al, 2014; Bordas et al, 2015). We demonstrated that, similar to other cortical and brainstem areas, AHP and SFA are also influenced by M-current in the raphe nuclei. Differences in afterhyperpolarization kinetics were previously shown between DR and MR serotonergic neurons and between different areas of the DR (Beck et al, 2004). As AHP is influenced by the M-current and we revealed differences in proportions of neurons having M-current in different raphe regions, these differences in M-current might explain the regional differences of AHP.

To our knowledge, this is the first demonstration that HTOs are present on raphe serotonergic neurons. Surprisingly, in contrast with the previous findings of the laboratory on PPN cholinergic neurons (Bordás et al, 2015), the presence or absence of the M-current does not influence this phenomenon. Rather, the power amplitude of these oscillations is

directly, the oscillatory frequency at power maximum is inversely proportional to the input resistance.

It is well revealed by literature data that DR and MR serotonergic neurons have different subgroups in terms of projection, neurochemical markers, development and gene expression, as well as in vitro and in vivo electrophysiological properties. Raphe serotonergic neurons developmentally originate from six rhombomeres and neurons from different rhombomeres display differences in gene expression pattern. Raphe serotonergic neurons have 11 transcriptomic clusters; among which, besides other important differences, genes encoding ion channels are also expressed in a different way and contribute to forming distinct neuronal populations within raphe serotonergic neurons (Ren et al, 2019; Okaty et al, 2015).

Different regions of raphe nuclei (namely, the MR and the rostral dorsal, the dorsal, the ventral parts and the lateral wing of the DR) project to different brain areas (Hale and Lowry, 2011). The MR projects to septohippocampal systems and hypothalamic areas inhibiting the hypothalamic-pituitary-adrenal system (Vertes et al., 1999; Hale and Lowry, 2011,). The rostral DR sends axons to substantia innominata, basal ganglia and the motor cortex (Imai et al., 1986; Waterhouse et al., 1986; Grove, 1988; Canteras et al., 1990; Hale and Lowry, 2011). The dorsal DR projects to the nucleus accumbens, the amygdala, and the medial prefrontal cortex (Van Bockstaele et al., 1993; Kathryn et al., 2003; Hale et al., 2008; Hale and Lowry, 2011). The ventral DR innervates the caudate putamen and cortical areas (Steinbusch et al., 1980; Waterhouse et al., 1986; Hale and Lowry, 2011). The lateral wing of the DR projects to brainstem structures, the lateral hypothalamus, and structures involved in visual processing (Waterhouse et al., 1993; Ljubic-Thibal et al., 1999; Hale and Lowry, 2011). According to the projections, the DR has a topographical organization along its dorsoventral axis (Ren et al., 2018).

DR and MR serotonergic neurons projecting to the basolateral amygdala, the dorsal hippocampus and the medial prefrontal cortex have different firing properties. Neurons projecting to the basolateral amygdala had significantly lower AHP amplitude than others (Fernandez et al, 2016), DR neurons sending axons to the forebrain fire bursts (Hajós and Sharp, 1996, Hajós et al., 2007). Based on firing frequency and action potential morphology, lateral wing DR neurons are also distinct from the ones in ventromedial location (Crawford et al., 2010).

The existence of raphe neuronal subgroups was further supported by in vivo electrophysiological studies. A subpopulation phase-locked to hippocampal theta rhythm was distinguished from another one not related to this rhythm but possessing clock-like activity (Kocsis et al., 2006). Furthermore, the burst firing neuronal subgroup of the DR can be distinguished on the basis of its in vivo electrophysiological properties (Gartside et al., 2000).

The MR and the various subregions of the DR have certain well established functional differences. Development of phobic and anxietic syndromes is caused if DR activity is stronger than MR activity, whereas stronger MR activity facilitates development of psychotic syndromes (Lechin et al., 2006). Amygdala-projecting serotonergic neurons of the DR are active during anxiety, whereas frontal cortex projecting ones stimulate active coping with challenges (Ren et al., 2018).

The M-current of the PPN has an important contribution to autoregulation and neuronal synchronization (see above). The best known regulatory mechanism on the M-current is its inhibition via muscarinic activation (Brown and Passmore, 2009). Based on this, it is feasible to hypothesize that serotonergic neurons with M-current are extensively regulated by cholinergic inputs. However, besides this regulation on M-current, the role of 5HT2C receptor in regulation of the M-current is also known (Roepke et al., 2012). One can also hypothesize that the M-current is a tool of serotonergic autoregulation of this nucleus. These cholinergic or serotonergic neuromodulatory actions might target the dorsal MR and the rostral DR. The rostral DR is known to contribute to movement-related stress tolerance (Greenwood et al., 2003; Hale and Lowry, 2011), whereas the MR has a role in adaptation to chronic psychosocial stress (Graeff et al., 1996; Hale and Lowry, 2011), neuromodulatory regulation by M-current could be a mechanism for adaptation to stress. In agreement with the recent literature (Zhao et al, 2017) we can conclude that M-current is a possible target for anxiolytic therapy.

7.6. CnF and PPN glutamatergic neurons are functionally distinct

The MLR is a functionally-defined mesencephalic area consisting of the PPN and the cuneiform nucleus (CnF), which has been typically identified as an output station of forebrain systems reaching lower motor circuits (Capelli et al., 2017, Kim et al., 2017, Garcia-Rill et al., 1983). Activation of these structures has been proposed to evoke different types of movement, but how the differences in morphological and functional properties underline their roles in regulation of motor activity is not clear yet.

Based on our finding, we showed that CnF glutamatergic neurons are more homogeneous electrophysiologically than PPN neurons. For the physiological characteristics, we showed that PPN neurons composed of a heterogeneous group displaying a range of adapting responses, whereas most CnF neurons are fast-adapting. In the PPN, 48.8% of recorded neurons were fast-adapting neurons, 30.2% non-adapting neurons, and 21% slow adapting, suggesting that neuronal profiles are more heterogenous than in the CnF.

Furthermore, in accordance with the data from our collaborating partner (Dr. Juan Mena-Segovia), CnF glutamatergic neurons have mostly short-range connectivity, but PPN glutamatergic neurons are heterogeneous and maintain long-range connections, particularly with the basal ganglia. CnF neurons produced short-lasting muscle activation driving involuntary motor activity by optogenetic activation. On the other hand, PPN neurons activation produced long-lasting increases in muscle tone that reduced motor activity and disrupted gait. These results highlight key biophysical and functional feature among MLR neurons that support their differential contribution to motor behavior in normal and pathological conditions.

8. SUMMARY

The pedunculopontine nucleus (PPN) is a cholinergic area of the reticular activating system (RAS). It is a source of cholinergic neuromodulation which also undergoes cholinergic autoregulation. It contributes to regulation of sleep-wakefulness cycles and movement as a part of the mesencephalic locomotor region (MLR). Rostral serotonergic members of the RAS are the dorsal and median raphe nuclei (DR and MR, respectively) which are also targeted by cholinergic neuromodulation and involved in regulation of sleep-wakefulness cycles, movement and affective states.

The M-current is a voltage-gated potassium current which is under regulation of several G-protein coupled receptors as muscarinic acetylcholine receptor. Channels for the M-current are composed of KCNQ (Kv7) subunits. Particularly, KCNQ4 expression is exclusively found in some brainstem structures as RAS nuclei in the central nervous system (CNS).

In this project, the presence and functional significance of KCNQ4 in the PPN was tested using morphological, behavioral and electrophysiological studies. We found that the lack of KCNQ4 leads to alterations in adaptation of activity to environmental light conditions. Although the M-current is an electrophysiological hallmark of the cholinergic neurons, only a subpopulation of these neurons possessed KCNQ4-dependent M-current. Cholinergic innervation of the PPN can effectively inhibit M-current in wild type (WT) animals. This current is involved in synchronization of neighboring PPN neurons and neuronal synchronization is decreased by inhibition of the M-current.

We found that serotonergic neurons displaying M-current are found in rostral positions in the DR and in the dorsal part of the MR. The M-current regulates firing frequency, action potential morphology and adaptation index (AI). Our findings indicate that the M-current seems to effectively set firing properties of certain serotonergic neurons and it might be a part of cholinergic and local serotonergic neuromodulatory regulation.

The MLR is a mesencephalic area consisting of the PPN and the cuneiform nucleus (CnF). We showed that CnF glutamatergic neurons are functionally more homogeneous than PPN neurons. In PPN, the electrophysiological diversity is greater.

10. KEYWORDS

Pedunculopontine nucleus (PPN), M-current, neuronal synchronization, spike frequency adaptation, KCNQ4 (Kv7.4), non-syndromic hearing loss (DFNA2), acetylcholine, dorsal raphe (DR), median raphe (MR), serotonergic neuron, cuneiform nucleus (CnF)

Nucleus pedunculopontinus (PPN), M-áram, neuronális szinkronizáció, tüzelési frekvencia adaptáció, KCNQ4 (Kv7.4), nonszindromatikus halláscsökkenés (DFNA2), acetilkolin, nucleus raphe dorsalis (DR), nucleus raphe medialis (MR), szerotoninerg neuronok, nucleus cuneiformis (CnF)

11. Acknowledgements

This work was carried out by Stipendium Hungaricum PhD programme and also supported by the Thematic Excellence Programme of the Ministry for Innovation and Technology in Hungary (Space Sciences thematical programme of the University of Debrecen; ED_18-1-2019-0028), the Argentinian-Hungarian Scientific and Technological Cooperation Grant (TÉT_15-1-2016-0087), the Hungarian National Brain Research Program and the OTKA Bridging Fund of the University of Debrecen.

First and foremost, I am extremely grateful to my supervisor, Dr. Pál Balázs for his invaluable advice, continuous support, and patience during my PhD study. His immense knowledge and plentiful experience have encouraged me in all the time of my academic research and daily life. I would like to express my sincere gratitude to Prof. László Csernoch for allowing me to do this work, within the framework of the Doctoral School of Molecular Medicine.

I greatly appreciate all my colleagues Adrienn Kovacs, Pocsai Krisztina, Csemer Andrea and Baneen E. Maamrah. It is their kind help and support that have made my study and life in Hungary a wonderful time. As well as I would like to appreciate Dr. Péter Szentesi (Department of Physiology, University of Debrecen) for his professional assistance in performing and interpreting the experiments.

I am also very grateful to collaborating partners Dr. Guillermo Spitzmaul and Dr. Juan Mena-Segovia and their teammates for wonderful collaboration.

I would like to thank Dr. Peter Szücs (Department of Anatomy, Histology and Embryology, Medical Faculty, University of Debrecen) for providing the mice (ChAT-cre, Vglut2-cre, Sert-cre)

Many thanks also to Dr. Rita Gálosi (University of Pécs, Hungary) for her valuable comments and to Kristóf Nagy for his help in the experiments.

Finally, I would like to express my gratitude to my family. Without their tremendous understanding and encouragement in the past few years, it would be impossible for me to complete my study.

12. References

1. Abrams J.K., Johnson P.L., Hay-Schmidt A., Mikkelsen J.D., Shekhar A., Lowry C.A. (2005) Serotonergic systems associated with arousal and vigilance behaviors following administration of anxiogenic drugs. Neuroscience; 133:983–997.
2. Adamantidis, A.R., Zhang, F., Aravanis, A.M., Deisseroth, K., and de Lecea, L. (2007). Neural substrates of awakening probed with optogenetic control of hypocretin neurons. Nature 450, 420–424.
3. Andrade R, Haj-Dahmane S. (2013) Serotonin neuron diversity in the dorsal raphe. ACS Chem Neurosci 4(1):22-5.
4. Aravanis, A.M., Wang, L.P., Zhang, F., Meltzer, L.A., Mogri, M.Z., Schneider, M.B., and Deisseroth, K. (2007). An optical neural interface: in vivo control of rodent motor cortex with integrated fiberoptic and optogenetic technology. J. Neural Eng. 4, S143–S156.
5. Arenkiel, B.R., Peca, J., Davison, I.G., Feliciano, C., Deisseroth, K., Augustine, G.J., Ehlers, M.D., and Feng, G. (2007). In vivo light-induced activation of neural circuitry in transgenic mice expressing channelrhodopsin-2. Neuron 54, 205–218.
6. Arguinchona, J. H., & Tadi, P. (2020). Neuroanatomy, Reticular Activating System. In StatPearls. StatPearls Publishing.
7. Armstrong D.M., Saper C.B., Levey A.I., Wainer B.H., & Terry R.D. (1983). Distribution of cholinergic neurons in rat brain: Demonstrated by the immunocytochemical localization of choline acetyltransferase. The Journal of Comparative Neurology, 216(1), 53–68.
8. Atasoy D., Aponte Y., Su H.H., and Sternson S.M. (2008). A FLEX switch targets Channelrhodopsin-2 to multiple cell types for imaging and long-range circuit mapping. J. Neurosci. 28, 7025–7030.
9. Baashar, A., Robertson, D., Mulders, W.H.A.M. (2015). A novel method for selectively labelling olivocochlear collaterals in the rat. Hear. Res. 325, 35–41
10. Baashar, A., Robertson, D., Yates, N. J., & Mulders, W. H. A. M. (2019). Targets of olivocochlear collaterals in cochlear nucleus of rat and guinea pig. The Journal of Comparative Neurology. 1-18, 24681
11. Baksa B., Kovács A., Bayasgalan T., Szentesi P., Kőszeghy Á., Szücs P., Pál B. (2019) Characterization of functional subgroups among genetically identified

cholinergic neurons in the pedunculopontine nucleus. Cell Mol Life Sci. 2019;76(14):2799-2815.

12. Banghart M., Borges K., Isacoff E., Trauner D., Kramer R.H. (2004) Light-activated ion channels for remote control of neuronal firing. Nat Neurosci 7: 1381–1386
13. Barbeau A. (1962) The pathogenesis of Parkinson's disease; a new hypothesis. Can. med. Ass. J. 87, 802-807.
14. Bayasgalan T., Stupniki S., Kovács A., Csemer A., Szentesi P., Pocsai K. (2020) The KCNQ4-mediated M-current regulates the circadian rhythm in mesopontine cholinergic neurons. BioRxiv, 2020; doi: https://doi.org/10.1101/2020.09.11.29342
15. Beck S.G., Pan Y.Z., Akanwa A.C, Kirby L.G. (2004) Median and dorsal raphe neurons are not electrophysiologically identical. Journal of Neurophysiology, 91(2), 994–1005.
16. Beckstead, RM, Domesick, VB, Nauta, WJH (1979) Efferent connections of the substantia nigra and ventral tegmental area in the rat. Brain Res. 175, 191-217.
17. Beisel K. W., Rocha-Sanchez S. M., Morris K. A., Nie L., Feng F., Kachar B., Yamoah E. N., and Fritzsch B. (2005) Differential expression of KCNQ4 in inner hair cells and sensory neurons is the basis of progressive high-frequency hearing loss. Neurosci. 25, 9285-9293.
18. Benarroch E.E. (2013) Pedunculopontine nucleus: functional organization and clinical implications. Neurology. 80(12):1148-55.
19. Beninato, M., Spencer, RF (1987) A cholinergic projection to the rat substantia nigra from the pedunculopontine tegmental nucleus. Brain Res. 412, 169-174.
20. Bernardi, G., Betta, M., Ricciardi, E., Pietrini, P., Tononi, G., & Siclari, F. (2019). Regional delta waves in human rapid-eye movement sleep. The Journal of Neuroscience, 2298–18.
21. Bi, A., Cui, J., Ma, Y.P., Olshevskaya, E., Pu, M., Dizhoor, A.M., and Pan, Z.H. (2006). Ectopic expression of a microbial-type rhodopsin restores visual responses in mice with photoreceptor degeneration. Neuron 50, 23–33.
22. Bigl V., Woolf N., Butcher L (1982) Cholinergic projections from the basal forebrain to frontal, parietal, temporal, occipital, and cingulate cortices: A combined fluorescent tracer and acetylcholinesterase analysis. Brain Res Bull 8: 727-749
23. Blom, Sigrid Marie; Schmitt, Nicole; Jensen, Henrik Sindal (2010). Differential Effects of ICA-27243 on Cloned KV7 Channels. Pharmacology, 86(3), 174–181.

24. Bordas C., Kovacs A., Pal B. (2015) The M-current contributes to high threshold membrane potential oscillations in a cell type-specific way in the pedunculopontine nucleus of mice. Front Cell Neurosci. 9-121
25. Bordas C. (2017), The pedunculopontin nucleus is directly neuronal and indirect, astrocyte-dependent neuromodulation mechanisms, University of Debrecen, http://hdl.handle.net/2437/244119
26. Boucetta S., Cissé Y., Mainville L., Morales M., and Jones B. E. (2014) Discharge profiles across the sleep-waking cycle of identified cholinergic, GABAergic, and glutamatergic neurons in the pontomesencephalic tegmentum of the rat. J Neurosci. 34, 4708-4727.
27. Boyden E.S., Zhang F., Bamberg E., Nagel G., Deisseroth K. (2005) Millisecond-timescale, genetically targeted optical control of neural activity. Nat Neurosci 8: 1263- 1268
28. Brainard G. C., Barger L. K., Soler R. R., and Hanifin J. P. (2016) The development of lighting countermeasures for sleep disruption and circadian misalignment during spaceflight. Curr Opin Pulm Med. 22, 535-544.
29. Brickel, N., Hewett, K., Rayner, K., McDonald, S., De'Ath, J., Daniluk, J., Cooper, J. (2020). Safety of retigabine in adults with partial-onset seizures after long-term exposure: focus on unexpected ophthalmological and dermatological events. Epilepsy & Behavior, 102, 106580.
30. Brown D. A., and Adams P. R. (1980) Muscarinic suppression of a novel voltage-sensitive K+ current in a vertebrate neurone. Nature. 283, 673-676.
31. Brown D.A., Passmore G.M. (2009) Neural KCNQ (Kv7) channels. Br J Pharmacol. 2009; 156(8):1185-95.
32. Brown, D.A. and H. Higashida (1988) lnositol 1,4,5-trisphosphate and diacylglycerol mimic bradykinin effects on mouse neuroblastoma X rat glioma hybrid cells, J. Physiol. 397, 185.
33. Brown, P. (2003). Oscillatory nature of human basal ganglia activity: relationship to the pathophysiology of Parkinson's disease. Mov. Disord. 18, 357–363.
34. Brudzynski, SM, Wu, M., Mogenson, J. (1988) Modulation of locomotor activity induced by injections of carbachol into the tegmental pedunculopontine nucleus and adjacent areas in the rat. Brain Res. 451, 119-125.

35. Brueggemann L. I., Haick J. M., Cribbs L. L., and Byron K. L. (2014) Differential activation of vascular smooth muscle Kv7.4, Kv7.5, and Kv7.4/7.5 channels by ML213 and ICA-069673. Mol Pharmacol. 86, 330-341.

36. Busskamp, V., Duebel, J., Balya, D., Fradot, M., Viney, T.J., Siegert, S., Groner, A.C., Cabuy, E., Forster, V., Seeliger, M. (2010). Genetic reactivation of cone photoreceptors restores visual responses in retinitis pigmentosa. Science 329, 413–417.

37. Caggiano V., Leiras R., Goñi-Erro H. (2018) Midbrain circuits that set locomotor speed and gait selection. Nature. 553(7689):455-460

38. Caminos E., Vaquero C. F., and Martinez-Galan J. R. (2015) Relationship between rat retinal degeneration and potassium channel KCNQ5 expression. Exp Eye Res. 131, 1-11.

39. Canteras N.S., Shammah-Lagnado S.J., Silva B.A., Ricardo J.A. (1990) Afferent connections of the subthalamic nucleus: a combined retrograde and anterograde horseradish peroxidase study in the rat. Brain Res. 513(1):43-59.

40. Capelli P, Pivetta C, Esposito MS, Arber S. (2017) Locomotor speed control circuits in the caudal brainstem. Nature. 551, pages373–377

41. Carignano C., Barila E. P., Rías E. I., Dionisio L., Aztiria E., and Spitzmaul G. (2019) Inner hair cell and neuron degeneration contribute to hearing loss in a DFNA2-like mouse model. Neurosci. 410, 202-216.

42. Chow B.Y., Han X., Dobry A.S., Qian X., Chuong A.S., Li M., Henninger M.A., Belfort G.M., Lin Y, Monahan P.E, Boyden E.S. (2010) High-performance genetically targetable optical neural silencing by light-driven proton pumps. Nature. 463(7277):98-102.

43. Ciocchi, S., Herry, C., Grenier, F., Wolff, S.B., Letzkus, J.J., Vlachos, I., Ehrlich, I., Sprengel, R., Deisseroth, K., Stadler, M.B., et al. (2010). Encoding of conditioned fear in central amygdala inhibitory circuits. Nature 468, 277–282.

44. Clarke, PB, Hommer, DW, Pert, A., Skirboll, LR (1987) Innervation of substantia nigra neurons by cholinergic afferents from the pedunculopontine nucleus in the rat. Neuroanatomical and electrophysiological evidence. Neuroscience 23, 1011-1019.

45. Clements J.R, & Grant S. (1990). Glutamate-like immunoreactivity in neurons of the laterodorsal tegmental and pedunculopontine nuclei in the rat. Neurosci Lett, 120(1), 70–73.

46. Cooper, Edward C.; Harrington, Emily; Jan, Yuh Nung; Jan, Lily Y. (2001). M Channel KCNQ2 Subunits Are Localized to Key Sites for Control of Neuronal Network Oscillations and Synchronization in Mouse Brain. The Journal of Neuroscience, 21(24), 9529–9540.
47. Cooper, Edward C.; Jan, Lily Y. (2003). M-Channels. Archives of Neurology, 60(4), 496
48. Cox J, Pinto L, Dan Y. (2016) Calcium imaging of sleep-wake related neuronal activity in the dorsal pons. Nat Commun. 7: 763.
49. Crawford L.K., Craige C.P., Beck S.G. (2010) Increased intrinsic excitability of lateral wing serotonin neurons of the dorsal raphe: a mechanism for selective activation in stress circuits. J Neurophysiol. 103(5):2652-63.
50. Dailey J.W., Cheong J.H., Ko K.H., Adams-Curtis L.E. and Jobe P.C. (1995) Anticonvulsant properties of D-20443 in genetically epilepsy-prone rats: Prediction of clinical response. Neurosci Lett 195:77–80.
51. Datta, S., Siwek, DF (2002) Single cell activity patterns of pdenculopontine tegmentum, 70(4):611-21
52. De Leenheer E. M., Ensink R. J., Kunst H. P., Marres H. A., Talebizadeh Z., Declau F., Smith S. D., Usami S., Van de Heyning P. H., Van Camp G., Huygen P. L., and Cremers C. W. (2002) DFNA2/KCNQ4 and its manifestations. Adv Otorhinolaryngol. 61, 41-46.
53. DeFeudis, F. V. (1974) Central cholinergic systems and behavior. Academic Press: New York. 33:1043–1048
54. Deisseroth K., Feng G., Majewska A.K., Miesenbock G., Ting A., Schnitzer M.J. (2006) Next-generation optical technologies for illuminating genetically targeted brain circuits. J Neurosci.26:10380–86.
55. Deisseroth K. (2010) Controlling the brain with light. Sci Am.303:48–55.
56. Deisseroth K. (2011) Optogenetics. Nat Methods. 8:26–29.
57. Delmas P., and Brown D. A. (2005) Pathways modulating neural KCNQ/M (Kv7) potassium channels. Nat Rev Neurosci. 6, 850-862.
58. Diester, I., Kaufman, M.T., Mogri, M., Pashaie, R., Goo, W., Yizhar, O., Ramakrishnan, C., Deisseroth, K., and Shenoy, K.V. (2011). An optogenetic toolbox designed for primates. Nat. Neurosci. 14, 387–397.
59. Dittgen, T., Nimmerjahn, A., Komai, S., Licznerski, P., Waters, J., Margrie, T.W., Helmchen, F., Denk, W., Brecht, M., and Osten, P. (2004). Lentivirusbased genetic

manipulations of cortical neurons and their optical and electrophysiological monitoring in vivo. Proc. Natl. Acad. Sci. USA 101, 18206–18211.

60. Dong-Gon Park; Sang Sung Nam; Keon Kim; Hyoungman Kim (1989). Effect of high pressure on the light-induced structural change of bacteriorhodopsin reconstituted in liposome. , 973(1), 0–22.
61. Drion G., Bonjean M., Waroux O., Scuvée-Moreau J., Liégeois J. F., Sejnowski T. J., Sepulchre R., and Seutin V. (2010) M-type channels selectively control bursting in rat dopaminergic neurons. Eur J Neurosci. 31, 827-835.
62. Dun, N. J., Dun, S. L., Hwang, L. L., and Forstermann, U. (1995). Infrequent co-existence of nitric oxide synthase and parvalbumin, calbindin and calretinin immunoreactivity in rat pontine neurons. Neurosci. Lett. 191, 165–168.
63. Eckenstein, F., Sofroniew, MV (1986) Identification of central cholinergic neurons containing both choline acetyltransferase and acetylcholinesterase and of central neurons containing only acetylcholinesterase. J. Neurosci. 11, 2286-2291.
64. Elena Caminos; Elisabet Garcia-Pino; Juan Ramon Martinez-Galan; José M. Juiz (2007). The potassium channel KCNQ5/Kv7.5 is localized in synaptic endings of auditory brainstem nuclei of the rat. , 505(4), 363–378
65. F. Zhang, L.P. Wang, M. Brauner, J.F. Liewald, K. Kay, N. Watzke, P.G. Wood, E. Bamberg, G. Nagel, A. Gottschalk, K. Deisseroth (2007) Multimodal fast optical interrogation of neural circuitry, Nature, 446, pp. 633-639
66. Feldbauer, K.; Zimmermann, D.; Pintschovius, V.; Spitz, J.; Bamann, C.; Bamberg, E. (2009). Channelrhodopsin-2 is a leaky proton pump. Proceedings of the National Academy of Sciences, 106(30), 12317–12322
67. Fernandez SP, Cauli B, Cabezas C, Muzerelle A, Poncer JC, Gaspar P. (2016) Multiscale single-cell analysis reveals unique phenotypes of raphe 5-HT neurons projecting to the forebrain. Brain Struct Funct. 221(8):4007-4025.
68. Fidzinski P., Korotkova T., Heidenreich M., Maier N., Schuetze S., Kobler O., Zuschratter W., Schmitz D., Ponomarenko A., and Jentsch T. J. (2015) KCNQ5 K+ channels control hippocampal synaptic inhibition and fast network oscillations. Nat Commun. 6, 6254.
69. Ford B, Holmes CJ, Mainville L, & Jones BE (1995). GABAergic neurons in the rat pontomesencephalic tegmentum: codistribution with cholinergic and other tegmental neurons projecting to the posterior lateral hypothalamus. J Comp Neurol, 363(2), 177–196.

70. Fortin, M., Parent, A. (1999) Calretinin-immunoreactive neurons in primate pedunculopontin and laterodorsal tegmental nuclei. Neuroscience 88, 535–547.
71. Furman, M., Zhan, Q., McCafferty, C., Lerner, BA, Motelow, JE, Meng, J., Ma, C., Buchanan, GF, Witten, IB, Deisseroth, K., Cardin, JA, Blumenfeld, H. (2015) Optogenetic stimulation of cholinergic brainstem neurons during focal limbic seizures: Effects on cortical physiology. Epilepsy. 56 (12): e198-202.
72. G. Moruzzi, H.W. Magoun (1949) Brain stem reticular formation and activation of the EEG, Electroencephalography and Clinical Neurophysiology, Volume 1, Issues 1–4, pages 455-473
73. Garcia-Rill E, Houser CR, Skinner RD, Smith W, Woodward DJ. (1987) Locomotion-inducing sites in the vicinity of the pedunculopontine nucleus. Brain Res Bull. 18, 731–738.
74. Garcia-Rill E, Skinner RD, Fitzgerald JA. (1983) Activity in the mesencephalic locomotor region during locomotion. Exp Neurol. 82(3):609-22.
75. Garcia-Rill, E. (1991) The pedunculopontine nucleus. Prog Neurobiol. 36: 363–389
76. Garcia-Rill, E. (2009). Reticular Activating System. Encyclopedia of Neuroscience, 137–143.
77. Garin Shkolnik T., Feuerman H., Didkovsky E. (2014) Blue-Gray Mucocutaneous Discoloration: A New Adverse Effect of Ezogabine. *JAMA Dermatol*. 150(9):984–989. doi:10.1001/jamadermatol.2013.8895
78. Gartside S.E., Hajós-Korcsok E., Bagdy E., Hársing L.G. Jr, Sharp T., Hajós M. (2000) Neurochemical and electrophysiological studies on the functional significance of burst firing in serotonergic neurons. Neuroscience. 98(2):295-300.
79. Gillet C., Goyer D., Kurth S., Griebel H., Kuenzel T. (2018). Cholinergic innervation of principal neurons in the cochlear nucleus of the Mongolian gerbil. J. Comp. Neurol. 526, 1647–1661.
80. Gillet, C., Kurth, S., & Kuenzel, T. (2020). Muscarinic modulation of M and h currents in gerbil spherical bushy cells. PloS one, 15(1), e0226954.
81. Goard M, Dan Y. (2009) Basal forebrain activation enhances cortical coding of natural scenes. Nat Neurosci. 12(11):1444-9.
82. Goetz L, Bhattacharjee M, Ferraye MU, (2019) Deep Brain Stimulation of the Pedunculopontine Nucleus Area in Parkinson Disease: MRI-Based Anatomoclinical Correlations and Optimal Target. Clin Neurosurg. 84(2):506-518.

83. Goldsmith, M., Van Der Kooy, D. (1988) Separate non-cholinergic descending projections and cholinergic ascending projections from the nucleus tegmenti pedunculopontinus. Brain Res. 445, 386-391.

84. Gong, S., Doughty, M., Harbaugh, C.R., Cummins, A., Hatten, M.E., Heintz, N., and Gerfen, C.R. (2007). Targeting Cre recombinase to specific neuron populations with bacterial artificial chromosome constructs. J. Neurosci. 27, 9817–9823.

85. Gong, S., Doughty, M., Harbaugh, C.R., Cummins, A., Hatten, M.E., Heintz, N., and Gerfen, C.R. (2007). Targeting Cre recombinase to specific neuron populations with bacterial artificial chromosome constructs. J. Neurosci. 27, 9817–9823.

86. Gonzalez-Lima, F., & Scheich, H. (1985). Ascending reticular activating system in the rat: A 2-deoxyglucose study. Brain Research, 344(1), 70–88.

87. Gorman M. R., and Elliott J. A. (2003) Entrainment of 2 subjective nights by daily light:dark:light:dark cycles in 3 rodent species. J Biol Rhythms. 18, 502-512. doi: 10.1177/0748730403260219

88. Grace AA, Onn SP. (1989) Morphology and electrophysiological properties of immunocytochemically identified rat dopamine neurons recorded in vitro. J Neurosci. 9(10):3463-81.

89. Gradinaru, V., Mogri, M., Thompson, K.R., Henderson, J.M., and Deisseroth, K. (2009). Optical deconstruction of parkinsonian neural circuitry. Science 324, 354–359.

90. Gradinaru, V., Thompson, K.R., and Deisseroth, K. (2008). eNpHR: a Natronomonas halorhodopsin enhanced for optogenetic applications. Brain Cell Biol. 36, 129–139.

91. Graeff FG, Guimaraes FS, De Andrade TG, Deakin JF (1996) Role of 5-HT in stress, anxiety, and depression. Pharmacol Biochem Behav 54:129–141

92. Graeff FG, Guimaraes FS, De Andrade TG, Deakin JF. (1996) Role of 5-HT in stress, anxiety, and depression. Pharmacol Biochem Behav 54:129–141.

93. Graeff, F.G. (2002). On serotonin and experimental anxiety. Psychopharmacology, 163, 467-476

94. Gray JA, McNaughton N. (2000) The neuropsychology of anxiety. 2nd Edition. Oxford University Press, Oxford.

95. Greenwood BN, Foley TE, Day HE, Campisi J, Hammack SH, Campeau S, Maier SF, Fleshner M. (2003) Freewheel running prevents learned helplessness/behavioral depression: role of dorsal raphe serotonergic neurons. J Neurosci. 23(7):2889-98.

96. Grove EA. (1988) Neural associations of the substantia innominata in the rat: afferent connections. J Comp Neurol 277(3):315-46.

97. Guan D, Higgs MH, Horton LR, Spain WJ, Foehring RC. (2011) Contributions of Kv7-mediated potassium current to sub- and suprathreshold responses of rat layer II/III neocortical pyramidal neurons. J Neurophysiol. 106(4):1722-33.

98. Guinan JJ Jr. (2006) Olivocochlear efferents: anatomy, physiology, function, and the measurement of efferent effects in humans. Ear Hear. 27(6):589-607.

99. Gunthorpe M. J., Large C. H., and Sankar R. (2012) The mechanism of action of retigabine (ezogabine), a first-in-class K+ channel opener for the treatment of epilepsy. Epilepsia. 53, 412-424.

100. Ha G. H., and Cheong E. (2017) Spike frequency adaptation in neurons of the central nervous system. Exp Neurobiol. 26, 179-185.

101. Hajós M, Allers KA, Jennings K, Sharp T, Charette G, Sík A, (2007) Neurochemical identification of stereotypic burst-firing neurons in the rat dorsal raphe nucleus using juxtacellular labelling methods. Eur J Neurosci. 25(1):119-26.

102. Hajos M, Gartside SE, Villa AE, Sharp T. (1995) Evidence for a repetitive (burst) firing pattern in a sub-population of 5- hydroxytryptamine neurons in the dorsal and median raphe nuclei of the rat. Neuroscience 69, 189–197.

103. Hajós M, Sharp T. (1996) Burst-firing activity of presumed 5-HT neurones of the rat dorsal raphe nucleus: electrophysiological analysis by antidromic stimulation. Brain Res. 740(1-2):162-8.

104. Hale MW, Hay-Schmidt A, Mikkelsen JD, Poulsen B, Bouwknecht JA, Evans AK (2008). Exposure to an open-field arena increases c-Fos expression in a subpopulation of neurons in the dorsal raphe nucleus, including neurons projecting to the basolateral amygdaloid complex. Neuroscience 157(4):733-48.

105. Hale MW, Lowry CA. (2011) Functional topography of midbrain and pontine serotonergic systems: implications for synaptic regulation of serotonergic circuits. Psychopharmacology (Berl) 213(2-3):243-64.

106. Han, X., Chow, B. Y., Zhou, H., Klapoetke, N., Chuong, A., Rajimehr, R., et al. (2011). A high-light sensitivity optical neural silencer: Development and application to optogenetic control of non-human primate cortex. Frontiers in Systems, Neuroscience, 5, 18.

107. Han, X., Qian, X., Bernstein, J.G., Zhou, H.H., Franzesi, G.T., Stern, P., Bronson, R.T., Graybiel, A.M., Desimone, R., and Boyden, E.S. (2009). Millisecond-

timescale optical control of neural dynamics in the nonhuman primate brain. Neuron 62, 191–198.

108. Handley SL. (1995) 5-Hydroxytryptamine pathways in anxiety and its treatment. Pharmacol Ther. 66(1):103-48.

109. Hansen H. H., Waroux O., Seutin V., Jentsch T. J., Aznar S., and Mikkelsen J. D. (2008) Kv7 channels: interaction with dopaminergic and serotonergic neurotransmission in the CNS. J Physiol. 586, 1823-1832.

110. Harrison E. M., Walbeek T. J., Sun J., Johnson J., Poonawala Q., and Gorman M. R. (2016) Extraordinary behavioral entrainment following circadian rhythm bifurcation in mice. Sci Rep. 6, 38479. doi: 10.1038/srep38479

111. Haubensak, W., Kunwar, P.S., Cai, H., Ciocchi, S., Wall, N.R., Ponnusamy, R., Biag, J., Dong, H.W., Deisseroth, K., Callaway, E.M., et al. (2010). Genetic dissection of an amygdala microcircuit that gates conditioned fear. Nature 468, 270–276.

112. Heidenreich M., Lechner S.G., Vardanyan V., Wetzel C., Cremens C. W., De Leenheer E. M., Aránguez G., Moreno-Pelayo M. A., Jentsch T. J., and Lewin G. R. (2011) KCNQ4 K+ channels tune mechanoreceptors for normal touch sensation in mouse and man. Nat Neurosci. 15, 138-145

113. Henderson Z. (1981) A projection from acetylcholinesterase-containing neurons in the diagonal band to the occipital cortex of the rat. Neuroscience 6, 1081-1088.

114. Hepp DH, Ruiter AM, Galis Y, (2013). Pedunculopontine cholinergic cell loss in hallucinating Parkinson disease patients but not in dementia with Lewy bodies patients. J Neuropathol Exp Neurol. 72(12):1162-70

115. Hernandez C. C., Zaika O., Tolstykh G. P., and Shapiro M. S. (2008) Regulation of neural KCNQ channels: signalling pathways, structural motifs and functional implications. J Physiol. 586, 1811-1821.

116. Hilgemann D.W., Feng,S. and Nasuhoglu,C. (2001) The complex and intriguing lives of PIP2 with ion channels and transporters. Sci. STKE, 111, RE19.

117. Hirsch EC, Graybiel AM, Duyckaerts C, Javoy-Agid F. (1987) Neuronal loss in the pedunculopontine tegmental nucleus in Parkinson disease and in progressive supranuclear palsy. Proc Natl Acad Sci U S A. 84(16):5976-80

118. Honda T., and Semba K. (1995) An ultrastructural study of cholinergic and non-cholinergic neurons in the laterodorsal and pedunculopontine tegmental nuclei in the rat. Neurosci. 68, 837-853.

119. Hornung, JP. (2003) The human raphe nuclei and the serotonergic system. Journal of Chemical Neuroanatomy, 26(4), 331–343.
120. Horowitz LF, Hirdes W, Suh BC, Hilgemann DW, Mackie K, Hille B. (2005) Phospholipase C in living cells: activation, inhibition, Ca2+ requirement, and regulation of M current. J Gen Physiol.;126:243–262.
121. Horváth M, Kraus KS, Illing RB. (2000) Olivocochlear neurons sending axon collaterals into the ventral cochlear nucleus of the rat. Journal of Comparative Neurology. 422:95–105.
122. Huang H., and Trussell L. O. (2011) KCNQ5 channels control resting properties and release probability of a synapse. Nat Neurosci. 14, 840-847.
123. Idnurm A., Howlett B.J., (2001) Characterization of an opsin gene from the ascomycete Leptosphaeria maculans. Genome. 44: 167-171
124. Imai H, Steindler DA, Kitai ST. (1986) The organization of divergent axonal projections from the midbrain raphe nuclei in the rat. J Comp Neurol. 243(3):363-80.
125. Ishizuka, T., Kakuda, M., Araki, R., and Yawo, H. (2006). Kinetic evaluation of photosensitivity in genetically engineered neurons expressing green algae light-gated channels. Neurosci. Res. 54, 85–94.
126. Jackson A, Crossman AR (1981) Basal ganglia and other afferent projections to the peribrachial region in the rat: a study using retrograde and anterograde transport of horseradish peroxidase. Neuroscience 6: 1537–1549
127. Jackson A, Crossman AR (1983) Nucleus tegmenti pedunculopontinus: efferent connections with special reference to the basal ganglia, studied in the rat by anterograde and retrograde transport of horseradish peroxidase. Neuroscience 10: 725–765
128. Jackson, A., Crossman, AR (1983) Nucleus tegmenti pedunculopontinus: Efferent connections with special reference to the basal ganglia, studies in the rat by anterograde and retrograde transport of horseradish peroxidase. Neuroscience 10, 725–765.
129. Jellinger K. (1988) The pedunculopontine nucleus in Parkinson's disease, progressive supranuclear palsy and Alzheimer's disease. J Neurol Neurosurg Psychiatry. 51(4):540-3

130. Jenkinson N, Nandi D, Miall RC, Stein JF, Aziz TZ. (2004) Pedunculopontine nucleus stimulation improves akinesia in a Parkinsonian monkey. Neuroreport. 15(17):2621-4

131. Jentsch T. J. (2000) Neuronal KCNQ potassium channels: physiology and role in disease. Nat Rev Neurosci. 1, 21–30.

132. Jepps T. A., Chadha P. S., Davis A. J., Harhun M. I., Cockerill G. W., Olesen S. P., Hansen R. S., and Greenwood I. A. (2011) Downregulation of Kv7.4 channel activity in primary and secondary hypertension. Circulation. 124, 602-611.

133. Jing M. Y., Han X., Zhao T. Y., Wang Z. Y., Lu G. Y., Wu N., Song R., and Li J. (2019) Re-examining the role of ventral tegmental area dopaminergic neurons in motor activity and reinforcement by chemogenetic and optogenetic manipulation in mice. Metab Brain Dis. 34, 1421-1430.

134. Johnson, Steven & North, R.A.. (1992). Johnson SW, North RA. Opioids excite dopamine neurons by hyperpolarization of local interneurons. J Neurosci 12: 483-488. The Journal of neuroscience : the official journal of the Society for Neuroscience. 12. 483-8.

135. Johnston MV, McKinney M, Coyle JT (1981) Neocortical cholinergic innervation: a description of extrinsic and intrinsic components in the rat. Exp Brain Res 43:159–172

136. Jones, B. E. (1991). Noradrenergic locus coeruleus neurons: their distant connections and their relationship to neighboring (including cholinergic and GABAergic) neurons of the central gray and reticular formation. Neurobiology of the Locus Coeruleus, 15–30.

137. Jones, B. E. (1993). Chapter 5: The organization of central cholinergic systems and their functional importance in sleep-waking states. Progress in Brain Research, 61–71.

138. Jones, BE, Yang, TZ (1985) The efferent projections from the reticular formation and the locus coeruleus studied by anterograde and retrograde axonal transport in the rat. J. comp. Neurol. 242, 56-92.

139. Jones, E. G., & Leavitt, R. Y. (1974). Retrograde axonal transport and the demonstration of non-specific projections to the cerebral cortex and striatum from thalamic intralaminar nuclei in the rat, cat and monkey. The Journal of Comparative Neurology, 154(4), 349–377.

140. Josset N, Roussel M, Lemieux M, Lafrance-Zoubga D, Rastqar A, Bretzner F. (2018) Distinct Contributions of Mesencephalic Locomotor Region Nuclei to Locomotor Control in the Freely Behaving Mouse. Curr Biol. 28, 884–901

141. Juan Navarro-López; Lydia Jiménez-Díaz; Sandrine M. Géranton; Jonathan F. Ashmore (2009). Electrophysiological and Molecular Analysis of Kv7/KCNQ Potassium Channels in the Inferior Colliculus of Adult Guinea Pig. , 37(3), 263–268.

142. Kamondi A., Williams J. A., Hutcheon B., Reiner P. B. (1992). Membrane properties of mesopontine cholinergic neurons studied with the whole-cell patch-clamp technique: implications for behavioral state control. J. Neurophysiol. 68 1359–1372.

143. Kang Y, Kitai ST. (1990) Electrophysiological properties of pedunculopontine neurons and their postsynaptic responses following stimulation of substantia nigra reticulata. Brain Res. 535(1):79-95

144. Kathryn G Commons, K Ryan Connolley, Rita J Valentino. (2003) A neurochemically distinct dorsal raphe-limbic circuit with a potential role in affective disorders. Neuropsychopharmacology 28(2):206-15.

145. Katzel D., Zemelman B. V., Buetfering C., Wolfel M., Miesenbock G. (2011). The columnar and laminar organization of inhibitory connections to neocortical excitatory cells. Nat. Neurosci. 14, 100–107

146. Kaufman, E. F. S., & Rosenquist, A. C. (1985). Efferent projections of the thalamic intralaminar nuclei in the cat. Brain Research, 335(2), 257–279.

147. Kezunovic N, Hyde J, Simon C, Urbano FJ, Williams DK, Garcia-Rill E. (2012) Gamma band activity in the developing parafascicular nucleus. J Neurophysiol 107: 772–784.

148. Kezunovic, N., Urbano, FJ, Simon, C., Hyde, J., Smith, K., Garcia-Rill, E. (2011) Mechanism behind gamma band activity in the pedunculopontine nucleus. Eur J Neurosci. 34 (3): 404-15.

149. Kharkovets T., Dedek K., Maier H., Schweizer M., Khimich D., Nouvian R., Vardanyan V., Leuwer R., Moser T., and Jentsch T. J. (2006) Mice with altered KCNQ4 K+ channels implicate sensory outer hair cells in human progressive deafness. EMBO J. 25, 642-652.

150. Kharkovets T., Hardelin J. P., Safieddine S., Schweizer M., El-Amraoui A., Petit C., and Jentsch T. J. (2000) KCNQ4, a K+ channel mutated in a form of dominant

deafness, is expressed in the inner ear and the central auditory pathway. PNAS. 97, 4333-4338.

151. Kim LH, Sharma S, Sharples SA, Mayr KA, Kwok CHT, Whelan PJ. (2017) Integration of descending command systems for the generation of context-specific locomotor behaviors. Front Neurosci. 11:581.

152. Kishan, A. U., Lee, C. C., & Winer, J. A. (2011). Patterns of olivocochlear axonal branches. Open journal of neuroscience, 1, 2.

153. Klinger F., Gould G., Boehm S., and Shapiro M. S. (2011) Distribution of M-channel subunits KCNQ2 and KCNQ3 in rat hippocampus. Neuroimage. 58, 761-769.

154. Koch M, Kungel M, Herbert H. Cholinergic neurons in the pedunculopontine tegmental nucleus are involved in the mediation of prepulse inhibition of the acoustic startle response in the rat. Exp Brain Res. 1993;97:71–82.

155. Kocsis B, Varga V, Dahan L, Sik A. Serotonergic neuron diversity: identification of raphe neurons with discharges time-locked to the hippocampal theta rhythm. Proc Natl Acad Sci U S A. 2006; 103(4):1059-64.

156. Koyama S., and Appel S. B. (2006) Characterization of M-current in ventral tegmental area dopamine neurons. J Neurophysiol. 96, 535-543.

157. Kravitz, A.V., Freeze, B.S., Parker, P.R., Kay, K., Thwin, M.T., Deisseroth, K., and Kreitzer, A.C. (2010). Regulation of parkinsonian motor behaviours by optogenetic control of basal ganglia circuitry. Nature 466, 622–626.

158. Kroeger D., Ferrari L. L., Petit G., Mahoney C. E., Fuller P. M., Arrigoni E., and Scammell T. E. (2017) Cholinergic, glutamatergic, and GABAergic neurons of the pedunculopontine tegmental nucleus have distinct effects on sleep/wake behavior in mice. J Neurosci. 37, 1352-1366.

159. Kubisch C., Schroeder B. C., Friedrich T., Lütjohann B., El-Amraoui A., Marlin S., Petit C., and Jentsch T. J. (1999) KCNQ4, a novel potassium channel expressed in sensory outer hair cells, is mutated in dominant deafness. Cell. 96, 437-446.

160. Kuhlman, S.J., and Huang, Z.J. (2008). High-resolution labeling and functional manipulation of specific neuron types in mouse brain by Cre-activated viral gene expression. PLoS ONE 3(4):e2005.

161. Lacey MG, Mercuri NB, North RA. (1990) Actions of cocaine on rat dopaminergic neurones in vitro. Br J Pharmacol.98:731–735.

162. Lau B, Welter ML, Belaid H, (2015) The integrative role of the pedunculopontine nucleus in human gait. Brain. 138(Pt 5):1284-96

163. Lavoie B, Parent A. (1994) Pedunculopontine nucleus in the squirrel monkey: Cholinergic and glutamatergic projections to the substantia nigra. J Comp Neurol.. 344(2):232-41

164. Leão R. N., Tan H. M., and Fisahn A. (2009) Kv7/KCNQ channels control action potential phasing of pyramidal neurons during hippocampal gamma oscillations in vitro. J Neurosci. 29, 13353-13364.

165. Lechin F, van der Dijs B, Amat J, Lechin M. (1989) Neuroanatomical basis. In: Lechin F, van der Dijs B, editors. Neurochemistry and clinical disorders: circuitry of some psychiatric and psychosomatic syndromes. Boca Raton, FL' CRC Press. p. 9 – 12.

166. Lechin F, van der Dijs B, Hernandez-Adrian G. (2006) Dorsal raphe vs. median raphe serotonergic antagonism. Anatomical, physiological, behavioral, neuroendocrinological, neuropharmacological and clinical evidences: Relevance for neuropharmacological therapy, Progress in Neuro-Psychopharmacology & Biological Psychiatry 30: 565 – 585

167. Lechin F, van der Dijs B, Lechin E. (1979a) Anatomic – functional correlation. In: Lechin F, van der Dijs B, Lechin E, editors. The autonomic nervous system: physiological basis of psychosomatic therapy. Barcelona, Spain' Editorial Cientifico-Medica. p. 31 – 40.

168. Lechin F, van der Dijs B, Lechin ME. (2002b) Neuroautonomic, neuroendocrine and neuroimmune interactions. In: Lechin F, van der Dijs B, Lechin ME, editors. Neurocircuitry and neuroautonomic disorders Reviews and therapeutic strategies. Basel' Karger. p. 57 – 9.

169. Lee, J.H., Durand, R., Gradinaru, V., Zhang, F., Goshen, I., Kim, D.S., Fenno, L.E., Ramakrishnan, C., and Deisseroth, K. (2010). Global and local fMRI signals driven by neurons defined optogenetically by type and wiring. Nature 465, 788–792.

170. Lehmann J., Nagy J. 1., Atmadja S. and Fibiger H. C. (1980) The nucleus basalis magnocellularis: The origin of a cholinergic projection to the neocortex of the rat. Neurosci. 5, 1161-1174.

171. Leonard C. S. and Llinas R. (1990) Electrophysiology of mammalian pedunculopontine and laterodorsal tegmental neurons in vitro: implications for the

control of REM sleep. In Brain Chohnergic Systems (eds Steriade M. and Biesold D.), pp. 205-223.

172. Leonard CS, Llinás R. (1994) Serotonergic and cholinergic inhibition of mesopontine cholinergic neurons controlling rem sleep: An in vitro electrophysiological study. Neuroscience. 59(2):309-30

173. Leonard, CS, Llinás, R. (1994) Serotonergic and cholinergic inhibition of mesopontin cholinergic neurons controlling REM sleep: an in vitro electrophysiological study. Neuroscience; 59: 309–330.

174. Li, M., & Zhang, W. (2015). Oscillations in pedunculopontine nucleus in Parkinson's disease and its relationship with deep brain stimulation. Frontiers in neural circuits, 9, 47.

175. Li, X., Gutierrez, D.V., Hanson, M.G., Han, J., Mark, M.D., Chiel, H., Hegemann, P., Landmesser, L.T., and Herlitze, S. (2005). Fast noninvasive activation and inhibition of neural and network activity by vertebrate rhodopsin and green algae channelrhodopsin. Proc. Natl. Acad. Sci. USA 102, 17816–17821.

176. Liang, Gui-Hua; Liang, Gui-Hua; Jin, Zhe; Liang, Gui-Hua; Jin, Zhe; Ulfendahl, Mats; Järlebark, Leif (2006). Molecular analyses of KCNQ1–5 potassium channel mRNAs in rat and guinea pig inner ears: expression, cloning, and alternative splicing. Acta Oto-laryngologica, 126(4), 346–352.

177. Lima SQ, Miesenböck G. (2005) Remote control of behavior through genetically targeted photostimulation of neurons. Cell; 121:141–52.

178. Link, M. J., & Sloan, C. Y. (2003). Midbrain. Encyclopedia of the Neurological Sciences, 152–159.

179. Linley JE, Pettinger L, Huang D, Gamper N. M (2012) channel enhancers and physiological M channel block. J. Physiol. 590(Pt. 4), 793–807.

180. Ljubic-Thibal V, Morin A, Diksic M, Hamel E. (1999) Origin of the serotonergic innervation to the rat dorsolateral hypothalamus: retrograde transport of cholera toxin and upregulation of tryptophan hydroxylase mRNA expression following selective nerve terminals lesion. Synapse. 32(3):177-86.

181. Lobo, M.K., Covington, H.E., 3rd, Chaudhury, D., Friedman, A.K., Sun, H., Damez-Werno, D., Dietz, D.M., Zaman, S., Koo, J.W., Kennedy, P.J., et al. (2010). Cell type-specific loss of BDNF signaling mimics optogenetic control of cocaine reward. Science 330, 385–390.

182. Lowry CA. (2002) Functional subsets of serotonergic neurones: Implications for control of the hypothalamic-pituitary-adrenal axis. J Neuroendocrinol; 14:911–923.
183. Lucas-Meunier, Estelle & Fossier, Philippe & Baux, Gérard & Amar, Muriel. (2003). Cholinergic modulation of the cortical neuronal network. Pflügers Archiv : European journal of physiology. 446. 17-29.
184. Luquin, Esther & Huerta, Ibone & Aymerich, Maria & Mengual, Elisa. (2018). Stereological Estimates of Glutamatergic, GABAergic, and Cholinergic Neurons in the Pedunculopontine and Laterodorsal Tegmental Nuclei in the Rat. Frontiers in Neuroanatomy. 12. 34.
185. Macchi, G., & Bentivoglio, M. (1982). The organization of the efferent projections of the thalamic intralaminar nuclei: Past, present and future of the anatomical approach. The Italian Journal of Neurological Sciences, 3(2), 83–96.
186. MacLaren D. A. A., Ljungberg T. L., and Griffin M. E. (2018) Pedunculopontine tegmentum cholinergic loss leads to a progressive decline in motor abilities and neuropathological changes resembling progressive supranuclear palsy. Eur J Neurosci. 48, 3477-3497.
187. Madisen, L., Mao, T., Koch, H., Zhuo, J. M., Berenyi, A., Fujisawa, S., et al. (2012). A toolbox of Cre-dependent optogenetic transgenic mice for light-induced activation and silencing. Nat. Neurosci. 15, 793–802.
188. Madisen, L., Zwingman, T.A., Sunkin, S.M., Oh, S.W., Zariwala, H.A., Gu, H., Ng, L.L., Palmiter, R.D., Hawrylycz, M.J., Jones, A.R., et al. (2010). A robust and high-throughput Cre reporting and characterization system for the whole mouse brain. Nat. Neurosci. 13, 133–140.
189. Madison DV, Nicoll RA. (1984) Control of the repetitive discharge of rat CA1 pyramidal neurones in vitro. J. Physiol.; 354, 319–331.
190. Maier SF, Watkins LR. (2005) Stressor controllability and learned helplessness: the roles of the dorsal raphe nucleus, serotonin, and corticotropin-releasing factor. Neurosci Biobehav Rev.29(4-5):829-41.
191. Maier SF, Watkins LR. (1998) Stressor controllability, anxiety, and serotonin. Cognitive Therapy and Research.;6:595–613.
192. Manaye KF, Zweig R, Wu D, et al. Quantification of cholinergic and select non-cholinergic mesopontine neuronal populations in the human brain. Neuroscience. 1999. doi:10.1016/S0306-4522(98)00380-7

193. Marinelli S, Schnell SA, Hack SP, Christie MJ, Wessendorf MW, Vaughan CW. (2004) Serotonergic and nonserotonergic dorsal raphe neurons are pharmacologically and electrophysiologically heterogeneous. Journal of Neurophysiology, 92(6), 3532–3537.

194. Marrion NV. (1997) Control of M-current. Annu. Rev. Physiol. 59, 483–504. 10.1146/ annurev.physiol.59.1.483

195. Martinez-Gonzalez C, van Andel J, Bolam JP, Mena-Segovia J (2013) Divergent motor projections from the pedunculopontine nucleus are differentially regulated in Parkinsonism. Brain Struct Funct 219(4): 1451–1462.

196. Martinez-Gonzalez C, Wang HL, Micklem BR, Bolam JP, Mena-Segovia J. . (2012) Subpopulations of cholinergic, GABAergic and glutamatergic neurons in the pedunculopontine nucleus contain calcium-binding proteins and are heterogeneously distributed. Eur J Neurosci. 35(5):723-34.

197. Martinez-Gonzalez, C., Bolam, JP, Mena-Segovia, J. (2011) Topographical organization of the pedunculopontine nucleus. Front. Neuroanat. 2011. 5:22.

198. Mateos-Aparicio P, Murphy R, Storm JF. (2014) Complementary functions of SK and Kv7/M potassium channels in excitability control and synaptic integration in rat hippocampal dentate granule cells. J. Physiol. 592(Pt. 4), 669–693.

199. McGuier N. S., Rinker J. A., Cannady R., Fulmer D. B., Jones S. R., Hoffman M., and Mulholland P. J. (2018) Identification and validation of midbrain Kcnq4 regulation of heavy alcohol consumption in rodents. Neuropharmacology. 138, 10-19.

200. Mellott J. G., Motts S. D., Schofield B. R. (2011). GABAergic projections in the auditory tectothalamic system in the guinea pig. Assoc. Res. Otolaryngol. Abstr, 441

201. Mena-Segovia J., and Bolam J. P. (2017) Rethinking the pedunculopontine nucleus: from cellular organization to function. Neuron. 94, 7-18.

202. Mena-Segovia J., Sims H. M., Magill P. J., and Bolam J. P. (2008) Cholinergic brainstem neurons modulate cortical gamma activity during slow oscillations. J Physiol. 586, 2947-2960.

203. Mena-Segovia, J., Bolam, JP, Magill, PJ (2004) Pedunculopontine nucleus and basal ganglia: distant relatives or part of the same family? Trends in Neurosci. 27, 585–588.

204. Mena-Segovia, J., Micklem, BR, Nair-Roberts, RG, Ungless, MA, Bolam, JP (2009) GABAergic neuron distribution in the pedunculopontin nucleus defines functional subterritories. J. Comp. Neurol. 515, 397–408.

205. Mesulam MM, Mufson EJ, Wainer BH, Levey AI (1983) Central cholinergic pathways in the rat: an overview based on an alternative nomenclature (Ch1-Ch6). Neuroscience 10:1185–1201

206. Mesulam, MM, Mufson, EJ, Levey, AI, Wainer, BH (1984) Atlas of cholinergic neurons in the forebrain and upper brain stem of the macaque based on monoclonal choline acetyltransferase immunohistochemistry and acetylcholinesterase histochemistry. Neuroscience 12, 669-686.

207. Millan MJ. (2003) The neurobiology and control of anxious states. Prog Neurobiol. Jun;70(2):83-244.

208. Mitani, A., Ito, K., Mitani, V., Mccarley, RW (1988) Descending projections from the gigantocellular field in the cat: Cells of origin and their brain stem and spinal cord trajectories. J. comp. Neurol. 268, 546-566.

209. Monahan, P.E., and Samulski, R.J. (2000). Adeno-associated virus vectors for gene therapy: more pros than cons? Mol. Med. Today 6, 433–440.

210. Monti J. M. (2010) The role of dorsal raphe nucleus serotonergic and non-serotonergic neurons, and of their receptors, in regulating waking and rapid eye movement (REM) sleep. Sleep Med Rev. 14, 319-327.

211. Monti JM. (2011) Serotonin control of sleep-wake behavior. Sleep Medicine Reviews,; 15(4), 269–281.

212. Moon-Edley, S., Graybiel, AM (1983) The afferent and efferent connections of the feline tegmenti pedunculopontinus, pars compacta. J. comp. Neurol. 217, 187–-215.

213. Moore, RY, Bloom, FE (1979) Central catecholamine neuron system: Anatomy and physiology of the norepinephrine and epinephrine system. A. Rev. Neurosci. 2, 113-168.

214. Mori, S., Sakamoto, T., Ohta, Y., Takakusaki, K., Matsuyama, K. (1989) Site-specific postural and locomotor changes evoked in awake, freely moving intact cats by stimulating the brainstem. Brain Res. 505, 65-74.

215. Nagel G, Szellas T, Huhn W, Kateriya S, Adeishvili N, Berthold P, Ollig D, Hegemann P, Bamberg E (2003) Channelrhodopsin-2, a directly light-gated cation-selective membrane channel. Proc Natl Acad Sci USA 100: 13940- 13945

216. Nagel, G., Brauner, M., Liewald, J.F., Adeishvili, N., Bamberg, E., and Gottschalk, A. (2005). Light activation of channelrhodopsin-2 in excitable cells of Caenorhabditis elegans triggers rapid behavioral responses. Curr. Biol. 15, 2279–2284.

217. Nakamura Y., Tokuno H., Moriizumi T., Kitao Y., Kudo M. (1989). Monosynaptic nigral inputs to the pedunculopontine tegmental nucleus neurons which send their axons to the medial reticular formation in the medulla oblongata. An electron microscopic study in the cat. Neurosci. Lett. 103, 145–150

218. Nandi D. (2002) Reversal of akinesia in experimental parkinsonism by GABA antagonist microinjections in the pedunculopontine nucleus. Brain. 125(11): 2418–2430

219. Nauta, WJH (1958) Hippocampal projections and related neural pathways to the midbrain in the cat. Brain Res. 81, 319-340.

220. Navarro-López J, Jiménez-Díaz L, Géranton SM, Ashmore JF. (2009) Electrophysiological and molecular analysis of Kv7/KCNQ potassium channels in the inferior colliculus of adult guinea pig. J Mol Neurosci. 37(3):263-8.

221. Nelson, J. P., McCarley, R. W., & Hobson, J. A. (1983). REM sleep burst neurons, PGO waves, and eye movement information. Journal of Neurophysiology, 50(4), 784–797.

222. neurons across the sleep-wake cycle in the freely moving rats. J Neurosci Res 70: 611–621.

223. Newman DB, Ginsberg CY. (1992) Brainstem reticular nuclei that project to the cerebellum in rats: a retrograde tracer study. Brain Behav Evol.;39(1):24-68.

224. Nie L. (2008) KCNQ4 mutations associated with nonsyndromic progressive sensorineural hearing loss. Curr Opin Otolaryngol Head Neck Surg. 16, 441-444.

225. Nigro MJ., Mateos-Aparicio P, Storm JF.. (2014) Expression and functional roles of Kv7/KCNQ/M-channels in rat medial entorhinal cortex layer II stellate cells. J. Neurosci, 34, 6807–6812.

226. Ohmura Y, Tsutsui-Kimura I, Sasamori H, Nebuka M, Nishitani N, Tanaka KF, Yamanaka A, Yoshioka M. (2020) Different roles of distinct serotonergic pathways in anxiety-like behavior, antidepressant-like, and anti-impulsive effects. Neuropharmacology. 1;167:107703.

227. Okaty BW, Freret ME, Rood BD, Brust RD, Hennessy ML, deBairos D (2015) Multi-scale molecular deconstruction of the serotonin neuron system. Neuron. 88(4):774-91.

228. Pahapill PA, Lozano AM. (2000) The pedunculopontine nucleus and Parkinson's disease. Brain.;123(Pt 9):1767-1783.

229. Pál B, Koszeghy A, Pap P, Bakondi G, Pocsai K, Szucs G, Rusznák Z. (2009) Targets, receptors and effects of muscarinic neuromodulation on giant neurones of the rat dorsal cochlear nucleus. Eur J Neurosci. 30(5):769-82.

230. Paxinos GF, K. B. (2013) The mouse brain in stereotaxic coordinates, 4th Edition. San Diego. Elsevier.

231. Paxinos, G. and Watson, C., (1982) The Rat Brain in Stereotaxic Coordinates, Academic Press, Sydney : 0-12-547623-X.

232. Perera T, Tan JL, Cole MH, et al. Balance control systems in Parkinson's disease and the impact of pedunculopontine area stimulation. Brain. 2018. doi:10.1093/brain/awy216

233. Petreanu, L., Mao, T., Sternson, S.M., and Svoboda, K. (2009). The subcellular organization of neocortical excitatory connections. Nature 457, 1142–1145.

234. Petzold A., Valencia M., Pál B., and Mena-Segovia J. (2015) Decoding brain state transitions in the pedunculopontine nucleus: cooperative phasic and tonic mechanisms. Front Neural Circuits. 9, 68.

235. Pollak Dorocic I, Fürth D, Xuan Y, Johansson Y, Pozzi L, Silberberg G, Carlén M, Meletis K. (2014) A whole-brain atlas of inputs to serotonergic neurons of the dorsal and median raphe nuclei. Neuron. 83(3):663-78.

236. Provence, A., Angoli, D., & Petkov, G. V. (2018). KV7 Channel Pharmacological Activation by the Novel Activator ML213: Role for Heteromeric KV7.4/KV7.5 Channels in Guinea Pig Detrusor Smooth Muscle Function. The Journal of pharmacology and experimental therapeutics, 364(1), 131–144.

237. R.H. Kramer, J.J. Chambers, D. Trauner, (2005) Photochemical tools for remote control of ion channels in excitable cells, Nat. Chem. Biol., 1, pp. 360-365

238. Redgrave, P., Mitchell, IJ, Dean, P. (1987) Descending projections from the superior colliculus in rat: a study using orthograde transport of wheatgerm-agglutinin conjugated horseradish peroxidase. Exp Brain Res. 68 (1): 147-67

239. Reese NB, Garcia-Rill E, Skinner RD (1995) The pedunculopontine nucleus-auditory input, arousal and pathophysiology. Prog Neurobiol 47:105–133

240. Ren J, Friedmann D, Xiong J, Liu CD, Ferguson BR, Weerakkody T (2018). Anatomically defined and functionally distinct dorsal raphe serotonin sub-systems. Cell. 175(2):472-487.e20.

241. Ren J, Isakova A, Friedmann D, Zeng J, Grutzner SM, Pun A (2019) Single-cell transcriptomes and whole-brain projections of serotonin neurons in the mouse dorsal and median raphe nuclei. Elife.; 8:e49424.

242. Renouard, L., Bridi, M. C. D., Coleman, T., Arckens, L., & Frank, M. G. (2018). Anatomical correlates of rapid eye movement sleep-dependent plasticity in the developing cortex. Sleep. 41(10):zsy124

243. Roach J. P., Ben-Jacob E., Sander L. M., and Zochowski M. R. (2015) Formation and dynamics of waves in a cortical model of cholinergic modulation. PLoS Comput Biol. 11, e1004449.

244. Roach J. P., Sander L. M., and Zochowski M. R. (2016) Memory recall and spike-frequency adaptation. Phys Rev E. 93, 052307.

245. Roepke TA, Smith AW, Rønnekleiv OK, Kelly MJ. (2012) Serotonin 5-HT2C receptor-mediated inhibition of the M-current in hypothalamic POMC neurons. Am J Physiol Endocrinol Metab. 302(11):E1399-406.

246. Roš H, Magill PJ, Moss J, Bolam JP, Mena-Segovia J. (2010) Distinct types of non-cholinergic pedunculopontine neurons are differentially modulated during global brain states. Neuroscience. 170(1):78-91

247. Roseberry TK, Lee AM, Lalive AL, Wilbrecht L, Bonci A, Kreitzer AC. (2016) Cell-Type-Specific Control of Brainstem Locomotor Circuits by Basal Ganglia. Cell.. 164(3):526-37

248. Rundfeldt C, Netzer R. (2000) The novel anticonvulsant retigabine activates M-currents in Chinese hamster ovary-cells tranfected with human KCNQ2/3 subunits. Neurosci Lett. 282(1-2):73-6.

249. Rye DB, Wainer BH, Mesulam MM, Mufson EJ, Saper CB. (1984) Cortical projections arising from the basal forebrain: a study of cholinergic and noncholinergic components employing combined retrograde tracing and immunohistochemical localization of choline acetyltransferase. Neuroscience. 13(3):627-43.

250. Rye, DB, Lee, HJ, Saper, CB, Wainer, BH (1988) Medullary and spinal efferents of the pedunculopontine tegmental nucleus and adjacent mesopontine tegmentum in the rat. J. comp. Neurol. 269, 315-341.

251. Rye, DB, Saper, CB, Lee, HJ, Wainer, BH (1987) Pedunculopontine tegmental nucleus of the rat: Cytoarchitecture, cytochemistry and some extrapyramidal connections of the pontine tegmentum. J. Comp. Neurol. 259, 483-528.

252. S.D Moore, S.G Madamba, M Joels, G.R Siggins (1988) Somatostatin augments the M-current in hippocampal neurons, Science, 239 pp. 278-280

253. Saitoh, K., Hattori, S., Song, WJ, Isa, T., Takakusaki, K. (2003) Nigral GABAergic inhibition upon cholinergic neurons in the rat pedunculopontin tegmental nucleus. Eur. J. Neurosci. 18, 879–886.

254. Saitsu H, Kato M, Koide A, Goto T, Fujita T, Nishiyama K, Tsurusaki Y, Doi H, Miyake N, Hayasaka K, (2012) Whole exome sequencing identifies KCNQ2 mutations in Ohtahara syndrome. Ann Neurol 72: 298–300.

255. Sakai, K., El Mansari, M., Jouvet, M. (1990) Inhibition by carbachol microinjections of presumptive cholinergic PGO-on neurons in freely moving cats. Brain Res 527: 213–223

256. Sakai, K., Salvert, D., Touret, M., Jouvet, M. (1972) Afferent connections of the nucleus raphe dorsalis in the cat as visualized by the horseradish peroxidase technique. Brain Res. 137, 11-35.

257. Saper, C.B. (1984), Organization of cerebral cortical afferent systems in the rat. II. Magnocellular basal nucleus. J. Comp. Neurol., 222: 313-342.

258. Saper, CB, Loewy, AD (1982) Projections of the pedunculopontin tegmental nucleus in the rat: Evidence for additional extrapyramidal circuitry. Brain Res. 252, 367-372.

259. Sarter M, Bruno JP, Givens B. (2003) Attentional functions of cortical cholinergic inputs: what does it mean for learning and memory? Neurobiol Learn Mem. 80(3):245-56.

260. Satoh, K., Fibiger, HC (1986) Cholinergic neurons of the laterodorsal tegmental nucleus: Efferent and afferent connections. J. Comp. Neurol. 253, 277-302.

261. Scanziani M, Hausser M. (2009) Electrophysiology in the age of light. Nature.461:930–39.

262. Schofield, B. R., Motts, S. D., & Mellott, J. G. (2011). Cholinergic cells of the pontomesencephalic tegmentum: connections with auditory structures from cochlear nucleus to cortex. Hearing research, 279(1-2), 85–95.

263. Schwarz J. R., Glassmeier G., Cooper E. C., Kao T. C., Nodera H., Tabuena D., Kaji R., Bostock H. (2006) KCNQ channels mediate IKs, a slow K+ current regulating excitability in the rat node of Ranvier. J Physiol. 573(Pt 1), 17-34.

264. Serrano-Novillo C., Oliveras A., Ferreres J. C., Condom E., and Felipe A. (2020) Remodeling of Kv7.1 and Kv7.5 expression in vascular tumors. Int J Mol Sci. 21, 6019.

265. Shah M., Mistry M., Marsh S. J., Brown D. A., and Delmas P. (2002) Molecular correlates of the M-current in cultured rat hippocampal neurons. J Physiol. 544(Pt 1), 29-37.

266. Sherman D, Fuller PM, Marcus J, (2015) Anatomical location of the mesencephalic locomotor region and its possible role in locomotion, posture, cataplexy, and Parkinsonism. Front Neurol. 6:140.

267. Shik ML, Severin F V, Orlovskiĭ GN. (1966)[Control of walking and running by means of electric stimulation of the midbrain. Biofizika.11(4):659-666.

268. Simon C, Kezunovic N, Ye M, Hyde J, Hayar A, Williams DK, Garcia-Rill E. (2010) Gamma band unit activity and population responses in the pedunculopontine nucleus. J Neurophysiol 104: 463–474.

269. Sofroniew, M. V., Priestley, J. V., Consolazione, A., Eckenstein, F., & Cuello, A. C. (1985). Cholinergic projections from the midbrain and pons to the thalamus in the rat, identified by combined retrograde tracing and choline acetyltransferase immunohistochemistry. Brain Research, 329(1-2), 213–223.

270. Soiza-Reilly, M., & Commons, K. G. (2014). Unraveling the architecture of the dorsal raphe synaptic neuropil using high-resolution neuroanatomy. Frontiers in neural circuits, 8, 105

271. Soldovieri M.V., Miceli F., and Taglialatela M. (2011) Driving with no brakes: molecular pathophysiology of Kv7 potassium channels. Physiology (Bethesda). 26, 365-376.

272. Soldovieri MV, Boutry-Kryza N, Milh M, Doummar D, Heron B, Bourel E, Ambrosino P, Miceli F, De Maria M, Dorison N, Auvin S, Echenne B, Oertel J, Riquet A, Lambert L, Gerard M, Roubergue A, Calender A, Mignot C, Taglialatela M, Lesca G. (2014) Novel KCNQ2 and KCNQ3 mutations in a large cohort of families with benign neonatal epilepsy: first evidence for an altered channel regulation by syntaxin-1A. Hum Mutat. 35(3):356-67.

273. Spann, BM, Grofova, I. (1989) Origin of ascending and spinal pathways from the nucleus pedunculopontinus in the rat. J. comp. Neurol. 283, 13-27.

274. Steinbusch HW, van der Kooy D, Verhofstad AA, Pellegrino A (1980) Serotonergic and non-serotonergic projections from the nucleus raphe dorsalis to the caudate-putamen complex in the rat, studied by a combined immunofluorescence and fluorescent retrograde axonal labeling technique. Neurosci Lett 19(2):137-42.

275. Steriade M, Glenn LL. (1982) Neocortical and caudate projections of intralaminar thalamic neurons and their synaptic excitation from midbrain reticular core. J Neurophysiol. 48(2):352-71.

276. Steriade M, Paré D, Datta S, Oakson G, Curró Dossi R. (1990) Different cellular types in mesopontin cholinergic nuclei related to ponto-geniculo-occipital waves. J Neurosci. 10 (8): 2560-79.

277. Steriade, M., Dossi, R. C., Pare, D., & Oakson, G. (1991). Fast oscillations (20-40 Hz) in thalamocortical systems and their potentiation by mesopontine cholinergic nuclei in the cat. Proceedings of the National Academy of Sciences, 88(10), 4396–4400.

278. Stevens, S., & Hening, W. A. (2007). Sleep and Wakefulness. Textbook of Clinical Neurology, 21–33.

279. Storm JF. (1989) An after-hyperpolarization of medium duration in rat hippocampal pyramidal cells. J. Physiol. 409, 171–190.

280. Su M., Li L., Wang J., Sun H., Zhang L., Zhao C., Xie Y., Gamper N., Du X., and Zhang H. (2019) Kv7.4 channel contribute to projection-specific auto-inhibition of dopamine neurons in the ventral tegmental area. Front Cell Neurosci. 13, 557.

281. Sugimoto, T., Hattori, T. (1984) Organization and efferent projections of nucleus tegmenti pedunculopontinus pars compacta with special reference to cholinergic aspects. Neuroscience 11, 931-946.

282. Suh BC, Hille B. (2006) Does diacylglycerol regulate KCNQ channels? Pflugers Arch.453:293–301.

283. Susan D. Iversen (1984). 5-HT and anxiety. , 23(12-part-P2), 1553–1560.

284. Sverdlow, NR, Koob, GF (1987) Lesions of the dorsomedial nucleus of the thalamus, medial prefrontal cortex and pedunculopontine nucleus. Effects on locomotor activity medicated by nucleus accumbens-ventral pallidal pathway. Brain Res. 412, 233-243

285. Takakusaki K, Shiroyama T, Kitai ST. (1997) Two types of cholinergic neurons in the rat tegmental pedunculopontine nucleus: Electrophysiological and morphological characterization. Neuroscience. 79(4):1089-109.

286. Takakusaki K, Shiroyama T, Yamamoto T, Kitai ST (1996) Cholinergic and noncholinergic tegmental pedunculopontine projection neurons in rats revealed by intracellular labeling. J Comp Neurol 371(3):345–361

287. Thevathasan, W., Pogosyan, A., Hyam, JA, Jenkinson, N., Foltynie, T., Limousin, P., et al. (2012) Alpha oscillations in the pedunculopontin nucleus correlate with gait performance in parkinsonism. Brain 135, 148–160.

288. Tzingounis AV, Heidenreich M, Kharkovets T, Spitzmaul G, Jensen HS, Nicoll RA (2010) The KCNQ5 potassium channel mediates a component of the afterhyperpolarization current in mouse hippocampus. Proc Natl Acad Sci U S A. 107(22):10232-7.

289. Tzingounis AV, Nicoll RA. (2008) Contribution of KCNQ2 and KCNQ3 to the medium and slow afterhyperpolarization currents.Proc Natl Acad Sci U S A. 105(50):19974-9.

290. Van Bockstaele EJ, Biswas A, Pickel VM. (1993) Topography of serotonin neurons in the dorsal raphe nucleus that send axon collaterals to the rat prefrontal cortex and nucleus accumbens. Brain Res. 624(1-2):188-98.

291. Van Dort, CJ, Zachs, DP, Kenny, JD, Zheng, S., Goldblum, RR, Gelwan, NA, Ramos, DM, Nolan, MA, Wang, K., Weng, FJ, Lin, Y., Wilson, MA, Brown, EN (2015) Optogenetic activation of cholinergic neurons in the PPT or LDT induces REM sleep. Proc Natl Acad Sci US A. 112 (2): 584-9.

292. Vertes RP, Fortin WJ, Crane AM (1999) Projections of the median raphe nucleus in the rat. J Comp Neurol 407:555–582

293. Vincent SR (2000) The ascending reticular activating system: from aminergic neurons to nitric oxide. J Chem Neuroanat 18:23–30

294. Vincent, SR, Reiner, PB (1987) The immunohistochemical localization of choline acetyltransferase in the cat brain. Brain Res. Bull. 18, 371-415.

295. Viviana Gradinaru; Feng Zhang; Charu Ramakrishnan; Joanna Mattis; Rohit Prakash; Ilka Diester; Inbal Goshen; Kimberly R. Thompson; Karl Deisseroth (2010). Molecular and Cellular Approaches for Diversifying and Extending Optogenetics. , 141(1), 0–165.

296. Wainer BH, Levey AI, Rye DB, Mesulam MM, Mufson EJ. (1985) Cholinergic and non-cholinergic septohippocampal pathways. Neurosci Lett. 54(1):45-52.

297. Walter, B.L. & Shaikh, A.G.. (2014). Midbrain. 3, pp 152–159.

298. Wang HL, Morales M. (2009) Pedunculopontine and laterodorsal tegmental nuclei contain distinct populations of cholinergic, glutamatergic and GABAergic neurons in the rat. Eur J Neurosci. 29(2):340-58.

299. Wang, H.-S., Pan, Z., Brown, B. S., Wymore, R. S., Cohen, I. S., Dixon, J. E. & McKinnon, D. (1998). KCNQ2 and KCNQ3 potassium channel subunits: molecular correlates of the M-channel. Science 282, 18901893.

300. Waterhouse BD, Border B, Wahl L, Mihailoff GA. (1993) Topographic organization of rat locus coeruleus and dorsal raphe nuclei: distribution of cells projecting to visual system structures. J Comp Neurol. 336(3):345-61.

301. Waterhouse BD, Mihailoff GA, Baack JC, Woodward DJ. (1986) Topographical distribution of dorsal and median raphe neurons projecting to motor, sensorimotor, and visual cortical areas in the rat. J Comp Neurol. 249(4):460-76, 478-81.

302. Weckhuysen S, Mandelstam S, Suls A, Audenaert D, Deconinck T, Claes LR, Deprez L, Smets K, Hristova D, Yordanova I, Jordanova A, Ceulemans B, Jansen A, Hasaerts D, Roelens F, Lagae L, Yendle S, Stanley T, Heron SE, Mulley JC, Berkovic SF, Scheffer IE, de Jonghe P. (2012) KCNQ2 encephalopathy: emerging phenotype of a neonatal epileptic encephalopathy. Ann Neurol.71:15–25.

303. Wenk H., Bigl V. and Meyer U. (1980) Cholinergic projections from magnocellular nuclei of the basal forebrain to cortical areas in rats. Brain Res. Rev. 2, 295-316.

304. Wickenden A. D., Krajewski J. L., London B., Wagoner P. K., Wilson W. A., Clark S., Roeloffs R., McNaughton-Smith G., and Rigdon G. C. (2008) N-(6-chloro-pyridin-3-yl)-3,4-difluoro-benzamide (ICA-27243): a novel, selective KCNQ2/Q3 potassium channel activator. Mol Pharmacol. 73, 977-986.

305. Wilcox, KS, Grant, SJ Chgostophe, GG (1987) Electrophysiological properties of lateral dorsal tegmental neurons in vitro. Neurosci. Abstr. 13, 57.

306. Woolf NJ, Butcher LL. (2011) Cholinergic systems mediate action from movement to higher consciousness. Behav Brain Res. 221(2):488-98.

307. Woolf NJ, Eckenstein F, Butcher LL. (1984) Cholinergic systems in the rat brain: I. projections to the limbic telencephalon. Brain Res Bull. 13(6):751-84.

308. Woolf NJ. (1998) A structural basis for memory storage in mammals. Prog Neurobiol. 55(1):59-77.

309. Woolf, N. J., & Butcher, L. L. (1986). Cholinergic systems in the rat brain: III. Projections from the pontomesencephalic tegmentum to the thalamus, tectum, basal ganglia, and basal forebrain. Brain Research Bulletin, 16(5), 603–637.

310. Woolf, N. J., & Butcher, L. L. (1989). Cholinergic systems in the rat brain: IV. descending projections of the pontomesencephalic tegmentum. Brain Research Bulletin, 23(6), 519–540.

311. Yasin A., Gündüz A., Uludağ M., Örnek N. İ., Uzun N., Ünalan H., & Kızıltan M. (2018). Pattern of startle reflex to somatosensory stimuli changes after spinal cord injury. The journal of spinal cord medicine, 41(1), 36–41.

312. Ye, M., Hayar, A., Strotman, B., Garcia-Rill, E. (2010) Cholinergic modulation of fast inhibitory and excitatory transmission to pedunculopontine thalamic projecting neurons. J Neurophysiology 103: 2417–2432.

313. Yizhar O, Fenno LE, Davidson TJ, Mogri M, Deisseroth K. (2011) Optogenetics in neural systems. Neuron.71:9–34.

314. Yu H, Wu M, Townsend SD, Zou B, Long S, Daniels JS et al. (2011). Discovery, synthesis, and structure activity relationship of a series of N-Aryl-bicyclo[2.2.1]heptane-2-carboxamides: characterization of ML213 as a novel KCNQ2 and KCNQ4 potassium channel opener. ACS Chem Neurosci. 2: 572–577

315. Yu H, Wu M, Townsend SD, Zou B, Long S, Daniels JS, (2011) Discovery, synthesis, and structure activity relationship of a series of N-Aryl-bicyclo[2.2.1]heptane-2-carboxamides: characterization of ML213 as a novel KCNQ2 and KCNQ4 potassium channel opener. ACS Chem Neurosci. 2:572–577.

316. Yuan Mei; Feng Zhang (2012). Molecular Tools and Approaches for Optogenetics. , 71(12):1033-8.

317. Zaborszky, L., Csordas, A., Mosca, K., Kim, J., Gielow, M.R., Vadasz, C., and Nadasdy, Z. (2015a). Neurons in the basal forebrain project to the cortex in a complex topographic organization that reflects corticocortical connectivity patterns: an experimental study based on retrograde tracing and 3D reconstruction. Cereb. Cortex 25, 118–137.

318. Zaczek R, Chorvat RJ, Saye JA, Pierdomenico ME, Maciag CM, Logue AR, Fisher BN, Rominger DH, Earl RA. (1998) Two new potent neurotransmitter release enhancers, 10,10-bis(4-pyridinylmethyl)-9(10H)-anthracenone and 10,10-bis(2-fluoro-4-pyridinylmethyl)-9(10H)-anthracenone: comparison to linopirdine. J Pharmacol Exp Ther.285:724–730.

319. Zemelman BV, Lee GA, Ng M, Miesenböck G. (2002) Selective photostimulation of genetically chARGed neurons. Neuron.33:15–22.

320. Zhang F, Wang L-P, Brauner M, Liewald JF, Kay K, Watzke N, Wood PG, Bamberg E, Nagel G, Gottschalk A, et al (2007) Multimodal fast optical interrogation of neural circuits. Nature 446: 633- 639

321. Zhang, F., Prigge, M., Beyrie`re, F., Tsunoda, S.P., Mattis, J., Yizhar, O., Hegemann, P., and Deisseroth, K. (2008). Red-shifted optogenetic excitation: a tool for fast neural control derived from Volvox carteri. Nat. Neurosci. 11,631–633.

322. Zhang, F., Wang, L.P., Boyden, E.S., and Deisseroth, K. (2006). Channelrhodopsin-2 and optical control of excitable cells. Nat. Methods 3, 785–792.

323. Zhao C., Su M., Wang Y., Li X., Zhang Y., Du X., and Zhang H. (2017) Selective modulation of K+ channel Kv7.4 significantly affects the excitability of DRN 5-HT neurons. Front Cell Neurosci. 11, 405.

324. Zhao, C., Su, M., Wang, Y., Li, X., Zhang, Y., Du, X., et al. (2017). Selective modulation of K + channel Kv7.4 significantly affects the excitability of DRN 5-HT neurons. Front. Cell. Neurosci. 14, 11–405.

325. Zhao, S., Cunha, C., Zhang, F., Liu, Q., Gloss, B., Deisseroth, K., Augustine, G.J., and Feng, G. (2008). Improved expression of halorhodopsin for lightinduced silencing of neuronal activity. Brain Cell Biol. 36, 141–154.

326. Zhuang X, Gross C, Santarelli L, Compan V, Trillat AC, Hen R (1999) Altered emotional states in knockout mice lacking 5-HT1A or 5-HT1B receptors. Neuropsychopharmacol 21: S52-S60.

327. Zweig RM, Jankel WR, Hedreen JC, Mayeux R, Price DL. (1989) The pedunculopontine nucleus in Parkinson's disease. Ann Neurol. 26(1):41-6.

328. Zweig RM, Whitehouse PJ, Casanova MF, Walker LC, Januarykel WR, Price DL. (1987) Loss of pedunculopontine neurons in progressive supranuclear palsy. Ann Neurol. 22(1): 18-25

DEBRECENI EGYETEM
EGYETEMI ÉS NEMZETI KÖNYVTÁR
H-4002 Debrecen, Egyetem tér 1, Pf.: 400
Tel.: 52/410-443, e-mail: publikaciok@lib.unideb.hu

Nyilvántartási szám: DEENK/377/2021.PL
Tárgy: PhD Publikációs Lista

Jelölt: Bayasgalan, Tsogbadrakh
Doktori Iskola: Molekuláris Orvostudomány Doktori Iskola

A PhD értekezés alapjául szolgáló közlemények

1. **Bayasgalan, T.**, Stupniki, S., Kovács, A., Csemer, A., Szentesi, P., Pocsai, K., Dionisio, L., Spitzmaul, G., Pál, B.: Alteration of mesopontine cholinergic function by the lack of KCNQ4 subunit.
   Front. Cell. Neurosci. 15, 1-16, 2021.
   IF: 5.505 (2020)
2. Dautan, D., Kovács, A., **Bayasgalan, T.**, Diaz-Acevedo, M. A., Pál, B., Mena-Segovia, J.: Modulation of motor behavior by the mesencephalic locomotor region.
   Cell Reports. 36 (8), 1-53, 2021.
   IF: 9.423 (2020)
3. **Bayasgalan, T.**, Csemer, A., Kovács, A., Pocsai, K., Pál, B.: Topographical Organization of M-Current on Dorsal and Median Raphe Serotonergic Neurons.
   Front. Cell. Neurosci. 15, 1-8, 2021.
   DOI: http://dx.doi.org/10.3389/fncel.2021.614947
   IF: 5.505 (2020)

DEBRECENI EGYETEM Egyetemi és Nemzeti Könyvtár

DEBRECENI EGYETEM
EGYETEMI ÉS NEMZETI KÖNYVTÁR
H-4002 Debrecen, Egyetem tér 1, Pf.: 400
Tel.: 52/410-443, e-mail: publikaciok@lib.unideb.hu

További közlemények

4. Baksa, B., Kovács, A., **Bayasgalan, T.**, Szentesi, P., Kőszeghy, Á., Szűcs, P., Pál, B.: Characterization of functional subgroups among genetically identified cholinergic neurons in the pedunculopontine nucleus.
Cell. Mol. Life Sci. 76 (14), 2799-2815, 2019.
DOI: http://dx.doi.org/10.1007/s00018-019-03025-4
IF: 6.496

5. Kovács, A., Baksa, B., **Bayasgalan, T.**, Szentesi, P., Csemer, A., Pál, B.: Orexinergic actions modify occurrence of slow inward currents on neurons in the pedunculopontine nucleus.
Neuroreport. 30 (14), 933-938, 2019.
DOI: http://dx.doi.org/10.1097/WNR.0000000000001298
IF: 1.394

A közlő folyóiratok összesített impakt faktora: 28,323
A közlő folyóiratok összesített impakt faktora (az értekezés alapjául szolgáló közleményekre): 20,433

A DEENK a Jelölt által az iDEa Tudóstérbe feltöltött adatok bibliográfiai és tudománymetriai ellenőrzését a tudományos adatbázisok és a Journal Citation Reports Impact Factor lista alapján elvégezte.

Debrecen, 2021.08.27.